LEANDRO GOULART DE ARAUJO

PHOTO-OXIDATIVE DEGRADATION OF BISPHENOL A BY H_2O_2/UV: PROCESS STUDY AND KINETIC MODELLING

São Paulo

2018

LEANDRO GOULART DE ARAUJO

PHOTO-OXIDATIVE DEGRADATION OF BISPHENOL A BY H_2O_2/UV: PROCESS STUDY AND KINETIC MODELLING

Tese apresentada à Escola Politécnica da Universidade de São Paulo para obtenção do título de Doutor em Ciências

São Paulo
2018

LEANDRO GOULART DE ARAUJO

PHOTO-OXIDATIVE DEGRADATION OF BISPHENOL A BY H_2O_2/UV: PROCESS STUDY AND KINETIC MODELLING

Tese apresentada à Escola Politécnica da Universidade de São Paulo para obtenção do título de Doutor em Ciências

Área de concentração: Engenharia Química

Orientador: Prof. Dr. Antonio Carlos Silva Costa Teixeira

São Paulo

2018

Este exemplar foi revisado e corrigido em relação à versão original, sob responsabilidade única do autor e com a anuência de seu orientador.

São Paulo, _____ de _____ de _____

Assinatura do autor: _____

Assinatura do orientador: _____

Catalogação-na-publicação

Araujo, Leandro Goulart de
Photo-oxidative degradation of bisphenol A by H2O2/UV: process study and kinetic modelling / L. G. Araujo -- versão corr. -- São Paulo, 2018.
103 p.

Tese (Doutorado) - Escola Politécnica da Universidade de São Paulo. Departamento de Engenharia Química.

1.FOTOQUÍMICA 2.REATORES QUÍMICOS 3.PROCESSOS QUÍMICOS 4.CINÉTICA QUÍMICA I.Universidade de São Paulo. Escola Politécnica. Departamento de Engenharia Química II.t.

Ao meu pai pela imensa saudade e a minha mãe por todo amor.

AGRADECIMENTOS

Ao Professor Antonio Carlos Silva Costa Teixeira, pela oportunidade, dedicação e orientação transmitida durante todo o trabalho.

Me gustaría expresar mi agradecimiento al Profesor Orlando M. Alfano por recibirme en su grupo de investigación, contribuyendo a mi desarrollo profesional y personal.

Mi más sincero agradecimiento a los investigadores Dr. Leandro Conte y Dra. Agustina V. Schenone por ayudarme en mi aprendizaje y en la adquisición de nuevos conocimientos.

Aos meus pais: Álvaro (*in memoriam*) e Valdete, por todo carinho e amor. Vocês são meus maiores exemplos de vida. Também quero agradecer a minha irmã Luciana, por acreditar em mim e pelo carinho.

À minha companheira Thalita, por todo amor, carinho e aos maravilhosos momentos juntos. Obrigado por cuidar de mim nos instantes difíceis, por não me deixar desistir e pela paciência e suporte durante minha estadia no exterior.

Mi gratitud al Sr. Antonio Carlos Negro, por la amistad y los esfuerzos en ayudarme.

A mis profesores y amigos del Jiu Jitsu y de asados de la ciudad de Santa Fe, AR. En especial, a mi profesor Emiliano Riestra y mis amigos Ruben F. Zapata por la gran amistad y compañerismo, y Diego “Carioca” por la amistad.

A mis amigos del postgrado de la UNL, Isaías y Joana, por la amistad y compañía.

Aos amigos José Eduardo pela imensa ajuda e paciência, e ao José Otávio pelas valiosas dicas.

Ao Professor Moisés T. dos Santos do Departamento de Engenharia Química e a Professora Adriana Bauer da Faculdade de Educação pela atenção, ensinamentos e colaboração para o meu desenvolvimento como monitor no programa de aperfeiçoamento de ensino (PAE).

À Professora Cristina Borba da Escola Politécnica, Poli-USP, e a Msc. Marina Lunndo Letramento Acadêmico da Faculdade de Filosofia, Letras e Ciências Humanas, FFLCH - USP, ambas pelas sugestões referentes à adequação da escrita em inglês para o exame de qualificação.

À Dra. Adriana C. Velosa e à Professora Kátia R. B. Nogueira pelos ensinamentos.

Ao Murilo Moya e à Flaviane (Flavis) Santos pelos trabalhos feitos em conjunto.

Ao grupo Dempster MS Lab, em especial a Lidiane, Meriellen e Anita, por toda ajuda e esforços.

Ao Professor Julio T. Marumo do IPEN, pelas sugestões e amizade.

Ao Dr. Paulo Firmino Moreira Junior por toda ajuda e esforços.

Aos “monstros” do laboratório Rodrigo e Joel, por toda ajuda e amizade.

Aos amigos de departamento, pelas risadas e ótimas discussões no almoço, cafés e churrascos.

Aos meus professores de jiu jitsu em São Paulo: Igor Schneider (Tigrão) e Julio, e aos amigos e companheiros de equipe: Vinicius, Daniel, Milani, Julião e muitos outros, pelos treinos, rodízios, açaís e amizade.

Aos meus amigos de Poços de Caldas, MG, pelos bons momentos. Em especial ao Tiago, pela ajuda na mudança de formato de alguns gráficos.

Ao grupo AdOx, pelas valorosas contribuições. Em especial a Patrícia Metolina por sempre estar disposta a ajudar.

Ao pessoal da secretaria, Elisete, Alexandre e Graça, pelos auxílios.

Ao programa de Pós-Graduação em Engenharia Química e a CAPES pelo auxílio financeiro.

A todos que contribuíram direta ou indiretamente no desenvolvimento deste trabalho.

“The important work of moving the world forward does not wait to be done by perfect men.”

(George Eliot)

RESUMO

O bisfenol A (BPA) é amplamente utilizado na fabricação de plásticos, resinas epóxi e policarbonatos. Trata-se de um composto tóxico e um desregulador endócrino. Diferentes estudos evidenciam a presença do BPA em diversos compartimentos ambientais em todo planeta, identificando-o como um poluente persistente e resistente à degradação biológica, que apresenta efeitos sinergéticos com outros poluentes. Nesse contexto, os processos oxidativos avançados (POA) têm recebido atenção devido a sua capacidade em degradar poluentes com tais características, transformando-os em compostos menos perigosos ou até mesmo mineralizando-os totalmente. Apesar de haver trabalhos na literatura acerca da utilização de POA para degradação de BPA, estudos sistemáticos dos efeitos de variáveis de processo junto com a interpretação estatística dos resultados são virtualmente inexistentes. Além disso, até onde se sabe um modelo cinético rigoroso ainda não foi proposto para a degradação desse poluente por meio do processo H_2O_2/UV. Este trabalho teve por objetivo avaliar a degradação do BPA pelo processo H_2O_2/UV, investigando os efeitos da concentração inicial de H_2O_2 e da taxa específica de emissão de fótons ($E_{P,0}$) por meio de um projeto experimental Doehlert, combinado com a análise de superfície de resposta. Os experimentos foram realizados em um reator tubular fotoquímico equipado com uma lâmpada UV de 254 nm, para $[H_2O_2]_0$ e $E_{P,0}$ entre 1,6-9,6 mmol L^{-1} e $0,87 \times 10^{18}$ - $3,6 \times 10^{18}$ fótons L^{-1} s^{-1}, respectivamente. Todos os experimentos sob H_2O_2/UV resultaram em total degradação do BPA após 60 min de irradiação. Nesse caso, as melhores condições foram $[H_2O_2]_0$ = 7,6 mmol L^{-1} e $E_{P,0} = 3,6 \times 10^{18}$ fótons L^{-1} s^{-1}, para as quais se obteve o melhor desempenho quanto à taxa de degradação de BPA e à remoção após 15 min, e a segunda maior remoção de COT após 180 min. Entretanto, na maioria dos experimentos menos de 75% de remoção de COT foram observados, com 95% de mineralização obtida apenas para os maiores $[H_2O_2]_0$ e $E_{P,0}$. Elaborou-se um modelo matemático que considera as características do reator utilizado e o campo de radiação, baseado no modelo de fonte linear de emissão em planos paralelos (LSPP), combinado à equação de transferência radiativa (RTE), aos balanços materiais e a um modelo cinético detalhado do processo H_2O_2/UV. Foi empregada a aproximação de estado estacionário para todas as espécies radicalares. Na estimativa das constantes cinéticas desconhecidas, utilizou-se o método de mínimos quadrados não linear. Esse modelo foi capaz de ajustar satisfatoriamente as concentrações experimentais de BPA e de H_2O_2 em função do tempo. Este trabalho mostra que o processo H_2O_2/UV constitui uma alternativa conveniente para a degradação de BPA em matrizes aquosas, com total degradação do composto alvo e

porcentagem de mineralização adequada nas condições ótimas de operação. Tais condições podem servir como diretrizes iniciais de processamento em escalas piloto e industrial. Por sua vez, simulações empregando o modelo matemático proposto permitem gerar informações úteis para projeto e aumento de escala de processos de pré- ou pós-tratamento de efluentes contendo esse poluente.

Palavras-chave: Bisfenol A, Processos oxidativos avançados, UV, H_2O_2/UV, Carbono orgânico total, modelagem cinética, modelagem do campo de radiação.

ABSTRACT

Bisphenol A (BPA) is widely used in the production of plastics, epoxy resins and polycarbonates. It is a toxic, endocrine disruptor compound. Different studies have shown the presence of BPA in several environmental systems, classifying it as a worldwide persistent pollutant which may act synergistically with other pollutants. In this context, advanced oxidation processes (AOP) have received great attention due to their ability to degrade pollutants with such characteristics, through their transformation into less hazardous compounds or even their mineralization. Although there are investigations on the use of AOPs for BPA degradation, systematic studies on the effects of process variables, coupled with the statistical interpretation of the results are virtually non-existent. Furthermore, to the best of our knowledge, a rigorous kinetic model has not yet been proposed for the degradation of this pollutant by the H_2O_2/UV process. The objective of this work was to evaluate BPA degradation by the H_2O_2/UV process, investigating the effects of the initial H_2O_2 concentration and the specific rate of photons emission ($E_{P,0}$) by means of a Doehlert experimental design, combined with the response surface methodology. The experiments were performed in a photochemical tubular reactor equipped with a 254-nm UV lamp, for $[H_2O_2]_0$ and $E_{P,0}$ in the ranges 1.6-9.6 mmol L^{-1} and 0.87×10^{18}-3.6×10^{18} photons L^{-1} s^{-1}, respectively. Total BPA degradation was achieved after 60 min of irradiation in all experiments. The best conditions were $[H_2O_2]_0$ = 7.6 mmol L^{-1} and $E_{P,0} = 3.6 \times 10^{18}$ photons L^{-1} s^{-1}, for which the best performance was obtained regarding the BPA degradation rate, BPA degradation after 15 min, and the second highest TOC removal after 180 min. However, in most experiments less than 75% TOC removal was observed, with 95% mineralization obtained only for the superior $[H_2O_2]_0$ and $E_{P,0}$. A mathematical model was developed, considering the reactor characteristics and the radiation field, based on the line source with parallel emission (LSPP) approach, in combination with the radiative transfer equation (RTE), mass balances, and a detailed kinetic model of the H_2O_2/UV process. The steady-state approximation was applied for all radical species. In the estimation of unknown kinetic constants, the non-linear least squares method was employed. The model was able to satisfactorily fit experimental BPA and H_2O_2 concentrations as a function of time. This work shows that the H_2O_2/UV process is a good alternative for BPA removal from aqueous streams, with total degradation of the target compound and adequate percent mineralization under optimal operating conditions. Such conditions may serve as first guidelines for pilot-plant and industrial processes operation. In addition, simulations using the proposed kinetic

model may provide useful information for the design and scale-up of pre- or post-treatment of effluents containing this pollutant.

Keywords: Bisphenol A, Advanced oxidation processes, UV, H_2O_2/UV, Total organic carbon, Kinetic modelling, Radiation field modelling.

LIST OF FIGURES

LIST OF TABLES

LIST OF ABBREVIATIONS AND ACRONYMS

1-D	One dimension
ANOVA	Analysis of variance
AOP	Advanced oxidation processes
BPA	Bisphenol A
CAS	Chemical Abstracts Service
CV	Control volume
DBP	Dibutyl phthalate
DOC	Dissolved organic carbon
EDC	Endocrine disruptor compound
ESVE	Extense source with volumetric emission
HPLC	High performance liquid chromatography
IC	Inorganic carbon
ICP	Inductively coupled plasma
IUPAC	International Union of Pure and Applied Chemistry
LC-MS	Liquid chromatography-mass spectrometry
LP	Low-pressure
LSEE	Line source with spherical emission
LSPP	Line source with parallel plane emission
LVEPA	Local volumetric rate of energy absorption
LVRPA	Local volumetric rate of photon absorption
MP	Medium-pressure
PPCP	Pharmaceutical and personal care products
RMSE	Root mean square error
RTE	Radiation transfer equation
SPE	Solid phase extraction
SPS	Sodium persulfate
SSA	Steady state approximation
TC	Total carbon
TOC	Total organic carbon
USEPA	U. S. Environmental Protection Agency

UV	Ultraviolet
VTG	Vitellogenin
WWF	World Wide Fund for Nature
YES	Yeast estrogen screen

NOMENCLATURE

A	Area	cm^2 or m^2
b	UV path length	cm or m
$[BPA]_0$	Initial BPA concentration	mg L^{-1} or mol m^{-3}
c	Speed of light	m s^{-1}
C	Constant	-
C_i	Concentration of the reacting species i	mg L^{-1} or mol m^{-3}
dA	Small area on the x coordinate	m^2
dEν	Total amount of radiative energy	Einstein
dq	radiation energy density flux	Einstein m^{-3}
D_{Lamp}	Lamp diameter	cm or m
$e_\lambda^a(x,t)$	Spectral local volumetric rate of photon absorption	Einstein L^{-1} s^{-1}
$E_{P,0}$	Specific rate of photons emission	photons L^{-1} s^{-1} or Einstein m^{-3} s^{-1}
$G_\nu(x,t)$	Spectral incident radiation	Einstein m^{-2} s^{-1}
$[H_2O_2]_0$	Initial H_2O_2 concentration	mmol L^{-1} or mol m^{-3}
$I_{\lambda,\Omega}$	Spectral specific intensity	W m^{-2} sr^{-1}
k_n	Rate constant for a reaction n	L mol^{-1} s^{-1}
K_{OC}	Soil/sediment adsorption coefficient	L kg^{-1}
K_{OW}	Octanol-water partition coefficient	-
l	Path length of irradiation	cm or m
L or L_L	Lamp length	cm or m
$\underline{n}$	Normal vector	-
N_i	Flux of convection-diffusion of the reacting species i	mol m^{-2} s^{-1}

P	Photon flow	mol s^{-1} (Einstein s^{-1})
q_i	Radiant flux	mol cm^{-2} s^{-1} (Einstein cm^{-2} s^{-1})
r	Perpendicular distance from the lamp to a point $P(r,z)$	m
R_1 and R_2	inner and outer radius of the photoreactor, respectively	m
R_i	Homogeneous reaction rate of the reacting species i	m^3 mol^{-1} s^{-1}
r_{LP} or R_{in}	Lamp radius	m
$r_{uv,i}$	Photolysis rate for the reacting species i	mol L^{-1} s^{-1}
S_L	Radiation energy emission	Einstein s^{-1} m^{-1}
s_r	Point of radiation entry in the photoreactor reaction space	-
t	Time	seconds
t_0	Initial time	seconds
V	Total volume	L or m^3
V_r	Irradiated volume	L or m^3
$\overline{x}$	Position in relation to the irradiation source in cylindrical coordinates	m
$W_{\Omega,\nu}^{a}$	Absorption contribution	W m^{-3} s^{-2} sr^{-1}
$W_{\Omega,\nu}^{e}$	Emission contribution	W m^{-3} s^{-2} sr^{-1}
$W_{\Omega,\nu}^{in-s}$	In-Scattering contribution	W m^{-3} s^{-2} sr^{-1}
$W_{\Omega,\nu}^{ou-s}$	Out-Scattering contribution	W m^{-3} s^{-2} sr^{-1}

Greek letters

dΩ or dω	Solid angle	degrees or radians
ε	Molar (decadic) absorption coefficient	$m^3\ mol^{-1}\ s^{-1}$
κ_i	Volumetric absorption coefficient of reacting species *i*	s^{-1}
ϕ_i	Quantum yield for the reacting species *i*	dimensionless
ρ_i	Distance from point *P*(*r, z*) to an arbitrary point of the lamp	m
θ	Angle between the irradiated area and the radiation source	degrees or radians
ν	Radiation frequency	Hz

CONTENTS

1. INTRODUCTION

Bisphenol A (BPA) is widely used as an intermediate compound in the production of several materials, such as plastics, epoxy and polycarbonate resins (BISPHENOL A GLOBAL INDUSTRY GROUP, 2003). End products of such production processes are powder paints, automotive lenses, compact disks, building materials, adhesives, among others (STAPLES *et al.*, 1998). BPA may be released into the environment from bottles, landfill leachates, paper, packaging and chemical industry effluents (TORRES *et al.*, 2008).

In 1998, Staples *et al.* (1998) showed that BPA toxicity is expected to be between low to moderate level (algal EC_{50} of 1000 μg L^{-1}). Moreover, previous studies revealed that this pollutant could show estrogenic activity at mg L^{-1} levels (DODDS and LAWSON, 1936, SODRÉ *et al.*, 2007, KUSVURAN and YILDIRIM, 2013). However, in Brazil, only plastic baby feeding bottles have specific regulations regarding this contaminant (RDC Resolution n. 41/2011), which forbid the importation and manufacture of these products containing BPA in their formulation. Furthermore, the U.S. Environmental Protection Agency (USEPA) and the World Wide Fund for Nature (WWF) consider BPA an endocrine disruptor compound (EDC) (ZHANG and LI, 2014; MOHAPATRA *et al.*, 2010).

BPA has been detected in wastewaters, and its removal using conventional treatment techniques, such as the biological approaches, revealed to be ineffective (FÜRHACKER *et al.* 2000, MOHAPATRA *et al.*, 2011). Therefore, alternative treatments capable of efficiently degrading this pollutant are becoming a great concern. In this context, Advanced Oxidation Processes (AOP) have been receiving great attention due to their capability to degrade persistent pollutants, through their transformation into less hazardous compounds or even their mineralization. Besides, they are easy to operate at room temperature and pressure, among other advantages, such as treating contaminants at low concentrations (mg L^{-1}-μg L^{-1}) (SHARMA *et al.*, 2011; TITUS *et al.*, 2004; DOMÈNECH *et al.*, 2004). These processes generate hydroxyl radicals ($HO^{\bullet}$), highly reactive, oxidative species capable of degrading many organic compounds (ZAHORODNA *et al.*, 2007). Hydroxyl radicals have a high redox potential (2.8 V HSE) in comparison with other oxidants, only lower than that of fluorine (PLANT and JEFF, 1994; HAGER, 1990).

Commonly applied AOPs for such purposes include Fenton (H_2O_2/Fe^{2+}) (MOHAPATRA *et al.*, 2011) and photo-Fenton (H_2O_2/Fe^{2+}/UV) reactions (KATSUMATA *et al.*, 2004), photocatalysis (RODRÍGUES *et al.*, 2010; SIN *et al.*, 2012), UV photolysis

(CHEN *et al.*, 2007), sonication and ozonation (O_3) (KUSVURAN and YILDIRIM, 2013; UMAR *et al.*, 2013), or their combination (CHEN *et al.*, 2006).

In this context, this work is aimed at investigating the use of the AOP based on the H_2O_2/UV system to remove BPA from water, focusing on the effect of the important operational variables, namely hydrogen peroxide initial concentration and specific rate of photons emission. To the best of our knowledge, the influence of these variables on BPA degradation through H_2O_2/UV process has not been previously investigated considering a detailed approach based on experimental design and response surface methodologies. Furthermore, a mathematical model is proposed for the process, which can be used for process optimization and scale-up.

2. OBJECTIVES

This study is aimed at investigating BPA degradation in water using the H_2O_2/UV process. The specific objectives are:

- To evaluate the effect of the specific rate of photons emission from the radiation source and the H_2O_2 initial concentration under UVC at 254 nm upon BPA degradation;
- To identify the optimal conditions of these variables for BPA degradation and total organic carbon (TOC) removal;
- To propose a mathematical model, phenomenological and empirical, for BPA degradation by the H_2O_2/UV process.

3. BACKGROUND

3.1 Endocrine Disruptors Compounds

An endocrine system in perfect conditions is primordial for reproduction, development, and growth of living organisms. Therefore, the identification of endocrine disrupting compounds (EDCs) is necessary, since these substances can interfere with hormone synthesis and/or hormone signalling (GUNNARSSON, 2008). According to the literature, the first reports on these substances were published in the mid-20th century. Over recent decades, research efforts to understand this problem have been intensively made (GUNNARSSON, 2008; LIU *et al.*, 2009).

According to the US Environmental Agency (USEPA), an EDC is defined as: "An exogenous agent that interferes with the synthesis, secretion, transport, binding, action, or elimination of natural hormones in the body that are responsible for the maintenance of homeostasis, reproduction, development, and/or behaviour" (EPA, 1997). This definition is generic, and, for this reason, more than 87,000 known chemicals are considered EDC (KOMESLI *et al.*, 2015).

EDCs, both natural and synthetic are released into the environment by humans (industry, agriculture, etc.) and animals. These substances, as well as other pharmaceutical and personal care products (PPCPs), may reach environmental compartments (soil, surface water, sediment and ground water) mainly through sewage treatment systems (LIU *et al.*, 2009; ROSENFELDT and LINDEN, 2004). The main distribution routes of EDCs into the environment are illustrated in Figure 3.1.

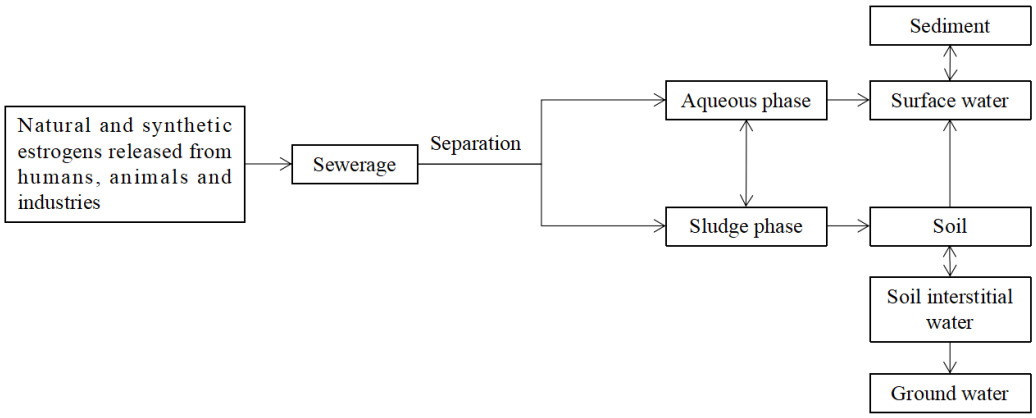

Figure 3.1 – Release and distribution of EDCs into the environment.
(Source: Modified from INGERSLEV and HALLING-SØRENSEN, 2003 *apud* LIU *et al.*, 2009)

Some preliminary work about estrogenic chemicals was carried out by DODDS and LAWSON (1936). Their first investigations on EDCs found that bisphenol A (BPA) showed full estrogenic activity. In short, the experiments were carried out by injecting about 70 mg kg^{-1} day^{-1} of BPA in ovariectomised adult rats, and changes were observed in vaginal epithelium, a common response caused by estrogens. Usually, BPA targets hormones as the thyroid, cortisol, and oestrogen.

3.2 BPA: Production and Process

BPA was discovered in 1905 and nowadays it has been mainly used to make compounds, such as plastics, epoxy resins, and polycarbonate resins (POLYCARBONATE/BPA GLOBAL GROUP, 2003). BPA production reached approximately 4.6 million metric tonnes in 2012, an increment of 372,000 tonnes compared to the record of 4.4 million in 2011 (MCGROUP, 2015).

One of the most common available processes for BPA production is the condensation of phenol with acetone using an acid as the catalyst (AGRAWAL and SUMAN, 2012). Figure 3.2 illustrates BPA production by this process.

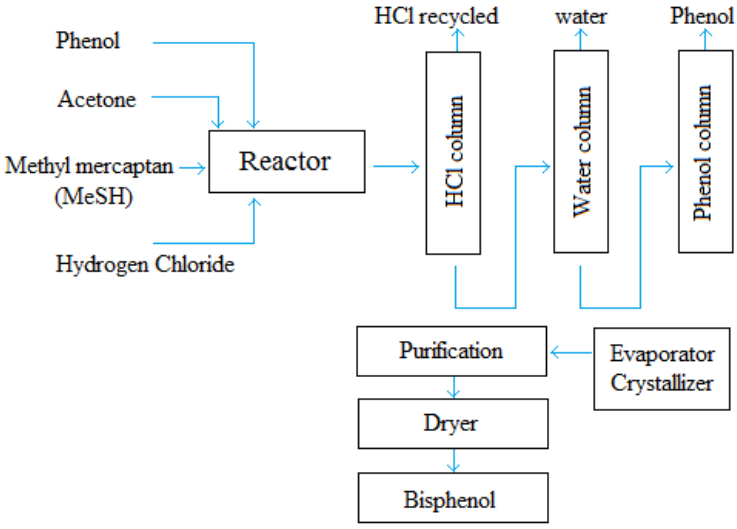

Figure 3.2 – Diagram of BPA production by acid catalysed phenol with acetone condensation. (Source: Modified from AGRAWAL and SUMAN, 2012)

According to the authors, the first step is the addition of phenol and acetone in a molar ratio of 3:1, under 50°C temperature and 1atm pressure. As indicated in Figure 3.2, anhydrous hydrogen chloride and methyl mercaptan (MeSH) are added to the reactor. Hydrogen chloride

and MeSH act as the catalysis and promoter, respectively. The residence time in the reactor is about 3 h. Since the reaction is exothermic, cooling water is required. The process is efficient, with 99% acetone conversion to BPA with the addition of phenol in excess. HCl can be recovered and recycled for further use. AGRAWAL and SUMAN (2012) stress the importance of temperature control, considering that higher temperatures cause BPA isomerization. The BPA solution is then purified by distillation and the water is separated. Simultaneously with the distillation process, some stabilizers are added in order to avoid BPA isomerization into o- and p- isomers. In the last distillation column, the reaction product is distilled under lower pressure. Finally, the subsequent steps are employed to remove remaining BPA isomers and purify the product through crystallization.

3.3 Physical and chemical properties of BPA

BPA is used for opposite purposes. As a plasticizer, BPA aims at increasing flexibility and malleability. On the other hand, as a hardener, BPA is added into the material aiming at increasing its resistance. Figure 3.3 presents the structural formula of BPA.

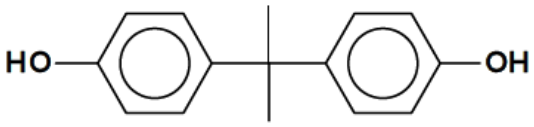

Figure 3.3 – Structural formula of bisphenol A.
(Source: FÜRHACKER *et al.*, 2000)

BPA is solid, colourless, soluble in organic solvents and slightly soluble in water (approximately 120 mg L^{-1}) (AGRAWAL and SUMAN, 2012; AGENSON and URASE, 2007). Table 3.1 lists the main properties of BPA.

Table 3.1 – Chemical and physical properties of BPA (STAPLES *et al.*, 1998; BISPHENOL A GLOBAL INDUSTRY GROUP, 2002; HAYNES, 2011; EUROPEAN UNION, 2012; FENT *et al.*, 2003; ZENG *et al.*, 2006; XU *et al.*, 2009; STAPLES *et al.*, 1998).

Main Properties	
Chemical formula	$C_{15}H_{16}O_2$
Molar weight	228 g mol^{-1}
CAS number	80-05-7
Solubility in water (25 ºC)	120 mg L^{-1}
Melting point	153 °C (1 atm)
Boiling point	360 °C (1 atm)
Henry's constant	4.0×10^{-8} mm Hg
K_{OC}	115-3886 (slight mobility in soil)
Log K_{OW}	3.4 (ambient pH)

3.4 Environmental contamination and toxicity

Since BPA is a widely-manufactured chemical, some concerns have been raised, regarding its concentration in various environments, such as marine, aquatic, and terrestrial (DORN *et al.*, 1987). In addition, the pollutant concentration is an important step to be considered before taking the necessary actions. Some EDCs were identified at μg L^{-1} level by a nationwide survey of pollutants in U.S. surface water, including BPA (12 μg L^{-1}) (KOPLIN *et al.*, 2002 *apud* ROSENFELDT and LINDEN, 2004). It is worth mentioning that there is a large amount of studies regarding the presence BPA in diverse environmental compartments around the globe. Table 3.2 details BPA concentrations measured in some of these sample sites.

Table 3.2 – Sample sites and corresponding BPA concentrations.

General overview	Specific sample spots	BPA concentration	Reference	Country or region
Industrial activities	Metal/wood industry	2.6-35 µg L^{-1}	FÜRHACKER *et al.* (2000)	Austria
	Chemical industry	2.5-50 µg L^{-1}	FÜRHACKER *et al.* (2000)	Austria
	Hospital	1 µg L^{-1}	FÜRHACKER *et al.* (2000)	Austria
	Paper production	28-72 µg L^{-1}	FÜRHACKER *et al.* (2000)	Austria
	Cloth washing company	1-8.9 µg L^{-1}	FÜRHACKER *et al.* (2000)	Austria
	Food industry	3.8 µg L^{-1}	FÜRHACKER *et al.* (2000)	Austria
	Household areas I	2.6 µg L^{-1}	FÜRHACKER *et al.* (2000)	Austria
	Household areas II	5.8 µg L^{-1}	FÜRHACKER *et al.* (2000)	Austria
	Influent	10-37 µg L^{-1}	FÜRHACKER *et al.* (2000)	Austria
	Effluent	2.5 µg L^{-1}	FÜRHACKER *et al.* (2000)	Austria
	Sewage leachates	1.3-5.4 µg mL^{-1} (without treatment); 0.5-5.1 ng mL^{-1}	KAWAGOSHI *et al.* (2003); COOR *et al.* (2003); YAMAMOTO *et al.*(2001); YAMADA *et al.*(1999)	Japan; Germany; Japan
	Food cans	4-23 µg L^{-1}	BROTONS *et al.* (1994)	Spain
	Serum	0.2×10^{-3}-20×10^{-3} µg L^{-1}	VANDERBERG *et al.* (2007)	Review article
Human body	Placental tissue	11.2×10^{-3} to 104.9×10^{-3} µg g^{-1} tissue	VANDERBERG *et al.* (2007)	Review article
	Breast milk	0.28-0.97 ng mL^{-1}	SUN *et al.* (2004)	Japan
	Urine	Male: 2.82-1.63 ng mL^{-1} Female: 2.76-1.12 ng mL^{-1}	CALAFAT *et al.* (2005); KIM *et al.* (2003)	United States; Korea
	Semen	Non-detected by high sensitive methods	VANDERBERG *et al.* (2007)	Review article
	Follicular fluid	2 ng mL^{-1}	IKEZUKI *et al.* (2002)	Japan
	Saliva	3.33-30 µg mL^{-1}	OLEA *et al.* (1996)	Spain

Table 3.2 (Cont.) – Sample sites and corresponding BPA concentrations.

General overview	Specific sample spots	BPA concentration	Reference	Country or region
Water in general	Drinking water	<1 μg L^{-1}	EPA (2010)	United States
	Shallow monitoring wells	up to 4.5 μg L^{-1}	ERICKSON (2012); ERICKSON *et al.* (2014)	United States
	Median surface fresh water	0.01 to 0.08 μg L^{-1}	KLECKA *et al.* (2009)	North America and Europe
	Water leaving waste treatment sites	up to 22 μg L^{-1}	LEE *et al.* (2007); LEE *et al.*(2011)	United States
Waste	Fly ash	2 μg kg^{-1}	MORIN *et al.* (2015)	Norway
	Plastics	63 to 313 mg kg^{-1}	MORIN *et al.* (2015)	Norway
	Landfill leachates	median of 17 μg L^{-1} (maximum 692 μg L^{-1})/ 0.1 to 17200 μg L^{-1}	ARP (2012)/SAKAMOTO *et al.* (2004); YASUHARA *et al.* (1997); YAMAMOTO *et al.* (2001); TARO *et al.* (2003); ASAKURA *et al.* (2004); KURATA *et al.* (2008)	Norway; Japan

The data provided by these studies yield convincing evidence that BPA is a widespread pollutant, although the measured concentrations were very contrasting at different sample spots.

As previously mentioned, BPA was identified as an estrogenic chemical. As regards to this characteristic, USEPA evaluated BPA as a weak estrogenic, five orders of magnitude lower than 17β-estradiol (CHEN *et al.*, 2002). Additionally, no mutagenicity was identified. BPA was considered toxic by the same agency, which used *Daphnia magna* as a reference organism to measure toxicity (EC_{50}=10 mg L^{-1} in a 48-h assay). Moreover, even low levels of this contaminant may be considered a major concern because of its physiological effect in living organisms (ROSENFELDT and LINDEN, 2004).

Despite the current discussion on the effects in humans, EDCs including BPA are known to present chemical persistence, microbial resistance and may show synergistic effects with other pollutants (TIJANI *et al.*, 2013).

3.5 *Advanced Oxidation Processes* (AOPs)

There are many types of pre-treatments aiming at removing EDCs from several matrices, such as chemical, mechanical, oxidative, biological or a combination of such types (SCRIMSHAW and LESTER, 2003). According to CONTRERAS *et al.* (2003), biological remediation is usually the most economical alternative to treat wastewater, ground water, and other aqueous wastes. Biological degradation relies on a variety of factors; including concentration, pH, and the chemical structure of the target compound (CONTRERAS *et al.*, 2003). The underlying argument against biological remediation is that many compounds are considered bio-recalcitrant and the data gathered in the literature suggests EDCs in sewage may be transferred to activate sludge because of their hydrophobic properties (LI *et al.*, 2011; CONTRERAS *et al.*, 2003). In the literature, BPA concentrations in sludge were found to be between 4 and 1363 ng g^{-1} (GATIDOU *et al.*, 2007; FROMME *et al.*, 2002). AOPs have shown to successfully degrade several EDCs (SILVA *et al.*, 2014; PUMA *et al.*, 2010; LAU *et al.*, 2007, TERNES *et al.*, 2003, ALUM *et al.*, 2004; KATSUMATA *et al.*, 2004; ROSENFELDT and LINDEN, 2004; ROSENFELDT *et al.*, 2007; SURI *et al.*, 2007).

According to OPPENLÄNDER (2003), and as already mentioned, AOPs involve the production of highly reactive and non-selective hydroxyl radicals ($HO^{\bullet}$), amongst other ROS, which are the most important oxidizing specie in aqueous media (STAEHELIN and HOIGNÉ, 1985). These radicals are generated by many different systems, with or without irradiation (Table 3.3).

Table 3.3 − Advanced Oxidation Processes. Adapted from CHENG *et al.* (2016).

Irradiated	Non irradiated
UV/O_3	O_3/H_2O_2
H_2O_2/UV	O_3/OH^-
Electron beam	H_2O_2/Fe^{2+} (Fenton)
$TiO_2/O_2/UV$	Electro-Fenton
$TiO_2/ H_2O_2/UV$	Ultrasound
Photo-Fenton	Wet air oxidation

Irradiated AOPs involve photochemistry concepts, which is a branch within the field of chemistry that studies the chemical and physical phenomena that may occur as a result of the interaction of chemical compounds with UV-visible radiation. This field of chemistry involves the interaction between photons and molecules, particularly, the mechanistic

interpretations of photoproducts formation, as well as their characterization and identification (OPPENLÄNDER, 2003).

Photochemical degradation may take place by direct or indirect photolysis. In experiments conducted by direct photolysis, the organic compounds may be degraded by absorbing UV-visible radiation. This degradation occurs by the interaction of compounds with photons, leading to electronic excitation and cleavage of molecule bonds (PARSONS, 2015; DOMÈNECH *et al.*, 2001). In this regard, degradation must be performed at the appropriate wavelength to reach the maximum efficiency. Parsons (2005) described the most common photochemical reactions occurring by homolytic cleavage (Equations 3.1 to 3.6).

$$AB + h\nu \rightarrow AB^* \quad (3.1)$$

$$AB^* \rightarrow (A^\bullet \dots B^\bullet)_{cage} \rightarrow A^\bullet + B^\bullet \quad (3.2)$$

$$(A^\bullet \dots B^\bullet)_{cage} \rightarrow AB \quad (3.3)$$

$$AB^* \rightarrow (A^+ \dots B^-)_{cage} \rightarrow A^+ + B^- \quad (3.4)$$

$$AB^* + O_2^3 \rightarrow AB^{\bullet +} + O_2^{\bullet -} \quad (3.5)$$

$$AB^* + O_2^3 \rightarrow AB + O_2^1 \quad (3.6)$$

UV absorption by a molecule is given by Equation 3.1, which results in compound excitation (highly energetic). The homolytic cleavage given by Equation 3.2 is the predominant step of these reactions, in which the radicals escape from the solvent cage and may undergo oxidation/reduction reactions. According to Equation 3.3, the recombination of primary radicals has a high possibility of taking place in the reaction medium, which explains the low quantum yield observed in some cases. In Equation 3.4, solvents with polar molecules, such as water, promote heterolytic scission (NICK *et al.*, 1992). Also, electrons and energy may be transferred to dissolved oxygen molecules, even though a lengthy lifetime of the excited state is necessary, as the triplet state. In this situation, many reactive oxygen species (ROS) are produced, such as the superoxide anion radical (Equation 3.5) and singlet oxygen (Equation 3.6) (PARSONS, 2005). As a result, dissolved oxygen plays an important role in the oxidative degradation of pollutants and affects the reaction rates, the intermediate products formed and the mineralization of the target compound (PARSONS, 2005).

An equally significant aspect of photolysis is the indirect degradation pathway. This process uses oxidants as initiators of the photochemical reactions or via light absorption by

natural substances, such as chromophoric dissolved organic matter (ZEPP and CLINE, 1976). As a consequence, this absorption may lead to the production of reactive oxygen species, such as $HO^{\bullet}$ and $^1O_2$, which react with organic contaminants by a series of oxidation reactions, usually generating CO_2 and water.

Among the photochemical processes, H_2O_2/UV has been found to be very effective in degrading organic micro-pollutants in many different matrices (IJPELAAR *et al.*, 2010; MAJCEN-LE MARECHAL *et al.*, 1997; DE LAAT *et al.*, 1999; RUPPERT *et al.*, 1994. The advantages of such system are the high reaction rates and the possibility to employ small, modular reactors. Figure 3.4 shows the four main oxidation mechanisms for the H_2O_2/UV process.

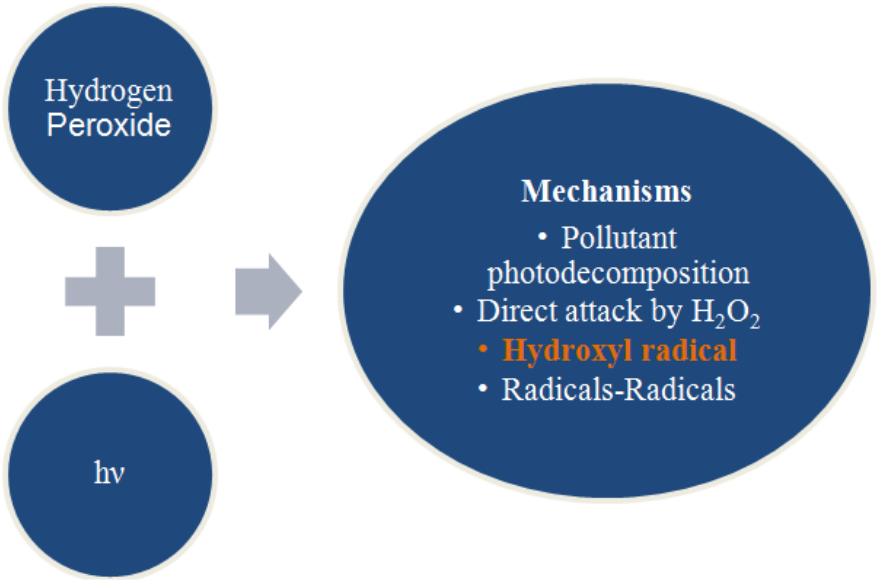

Figure 3.4 – Scheme of the main phenomena responsible for pollutant degradation by the H_2O_2/UV process.

BPA degradation has been extensively studied by the scientific community because of its potential impact on human health (DIAMANTI-KANDARAKIS *et al.*, 2009). As a consequence, many studies have been carried out on BPA degradation by AOPs in different conditions, matrices, processes and their combinations. For the sake of illustration, a few examples are given in the sequence.

MOHAPATRA *et al.* (2011) compared BPA degradation in wastewater sludge, as well as sludge solubilization by applying different pre-treatment methods, namely ultrasonication, Fenton's oxidation, and ferro-sonication. The investigations revealed that ferro-sonication led to improved sludge solubilization and the highest BPA degradation removal, 82.7%. This study demonstrated the effectiveness of the AOP even in solid matrices.

KATSUMATRA *et al.* (2004) studied BPA degradation in water by the photo-Fenton reaction. The authors confirmed the well-known influence of pH in this process. The optimum conditions resulted in complete degradation of 10 mg L^{-1} BPA after 9 min. BPA mineralization was observed by the formation of CO_2 using a TOC analyzer. CO_2 concentration was below the detection limit after 9 min, indicating that stable organic intermediate products were formed during the reaction. After 24 hours, only 54% BPA mineralization was observed, indicating that the products formed under these conditions and process are significant more persistent than BPA itself.

TAO *et al.* (2011) employed TiO_2-loaded MCM-41 catalyst under UV irradiation to degrade BPA. They observed the formation of 4-(1-hydroxy-1-methyl-ethyl)-phenol (HMEP) and phenol from the cleavage of phenyl groups, following HO• radicals attack. Furthermore, they observed the production of 4-hydroxyacetophenone and 2-methyl-2,3-dihydrobenzofuran. The mineralization into CO_2 and H_2O was achieved after further oxidation of the transformation products.

UMAR *et al.* (2013) reviewed BPA degradation by ozone in water and wastewater. They concluded that this process has a great potential for industrial scale application. Furthermore, they noticed that many by-products are formed, depending on process conditions.

3.5.1 BPA DEGRADATION BY THE H_2O_2/UV PROCESS

Only a few studies have been conducted regarding BPA degradation by the sole H_2O_2/UV process, which are summarized in Table 3.4.

Table 3.4 – Literature review for the oxidation of BPA by the H_2O_2/UV process.

Article	Compounds	Process	Quantification method	Equipment used for the H_2O_2/UV process	H_2O_2 concentration(mg L^{-1})	Fluence (UV*)**	BPA degradation	TOC removal
ROSENFELDT and LINDEN (2004)	BPA (0.233 µmol L^{-1}); ethinylestradiol; estradiol	UV and H_2O_2/UV	HPLC* ; TOC*	4 monochromatic 15-W low pressure lamps and a 1-kW medium-pressure lamp	15 and 24	1000 mJ cm^{-2}	5 and 15% (photolysis, LP and MP, respectively); 90% (H_2O_2/UV for both lamps)	Up to 65% (H_2O_2/UV)
CHEN *et al.* (2006)	BPA (60 µmol L^{-1} or 13.7 mg L^{-1})	UV and H_2O_2/UV	HPLC; YES*; VTG*	4 monochromatic 15-W low pressure Hg lamps	10, 25 and 50	100 to 5000 mJ cm^{-2}	Irrelevant degradation rates (photolysis); 99% (H_2O_2/UV)	-
CHEN *et al.* (2007)	BPA (60 µmol L^{-1} or 13.7 mg L^{-1})	UV and H_2O_2/UV	HPLC; YES; VTG	4 monochromatic 15-W low pressure Hg lamps	10, 25 and 50	100 to 5000 mJ cm^{-2}	Lower than 20% (photolysis); 97% (H_2O_2/UV)	-
FELIS *et al.* (2010)	BPA (10 mg L^{-1})	UV and H_2O_2/UV	HPLC; TOC	200-W medium pressure mercury lamp	10, 100 and 1000	754.78 W m^{-3}	About 97% (photolysis); below the limit of quantification (H_2O_2/UV)	Lower than 20% (photolysis); up to 42% (H_2O_2/UV; lower than 20% (H_2O_2//UV/HCO_3^-)
PARK *et al.* (2014)	BPA (9,14 mg L^{-1})	UV, H_2O_2/UV and Ozone/H_2O_2	HPLC	65 W, UV lamp	150 and 300	20 mW cm^{-2}	42,8% (photolysis and nitrate); 29,6% (photolysis)	-
ZHANG and LI (2014)	BPA (0.07, 0.13 and 0.26 mg g^{-1} dry weight); estrone; 17β-estradiol; estriol; 17α-ethinylestradiol; 4-nonylphenols	UV, H_2O_2/UV, photo-Fenton like	SPE*/HPLC; luminescence spectrometry; ICP*; DOC*	75-W low pressure Hg lamp	1700 to 68000	0.069 mW cm^{-2}	30 to 50 % (photolysis); up to 99% (H_2O_2/UV); up to 90% (H_2O_2/Fe^{2+}/UV)	-
OLMEZ-HANCI *et al.* (2014)	BPA (20 mg L^{-1} or 88 µmol L^{-1})	UV, H_2O_2/UV and UV/$S_2O_8^{2-}$	HPLC; *Vibrio fischeri* bioassay; YES; LC-MS*; TOC	6 UV-C lamps (8 W each)	85	21 W h L^{-1}	52% (photolysis); complete degradation (H_2O_2/UV and UV/$S_2O_8^{2-}$)	Not significant (photolysis); 70% (H_2O_2/UV and UV/$S_2O_8^{2-}$)
SHARMA *et al.* (2015; 2016)	BPA (0.22 mmol L^{-1}) and BPA (0.04-0.31 mmol L^{-1})	H_2O_2/UV and UV/$S_2O_8^{2-}$ (SPS)	HPLC; TOC	UV low pressure mercury lamps (total 40 W)	0.05 to 0.5	1.26×10^{-6} E s^{-1}	85% (H_2O_2/UV); up to 95% ($S_2O_8^{2-}$/UV)	55% (SPS/UV); 38% (H_2O_2/UV)
JAMIL *et al.* (2017)	BPA (0.175 mmol L^{-1}); paracetamol; DBP	UV, H_2O_2/UV, Fenton and photo-Fenton	HPLC	UV medium pressure mercury lamp (150 W)	0.17 to 1.02	1.32×10^{-5} E s^{-1}	100% (all processes)	80% (H_2O_2/UV); 90% (photo-Fenton)

*HPLC: High Performance Liquid Chromatography; TOC: Total Organic Carbon; YES: Yeast Estrogen Screen; VTG: Vitellogenin; SPE/HPLC: Solid Phase Extraction; ICP: Inductively Coupled Plasma; LC-MS: Liquid Chromatography-Mass Spectrometry; UV: Ultraviolet. DOC: Dissolved Organic Carbon; SPS: Sodium persulfate. **The data are given by using the original units from each article. Their transformation to the same unit was not possible, since some necessary data to perform conversions are missing.

ROSENFELDT and LINDEN (2004) compared the efficiency of BPA degradation by photolysis (UV-C) and by the combination H_2O_2/UV. The results showed that the polychromatic UV medium-pressure (MP) lamp was slightly more effective than the conventional UV low-pressure (LP) lamp. Furthermore, the combination H_2O_2/UV was much more effective when compared to direct UV photolysis. The photolysis resulted in BPA removals of approximately 5 and 15% for LP and MP lamps, respectively. In turn, the H_2O_2/UV process resulted in BPA removals of about 90% for both lamps. A model for the H_2O_2/UV process was developed and used by the authors to predict the degradation of some EDCs in different conditions.

CHEN *et al.* (2006) evaluated the use of direct photolysis with LP-UV lamps and the combination H_2O_2/UV. The authors showed that photolysis is not efficient to degrade BPA (irrelevant degradation rates). On the other hand, the H_2O_2/UV achieved the reduction in BPA concentration and estrogenic activity for both *in vitro* and *in vivo*. In vitro yeast estrogen screen (YES) and in vivo vitellogenin (VTG) resulted in EC_{50} values of 7.23 μmol L^{-1} and 14.7 μmol L^{-1}, respectively. The most efficient conditions were 5000 mJ cm^{-2} (UV fluence) and 50 mg L^{-1} H_2O_2, resulting in BPA and estrogenic activity removals higher than 99%.

CHEN *et al.* (2007) studied BPA photolysis by LP and MP lamps. LP-UV data were from CHEN *et al.* (2006). The study indicated that the MP-UV driven process was more efficient. The parameters evaluated were BPA concentration and estrogenic activity. The process efficiency was found to be similar regardless of the lamps for the H_2O_2/UV process. The most efficient result was achieved with 25 mg L^{-1} of H_2O_2 and fluence of 5000 mJ cm^{-2}, which resulted in BPA and estrogenic activity removals higher than 97%. According to the authors, the necessary fluence to achieve this result was even lower for 50 mg L^{-1} H_2O_2. It is worth mentioning that the photolysis experiments and UV+10 mg L^{-1} of H_2O_2 promoted a lower removal of estrogenic activity in comparison with BPA degradation. This result may suggest the formation of estrogenic degradation products and/or a synergistic response of these products with the remaining BPA. The results of CHEN *et al.* (2006) indicated that the degradation process did not result in the production of acutely toxic intermediates. However, in 2007, the authors observed a production of acidic intermediates in the process, which increased acute toxicity.

FELIS *et al.* (2010) investigated BPA degradation by means of sole UV-radiation and the H_2O_2/UV process in the absence or the presence of bicarbonate ions (HCO_3^-). Initial BPA concentration was 10 mg L^{-1}. They employed a medium-pressure Hg lamp (255 to 579 nm)

and a nominal power of 400W. HCO_3^- ions concentration was 100 mg L^{-1}. BPA degradation by direct photolysis was about 97% after 30 minutes. For the combination H_2O_2/UV, BPA concentration was below the limit of quantification after 15 minutes for all initial H_2O_2 concentrations: 10-1000 mg L^{-1}.

PARK *et al.* (2013) studied the effect of nitrate on BPA degradation by three different processes: UV, H_2O_2/UV, and H_2O_2/ozone. They observed that in the absence of H_2O_2, the use of nitrate improved BPA degradation as a result of the hydroxyl radicals produced from nitrate photolysis. This combination of photolysis with nitrate resulted in 42.8% BPA removal after 30 minutes. On the contrary, in the absence of nitrate the authors achieved 29.6% BPA degradation for the same reaction time. However, in the presence of H_2O_2, nitrate hindered BPA removal, acting as a radical scavenger.

ZHANG and LI (2014) also evaluated UV irradiation and the combination H_2O_2/UV in the degradation of BPA, estrone, 17β-estradiol, estriol, 17α-ethinylestradiol, and 4-nonylphenols. They spiked 11 different metal ions in the solutions, which varied from 0.05 to 5 mmol L^{-1}. The H_2O_2/UV process showed better results than UV alone. As indicated by the authors, the BPA percent removals at pH values of 3, 5 and 7 were 89, 84 and 74%, respectively, after 2 minutes under the H_2O_2/UV process. They also observed a positive impact of metal ions on the degradation of the target EDCs during the H_2O_2/UV process, due to enhanced Fenton-type reactions. For instance, 5 mmol L^{-1} Fe^{2+} or Fe^{3+} concentration increased BPA removal efficiency from ~15% to 100%.

OLMEZ-HANCI *et al.* (2014) investigated BPA degradation and detoxification using direct photolysis, H_2O_2/UV, and $S_2O_8^{2-}$/UV. BPA concentration was 20 mg L^{-1}. The oxidant doses were 2.5 mmol L^{-1}. They employed six lamps of 8 W each, with maximum emission band of the UV-C lamps at 253.7 nm. The UV-C light fluence was 2.27 W L^{-1}. Under direct photolysis, the degradation achieved was 52% after 120 min of irradiation. For the H_2O_2/UV process, complete BPA degradation was observed in less than 10 min. TOC was 40% removed after 120 min. The YES test indicated a rapid decline in estrogenic activity in the first 5 min of treatment and kept decreasing during TOC removal. A closer look at the data indicates that the UVC-driven treatment signalled more toxic by-products and with higher estrogenic activities than the original compound. In addition, the authors admit the possibility of complete mineralization under direct photolysis. However, this process requires a considerable length of time, energy, and also a higher possibility of toxic intermediates being formed.

SHARMA *et al.* (2015) also conducted experiments aiming at the degradation of BPA using the H_2O_2/UV or $S_2O_8^{2-}$/UV. For the H_2O_2/UV process, BPA removal reached 85% at the optimum conditions the authors considered. A low-pressure 40-W lamp emitting at 254 nm was used. The best H_2O_2 concentration was found to be 11.76 mmol L^{-1}. It is worth mentioning that oxidant concentrations at the higher levels showed an adverse effect, because of the quenching of hydroxyl radicals by H_2O_2 molecules.

In a subsequent study, SHARMA *et al*. (2016) showed a mechanistic study of BPA photo-oxidation employing the two different oxidants, H_2O_2 and sodium persulfate (SPS), irradiated at 254 nm using a 40-W lamp. BPA concentrations varied from 0.04 mmol L^{-1} (~10 mg L^{-1}) to 0.31 mmol L^{-1} (~70 mg L^{-1}). The irradiation time was 360 min. The best BPA removal (95.4%) for the H_2O_2/UV process was achieved for the inferior initial BPA concentration. On the other hand, the superior initial BPA concentration resulted in the lowest removal, with only 56. 8%. The evaluation of the TOC removal was undertaken only for the BPA concentration of 0.22 mmol L^{-1} (50 mg L^{-1}) and H_2O_2 concentration of 11.8 mmol L^{-1}. TOC removal was found to be 38.3% for the H_2O_2/UV system.

JAMIL *et al*. (2017) investigated the following homogeneous processes for degrading paracetamol, bisphenol A, and dibutyl phthalate: UV, H_2O_2/UV, Fenton (H_2O_2/Fe(II)), and photo-Fenton (H_2O_2/Fe(II)/UV) in water. Among them, the H_2O_2/UV system was found to be the second most efficient in removing TOC. Both processes were investigated at pH 3 and 60 minutes of irradiation. The H_2O_2/UV process achieved 80% TOC removal using H_2O_2 at 25 mmol L^{-1}. On the other hand, 90% TOC removal was attained using the photo-Fenton reaction with H_2O_2 and Fe(II) concentrations of 5 and 3.6 mmol L^{-1}, respectively.

Recent developments in BPA degradation by the H_2O_2/UV process allowed to conclude that the process is efficient to degrade the target compound and may lead to the formation of less toxic, non-endocrine disrupting intermediates. However, there is not a systematic evaluation of process parameters, such as the oxidant concentration and photon emissions rates from the same type of irradiation source. Usually, the comparison is made using different types of sources, such as low and medium pressure Hg lamps.

3.5.2 H_2O_2/UV REACTIONS

CRITTENDEN *et al.* (1999) listed 44 elementary reactions in the H_2O_2/UV process, obtained from independent published research. Since there are so many reactions involved, it

is usual to choose the most important reactions for the proposed mechanism. EDALATMANESH *et al.* (2008) listed 15 reactions to propose a kinetic model for phenol degradation under the H_2O_2/UV process. Some reactions are catalogued in Table 3.5.

Table 3.5 – Reactions of the H_2O_2/UV process. Modified from EDALATMANESH *et al.* (2008) and CRITTENDEN *et al.* (1999). *References: [a] target compound; [b] depends on the target organic compound.

Reaction number	Reaction	k
R1	$H_2O_2 \xrightarrow{\Phi_{H_2O_2}} 2HO^{\bullet}$	r_{uv,H_2O_2}
R2	$H_2O_2 + HO^{\bullet} \xrightarrow{k_{II}} H_2O + HO_2^{\bullet}$	$k_{II} = 2.7 \times 10^7 L\, mol^{-1}s^{-1}$
R3	$HO_2^- + HO^{\bullet} \xrightarrow{k_{III}} OH^- + HO_2^{\bullet}$	$k_{III} = 7.5 \times 10^9\ L\, mol^{-1}s^{-1}$
R4	$H_2O_2 + HO_2^{\bullet} \xrightarrow{k_{IV}} HO^{\bullet} + H_2O + O_2$	$k_{IV} = 3\ L\, mol^{-1}s^{-1}$
R5	$H_2O_2 + O_2^- \xrightarrow{k_V} HO^{\bullet} + OH^- + O_2$	$k_V = 0.13\ L\, mol^{-1}s^{-1}$
R6	$O_2^{\bullet -} + H^+ \xrightarrow{k_{VI}} HO_2^{\bullet}$	$k_{VI} = 1 \times 10^{10} L\, mol^{-1}s^{-1}$
R7	$HO_2^{\bullet} \xrightarrow{k_{VII}} O_2^{\bullet -} + H^+$	$k_{VII} = 1.58 \times 10^5 s^{-1}$
R8	$HO^{\bullet} + HO^{\bullet} \xrightarrow{k_{VIII}} H_2O_2$	$k_{VIII} = 5.5 \times 10^9 L\, mol^{-1}s^{-1}$
R9	$HO^{\bullet} + HO_2^{\bullet} \xrightarrow{k_{IX}} O_2 + H_2O$	$k_{IX} = 6.6 \times 10^9 L\, mol^{-1}s^{-1}$
R10	$HO_2^{\bullet} + HO_2^{\bullet} \xrightarrow{k_X} H_2O_2 + O_2$	$k_X = 8.3 \times 10^5 L\, mol^{-1}s^{-1}$
R11	$HO_2^{\bullet} + O_2^{\bullet -} \xrightarrow{k_{XI}} HO_2^- + O_2$	$k_{XI} = 9.7 \times 10^7 L\, mol^{-1}s^{-1}$
R12	$HO^{\bullet} + O_2^{\bullet -} \xrightarrow{k_{XII}} O_2 + OH^-$	$k_{XII} = 7 \times 10^9 L\, mol^{-1}s^{-1}$
R13	${R_1}^a + HO^{\bullet} \xrightarrow{k_{XIII}} intermediates \rightarrow CO_2 + H_2O$	k_{XIII}^b
R14	${R_1}^a \xrightarrow{\Phi_{R_1^a}} intermediates \rightarrow CO_2 + H_2O$	r_{uv,R_1^a}

The radical chain reactions are divided into (1) initiation: primary photolysis of H_2O_2 (R1); (2) propagation: (R2 to R4); (3) termination: (R8, R9 and R10); (4) degradation of the target compound: (R13 and R14). The oxidizing capability of hydroxyl radicals is much higher in comparison with other radical species. The rates of photolysis of H_2O_2 and the target compound (r_{UV,H_2O_2} and $r_{UV,BPA}$, respectively), appear in steps R1 and R14, and depend on two parameters, which are the molar absorption coefficient (ε_i) and the photolysis quantum yield (ϕ_i) (i species or oxidant). The molar (decadic) absorption coefficient indicates quantitatively how chemical species interact with light. This value is substrate specific and

wavelength dependent (OPPENLANDER, 2003), with $\varepsilon_{H_2O_2}$ = 19 L mol^{-1} cm^{-1} and ε_{BPA} = 840 L mol^{-1} cm^{-1}, both at 254 nm (OPPENLANDER, 2003; GOULART DE ARAUJO *et al.*, 2017)

The quantum yield is explained in the next section. More details about the reactions will be given in Section 8.

3.5.3 PHOTOLYSIS QUANTUM YIELD

The photolysis quantum yield is defined in photochemistry as a measure of the global efficiency of this process (BRAUN *et al.*, 1991). This parameter is of interest when related to H_2O_2 photochemistry. In theory, 1 mol of H_2O_2 should generate 2 moles of $HO^{\bullet}$ (R1, Table 3.5). Nonetheless, experimental values may change depending on the experimental situation (OPPENLÄNDER, 2003). For instance, in gas phase photolysis it is shown that other photophysical and/or photochemical reaction channels occur, producing less than 2 moles of $HO^{\bullet}$ for each mol of hydrogen peroxide. In the liquid phase, this situation is more critical, with the "cage effect" lowering the quantum yield of H_2O_2 photolysis to only 0.5. Furthermore, hydroxyl radicals within the aqueous cage rapidly recombine to regenerate hydrogen peroxide. Table 3.6 shows different quantum yields depending on the irradiation wavelength as well as the phase.

Table 3.6 – Quantum yields of H_2O_2 photolysis. Source: Adapted from OPPENLÄNDER (2003).

Oxidant	**Product**	**Irradiation wavelength λ nm^{-1}, phase**	**Quantum yield**
H_2O_2	$HO^{\bullet}$	200-354, gas phase	$\phi(-H_2O_2) = 1.0$
		254, in water	$\phi(-H_2O_2) = 0.5$
		313, in water	$\phi(-H_2O_2) = 0.30$
		254, in water	$\phi(+HO^{\bullet}) = 0.98$
		193, gas phase	$\phi(+HO^{\bullet}) = 1.22$
		248, gas phase	$\phi(+HO^{\bullet}) = 1.58$

3.6 Kinetic and photoreactor modelling

According to EDALATMANESH *et al.* (2007), the study of kinetic models for advanced oxidation processes is an important step to evaluate operation variables. Modelling promotes a better understanding of the system, enabling its optimization as well as the determination of the most relevant parameters for process design. However, oxidation experiments conducted in different reactors revealed large discrepancies regarding reaction kinetics (ZHANG *et al*., 2007, NAKASHIMA *et al*., 2003). In the case of studies using estrogens, for example, and as reported by LI-PUMA *et al.* (2010), the main reason for these differences is that the degradation rate constants were not set apart from the local volumetric rates of photon absorption (LVRPA, e^a) that took place for each reactor configuration. Consequently, the comparison between different research results may be a difficult task and even lead to inaccurate conclusions, limiting a potential scale-up of the oxidation system. Moreover, according to MOHAJERANI *et al*. (2012), the radiation field, in photochemical processes, is considered the main characteristic of the kinetics and photoreactors design. They also underline that the photochemical reaction rate is proportional to the local volumetric rate of energy absorption (LVREA), which is the same as LVRPA.

Similarly to conventional reactors, the analysis and modelling of photoreactors are based on fundamental principles related to thermodynamics and transport phenomena (moment, mass, and energy) (ALFANO *et al*., 1986). The study of photoreactors needs to take into consideration both non photo-activated and photo-activated steps to properly determine the reaction rates. As a result, the methodology must include dark steps (conventional reactors) and irradiated steps (photochemical reactions). For the latter, the LVRPA must be considered, since the reaction rate of photo-active steps depends essentially on the rate photons are absorbed within the reacting volume. This rate is based on the spatial distribution of radiant energy within the reaction space of the reactor, which relies on the geometrical characteristics of the photoreactor system; physical and chemical parameters; and on the concentration of the species capable of absorbing light. Figure 3.5 illustrates how these steps are connected in order to obtain a numerical solution.

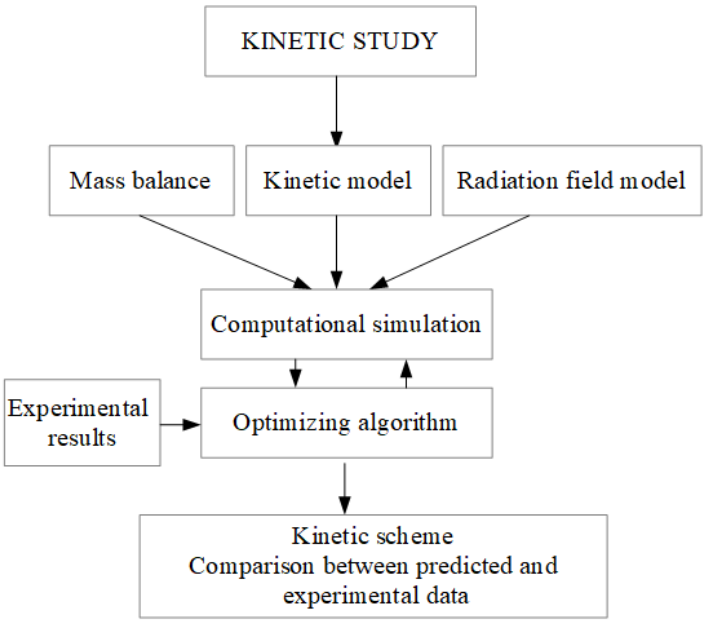

Figure 3.5 – Schematic diagram of the kinetic modelling strategy.
Source: Modified from IMOBERDORF *et al*. (2007)

There are two main explanations for non-uniformity in radiation field regarding homogeneous photo-reactors: the attenuation of radiation by energy absorption of photo-activated species (reagents and/or products) and the physical and geometric characteristics of the system (radiation source/reactor). The light attenuation caused by the absorbing species makes the LVRPA non-uniform.

The assessment of the LVRPA begins with a radiant energy balance at steady state condition in a homogeneous system. Furthermore, a radiation source model is required. A radiation source model can be obtained by the use of incidence models (GAERTNER and KENT, 1958) or by the application of emission models (HARRIS and DRANOFF, 1965):

i. *Incidence model*: a mathematical model that assumes a distribution of a given radiation in the vicinity of the reactor. The radiant energy on the reactor wall must be measured experimentally. It considers the energy in normal planes in the axis of the reactor and does not identify the dependency in regards to the axis coordinate;
ii. *Emission model*: This model proposes lamp emission fields. The incidence radiation fields are later obtained, such as the incidence algorithm. This algorithm provides the boundary condition for the radiant energy inside the reactor.

GARTER and KENT (1958) were one of the first to model photochemical reactions. They studied the photolysis of aqueous uranyl oxalate. The experiments were performed in an annular tubular reactor. The results demonstrated outstanding accuracy by assuming that the photolysis rate was proportional to the residence time multiplied by the irradiance in a chosen radial position. Reactant concentrations were not contemplated in their mathematical model. According to MOHAJERANI *et al*. (2012), GARTER and KENT's model could be applicable only for low conversions (<12%). Moreover, this model cannot be used without empirically adjusted parameters, which is a serious drawback for design purposes (ALFANO *et al.*, 1986).

Due to limitations of the incident models, an emission model will be applied in this work in order to incorporate the radiation field term into the kinetic model. The main emission models are the line source with parallel plane emission (LSPP), the line source with spherical emission (LSSE), and the extense source with volumetric emission (ESVE) (BRAUN *et al.*, 1993).

The next section gives a brief overview of these emission models, pointing out their main advantages and disadvantages, besides the general mathematical expressions used to calculate the LVRPA. Note that this parameter is crucial to achieve a complete kinetic expression and the choice of the model relies on the AOP employed and the experimental geometry. The review paper by ALFANO *et al.* (1986) offers in detail an overview and a critical discussion on this subject. Thenceforth, no conceptually new contributions have been accomplished on the matter of radiation source emission modeling.

3.6.1 LSPP MODEL

LSSP is considered the simplest emission model and it is based on the following assumptions (HARRIS and DRANOFF, 1965; ALFANO *et al*., 1986):

1. The source is seen as a line, with uniform emission along the axial direction (length);
2. The emitted radiation is on perpendicular planes regarding the lamp axis.

Figure 3.6 illustrates the LSPP model, where a point $P(r, z)$ receives radiation on perpendicular planes from a source, here considered linear. The variable r is distance from the

lamp to a point $P(r,z)$; R_{ext} is the maximum distance between the middle of the lamp and the outermost point of the photoreactor; L is the lamp length.

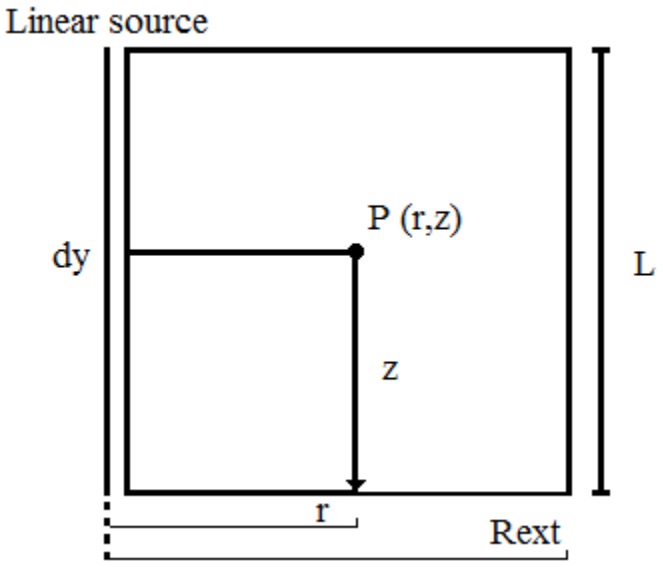

Figure 3.6 – LSPP model in perspective.

For this model, the LVRPA (e^a) is given by:

$$e^a = \kappa_i \frac{R_{in} q_i}{r} exp[-\kappa_i (r - R_{in})] \tag{3.17}$$

with

$$q_i = \frac{S_L}{2\pi R_{in}} = \frac{P}{L 2\pi R_{in}} \tag{3.18}$$

where κ_i is the volumetric absorption coefficient of reacting species (i), q_i is the radiant flux inmol cm^{-2} s^{-1} (Einstein cm^{-2} s^{-1}), S_L is the radiation energy in energy per unit time and unit length, and P is the photon flow in mol s^{-1} (Einstein s^{-1}). R_{in} is the radius of the irradiation source.

The simplicity of this model is considered attractive; however, this model does not predict experimental data within an acceptable error, except for a few cases (ROMERO *et al.* 1983). These few cases must present the following characteristics: (1) the lamp is situated very close to the reacting medium and (2) the ratio of the reactor length and its diameter must

be large. In our case, both characteristics are presented. For that reason, the LSPP model is considered adequate for our system.

3.6.2 LSSE MODEL

The lamp is viewed as a line source and each of its points emits radiation in every direction and isotropically, using three dimensions to describe the emission process (JACOB and DRANOFF, 1966). Furthermore, the source has a finite number of segments. Those contributions are added up to estimate the radiant energy distribution within the reactor (ALFANO *et al*., 1985).Figure 3.7 shows the geometry used for the LSSE model, where ρ is the distance between a point $A(r,z)$ to any point of the middle of the lamp (r = 0).

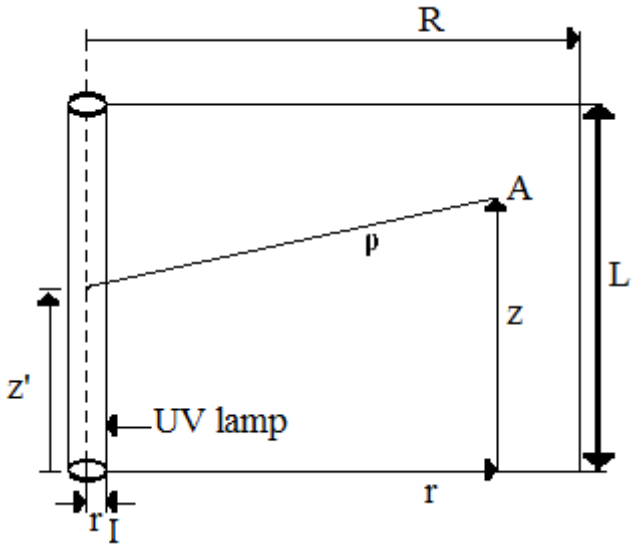

Figure 3.7 − LSSE model in perspective.

The value of e^a is given by (CERDA, 1978):

$$e^a = \frac{S_L \kappa}{4\pi r} \int_{\theta_1}^{\theta_2} exp\left\{-\kappa\left[\frac{(r - r_{LP}}{cos\theta}\right]\right\} d\theta \qquad (3.19)$$

where r_{LP} is the lamp radius and θ is the angle formed between discretized points and the irradiation source. More details about these angles will be given on Section 5.

According to ALFANO *et al.* (1986), line source models indicated satisfactorily good results under various experimental configurations with the use of annular reactors. Note that line source models are not suitable in the case of any kind of curved reflecting surface, a situation where the consideration of the lamp as a line source would be unrealistic.

3.6.3 ESVE MODEL

This model assumes that the radiant energy source has finite spatial dimensions. IRAZOQUI *et al.* (1973) considered the lamp as a perfect cylinder with null thickness. In other words, the volume is the own irradiation source. The lamp shows constant emission in the direction *z*. The term e^a is then given by (CASSANO *et al.* 1995):

$$e_v^a(x,t) = \frac{\kappa_v(x,t)P_{v,s}}{2\pi^2 R_L L_L}\int_{\varphi} d\varphi \int_{\theta(\varphi)} d\varphi\, d\theta sin\theta exp\left\{-\int_{\bar{s}=S_r}^{\bar{s}=s(x,\theta,\varphi)} \kappa_v(\bar{s},t)d\bar{s}\right\} \qquad (3.20)$$

It is worth mentioning that Equations 3.17-3.21 are the general forms used for each model. Since e^a is an irreducible function of position, the average value for the LVRPA ($\langle e^a \rangle$) is the value that will be included in the kinetic expression, and it depends on the system geometry. More details of the calculations for the LSPP model will be given in a later section as regards our experimental setup.

As discussed earlier, no conceptually new contributions have been made since the work published by ALFANO *et al.* (1986), and the present work is not intended to bring innovations in this direction. However, many works have been developed using these concepts. As there are many articles in which LVRPA has been added to the kinetic model, we are not going to review each of them but the most used in the development of the present work.

Studies demonstrated that under restricted optical and geometrical parameters, the variations in the radial and angular coordinates did not result in significant changes regarding the LVRPA (ALFANO *et al.*, 1985; ALFANO *et al.*, 1986a, ALFANO *et al.*, 1986b). ALFANO *et al.* (2001) presented a kinetic model to predict the degradation of 2,4-D and its transformation products under the H_2O_2/UV process. The experimental work was carried out in batch in a well-stirred tank irradiated underneath by a tubular lamp. They employed a one-dimensional model (LSPP) to describe the monochromatic LVRPA spatial distribution, since

in previous works they found that radial and angular variations were not very significant for their experimental apparatus (ALFANO *et al.*, 1985; ALFANO *et al.*, 1986; ALFANO *et al.*, 1986).

ROSSETTI *et al.* (2002) evaluated the decomposition of formic acid in water by the photo-Fenton reaction. A kinetic model was developed to predict the decomposition rates of formic acid and H_2O_2. The experimental study was performed in a flat-plate, well-stirred reactor located inside a batch recycling system. Both sides of the reactor were irradiated by two tubular lamps. The kinetic model selected was the same used by ALFANO *et al.* (2001). The kinetic model represented well the evolution of formic acid and hydrogen peroxide concentrations in a wide range of their initial molar concentrations. Furthermore, a deviation smaller than 9% between predicted and experimental data was achieved.

CONTE *et al.* (2012) also developed a kinetic model to predict the evolution of reactant concentrations in the photo-Fenton process. At first, they employed a well-stirred tank laboratory reactor, and then a pilot-plant solar reactor, created to capture UV, visible, and IR solar radiation. The pilot-plant photoreactor was able to achieve complete degradation of the target compounds after 60 min of treatment. In addition, a high mineralization was achieved after a longer period of treatment, 210 min. The computed values agreed with the experimental data, satisfactorily representing the process as well as the reactor.

BENZAQUÉN *et al.* (2012) studied absolute and apparent quantum efficiencies regarding atrazine degradation in water by the photo-Fenton process. They calculated the LVRPA and used it to evaluate the quantum efficiencies. LVRPA ($\langle e^a(x)_{V_R} \rangle$) ranged from 7.76×10^{10} to 15.8×10^{10} Einstein cm^{-3} s^{-1}. They noticed unequal increasing levels of LVRPA values compared to atrazine degradation rates. This behaviour indicated that the absolute quantum efficiency is more sensitive to the initial ferric iron concentrations than the apparent quantum efficiency.

BENZAQUÉN *et al.* (2015) proposed a kinetic model for atrazine degradation by the Fenton and photo-Fenton processes. From an accepted reaction mechanism, which included the LVRPA, they were able to reproduce the changes in ferric iron concentrations, hydrogen peroxide to atrazine molar ratios, and radiation level on the pollutant degradation rate.

3.7 Contributions of the Thesis

In sum, most studies reported in the literature focus on varying experimental conditions, such as different oxidant concentrations, pH, equipment, and so forth. Nevertheless, systematic investigations on the effects of process variables on BPA degradation, along with the statistical interpretation of the results are virtually inexistent in the literature. Moreover, as far as we know, a detailed kinetic model has not been proposed for BPA degradation by the H_2O_2/UV process. In this context, this Thesis has the following original contributions:

i. The influence of the process variables: initial H_2O_2 concentration ($[H_2O_2]_0$) and specific rate of photons emission ($E_{P,0}$) on BPA degradation by the H_2O_2/UV process is investigated, considering a detailed approach based on a Doehlert experimental design and response surface methodology;
ii. For the first time, a kinetic model is proposed for BPA degradation by the H_2O_2/UV process considering an expression for the radiation field, with kinetic constants estimated from experimental data. The results discussed here can be direct applied to scaling-up, since the obtained kinetic constants are independent of the reactor size, shape, and configuration.

4. MATERIALS AND METHODS

4.1 Chemicals

All the solutions were prepared using deionized water. Hydrogen peroxide 30% (Synth) and technical grade bisphenol A (Purity ≥ 99%, IUPAC: 2,2-bis(4-hydroxyphenyl) propane, 4,4'-isopropyl-idenediphenol, CAS number: 80-05-7) was supplied by Sigma-Aldrich. Aqueous solutions of H_2SO_4 1 mol L^{-1} (prepared with H_2SO_4 98% w/w, Vetec) or NaOH 1 mol L^{-1} (prepared with NaOH 97% w/w, Vetec) were used for pH correction. The reactants used for High Performance Liquid Chromatography (HPLC) analysis were acetonitrile (HPLC grade) and glacial acetic acid (100%), both HPLC grade and supplied by Merck.

4.2 Equipment and Procedures

4.2.1 DETERMINATION OF THE MOLAR ABSORPTION COEFFICIENT OF BPA ($\mathcal{E}$)

The UV-Vis absorption spectrum (200 to 300 nm) of BPA was measured with a UV-Vis spectrophotometer (Varian Cary 50), with a 1-cm path-length quartz cuvette. According to the Beer's Law, for dilute systems the graph of absorbance versus BPA concentration gives a straight line with slope equal to the molar absorption coefficient ε (L mol^{-1} cm^{-1}) at the given wavelength.

4.2.2 STUDY OF BPA PHOTO-DEGRADATION

H_2O_2/UV experiments were performed in a tubular photochemical reactor (Figure 4.1 and Figure 4.2), which consists of a borosilicate glass tube (lamp diameter, 0.025 m; inner diameter of the outer tube, 0.073 m; irradiated length, 1.027 m), equipped with a concentric low-pressure (LP) mercury vapour lamp (TUV Philips, 36 W), emitting UV radiation at 253.7 nm.

Figure 4.1 – Experimental apparatus.
Source: Leandro G. Araujo

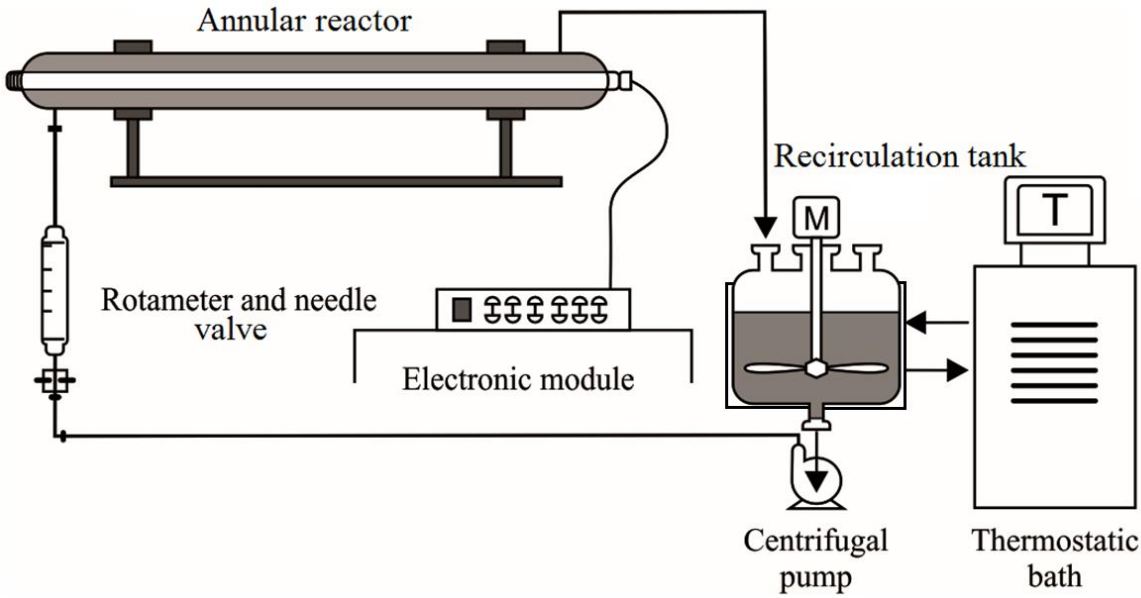

Figure 4.2 – Scheme of the experimental apparatus.
Source: ARAUJO *et al.* (2017)

According to the lamp supplier, the glass of this lamp filters out the 185-nm line. By homogeneously covering different fractions of the lamp surface with aluminum foils, acting as an opaque material (SILVA *et al.*, 2014), three different rates of photon emission on a per

unit reactor volume basis ($E_{P,0}$, photons L^{-1} s^{-1}) were experimentally obtained by ferrioxalate actinometry according to a procedure detailed elsewhere (BRAUN *et al.*, 1991). These values were 0.87×10^{18}, 1.41×10^{18}, and 3.6×10^{18} photons L^{-1} s^{-1} (SILVA *et al.*, 2014). For the kinetic study, the values of $E_{P,0}$ were converted to another unit, namely: 1.44×10^{-3}, 2.32×10^{-3}, and 5.98×10^{-3} Einstein m^{-3} s^{-1}. The radiation field inside the photochemical reactor was considered uniform in the axial direction, except for the radial coordinate. All the experiments were carried out in batch and the reactor was connected to a jacketed circulation vessel, from where the samples were withdrawn. The initial BPA concentration was 48.2 ± 0.9 mg L^{-1}. The initial concentrations of H_2O_2 were 1.6, 3.6, 5.6, 7.6, and 9.6 mmol L^{-1}. All the H_2O_2 solution was added at the beginning of the experiments and no further addition of oxidant was made. The temperature was kept at 25 ºC by means of a thermostatic bath and the total reaction time was 180 min. The initial pH was set at 7 at the beginning of the experiment, but uncontrolled over time. The solution was recirculated at a flow rate of 400 mL min^{-1}, and measured by a rotameter equipped with a needle valve. The total solution and the tubular reactor volume were 5.0 and 3.9 L, respectively. In the pH range of the experiments, BPA is protonated (*p*Ka BPA= 9.6) (ZENG *et al.*, 2006), and therefore no important influence of pH on our results was expected. Samples were withdrawn in times: 1, 2, 5, 10, 15, 30, 60, 75, 90, 105, 120, 135, 150, 165, and 180 min. A total of 20 mL was collected in each sampling. All the analyses were made immediately after sampling. The sampling protocol was the following:

Hydrolysis and photolysis experiments were performed in a previous work and are described elsewhere (GOULART DE ARAUJO *et al.*, 2017). The results confirmed that BPA hydrolysis over 24 hours was insignificant regardless of pH. BPA degradation due to direct photolysis at 254 nm was ~20% after 120 min of irradiation, under the following conditions: $[BPA]_0$ = 50 mg $L^{-1}$and $E_{P,0} = 1.41 \times 10^{18}$ photons L^{-1} s^{-1}.

4.2.3 EXPERIMENTAL DESIGN: DOEHLERT MATRIX

An experimental design was used to perform the H_2O_2/UV experiments, based on the Doehlert matrix (CAMPAÑA *et al.*, 1997) for two variables (initial H_2O_2 concentration, mmol L^{-1}, X_1; and specific rate of photons emission, $E_{P,0}$, X_2). The experimental runs were made in duplicate. Figure 4.3 and Table 4.1 detail these design points, and the values of $[H_2O_2]_0$ and $E_{P,0}$.

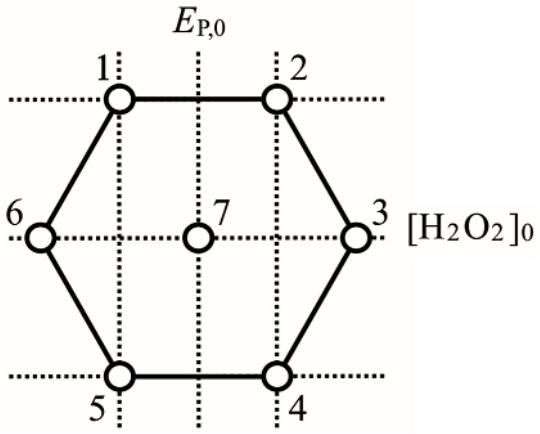

Figure 4.3 – Experimental design based on the Doehlert matrix for the H_2O_2/UV process.

Table 4.1 – Conditions of the H_2O_2/UV experiments.

Run	**X_1; X_2 (CODIFIED)**	**$[H_2O_2]_0$; $E_{P,0}$ (mmol L^{-1}; $\times 10^{18}$ photons L^{-1} s^{-1})**
1	–0.5; 0.866	3.6; 3.6
2	0.5; 0.866	7.6; 3.6
3	1.0; 0.0	9.6; 1.4
4	0.5; –0.866	7.6; 0.87
5	–0.5; –0.866	3.6; 0.87
6	–1.0; 0.0	1.6; 1.4
7	0.0; 0.0	5.6; 1.4

In short, seven experimental points were carried out for the system (k^2+ k +1, where k is the number of independent variables, two in this study), in duplicates (total of 14 experiments). The dependent variables (responses) were the apparent first-order BPA degradation rate constant (Y_1, min^{-1}), BPA degradation after 15 min (Y_2, %), and TOC removal after 120 min (Y_3, %). When necessary, the codified values corresponding to $[H_2O_2]_0$ were recalculated considering the actual measured values of this variable.

4.2.4 STATISTICAL ANALYSIS OF THE RESULTS

The effects of the variables involved in BPA degradation on each response were statistically assessed by means of response surface models (Equation 4.1), where X_i corresponds to the codified values of the independent variables, Y_i are the experimental responses, and a_0, a_i, a_{ii} and a_{ij}, are the model parameters. The analyses were performed using the software Statgraphics Plus v. 5.0.

$$Y_i = a_0 + a_1X_1 + a_2X_2 + a_{11}X_1^2 + a_{22}X_2^2 + a_{12}X_1X_2 \quad (4.1)$$

4.3 Analytical Techniques

4.3.1 HIGH-PERFORMANCE LIQUID CHROMATOGRAPHY

BPA analyses were performed employing an HPLC system (Shimadzu), equipped with a two-solvent delivery pump, a UV/Vis diode array detector (SPD 20A model), and a C18 column (Phenomenex, 250 mm×4.6 mm; 5 μm). The absorption wavelength, the oven temperature and the sample injection volume were 230 nm, 40 ºC, and 50 μL, respectively. The analyses were performed in isocratic mode. The eluents were (a) H_2O+0.2 % acetic acid and (b) acetonitrile at 50:50 ratio (v/v), at 1.0 mL min^{-1}. Under these conditions, the BPA retention time was 8 min. The detection and quantification limits were 0.41 and 1.26 mg L^{-1}, respectively.

4.3.2 TOTAL ORGANIC CARBON (TOC)

TOC analysis was performed in a Shimadzu equipment (TOC-5000A model). TOC was measured indirectly by the difference between total organic (TC) and inorganic carbon (IC).

4.3.3 HYDROGEN PEROXIDE DETERMINATION

H_2O_2 concentration was measured by the method described by Nogueira *et al.* (2004). Ammonium metavanadate was used in acidic medium, which resulted in the formation of a red-orange colour peroxovanadium cation, with a maximum absorbance at 450 nm, which was measured using a Varian Cary 50 UV-Vis spectrophotometer equipped with a 1-cm path length quartz cuvette. The concentration of H_2O_2 during the experiments was obtained by using the Beer-Lambert law (Equation 4.2) (OPPENLÄNDER, 2003):

$$A_{10} = \varepsilon \times c \times l \quad (4.2)$$

where,

A_{10}: Decadic absorbance of a beam of collimated monochromatic radiation in a homogeneous isotropic medium (VERHOEVEN, 1996 *apud* OPPENLÄNDER, 2003);
ε: molar (decadic) absorption coefficient in L mol^{-1} cm^{-1};
c: substrate concentration in mol L^{-1};
l: path length of irradiation in cm.

5. KINETIC MODELLING

This chapter is organized into three sections. The first describes the reaction mechanism. The main reactions involved in the H_2O_2/UV process are listed as well as the expressions and total rates obtained from these reactions. The second part deals with material balances, in which an expression related to our experimental system is presented. The third and last part of this chapter examines photo-reactor modelling for a homogeneous system. The main equations regarding this subject will be discussed. More information about the LSPP model will be also presented.

5.1 Reaction mechanisms and rate equations

As mentioned in the literature review, kinetic modelling is an essential tool for employing AOP in large scales. However, the development of a mathematical model for an AOP is considered arduous, due to the extensive number of reactions involved in those processes. Because of that, the assumption of pseudo-steady-state is very usual for the simulation of radical species concentrations, such as hydroxyl, peroxyl, and oxyl radicals (KANG *et al.*, 2002, ANDREOZZI *et al.*, 2000, ALNAIZY and AKGERMAN, 2000).

The proposed kinetic model for the BPA degradation under H_2O_2/UV is based on the reaction sequence proposed by HUANG and SHU (1995). The main interactions between H_2O_2 with UV radiation and free radicals are described by reactions (1)–(6) in Table 5.1, whereas reactions (7) and (8) represent the decomposition of any of the reacting organic compounds presented in the system.

Table 5.1 – Reaction scheme for BPA degradation under the H_2O_2/UV process.

Step	Reaction	nº
Initiation	$H_2O_2 \xrightarrow{\Phi_{H_2O_2}} 2HO^{\bullet}$	(1)
Propagation	$H_2O_2 + HO^{\bullet} \xrightarrow{k_2} HO_2^{\bullet} + H_2O$	(2)
	$H_2O_2 + HO_2^{\bullet} \xrightarrow{k_3} HO^{\bullet} + H_2O + O_2$	(3)
Termination	$2HO^{\bullet} \xrightarrow{k_4} H_2O_2$	(4)
	$2HO_2^{\bullet} \xrightarrow{k_5} H_2O_2 + O_2$	(5)
	$HO^{\bullet} + HO_2^{\bullet} \xrightarrow{k_6} H_2O + O_2$	(6)
Degradation of the target pollutant	$BPA + HO^{\bullet} \xrightarrow{k_7} products$	(7)
	$BPA \xrightarrow{\Phi_{BPA}} products$	(8)

The rate expressions for BPA and H_2O_2 are obtained from the following assumptions (ALFANO *et al.*, 1986):

i. The steady-state approximation (SSA) was applied for highly reactive intermediates, such as $HO^{\bullet}$ and $HO_2^{\bullet}$ radicals;
ii. Reaction step 3 is slower than others involving $HO_2^{\bullet}$ and can be neglected;
iii. Radical-radical termination reactions are neglected compared to propagation reactions.

With these assumptions, the expressions for the rates of H_2O_2 and BPA photolysis (r_{uv,H_2O_2} *and* $r_{uv,BPA}$), hydroxyl radical concentrations, and the total rates of H_2O_2 and BPA consumption can be described by the following equations:

$$r_{UV,H_2O_2} = \Phi_{H_2O_2} e^{a}_{254nm}(x,t) \tag{5.1}$$

$$r_{UV,BPA} = \Phi_{BPA} e^{a}_{254nm}(x,t) \tag{5.2}$$

$$C_{HO^{\bullet}}(x,t) = \frac{2r_{UV,H_2O_2}}{C_{H_2O_2}k_2 + C_{BPA}k_7} \tag{5.3}$$

$$R_{H_2O_2}(x,t) = -r_{UV,H_2O_2} - k_2 C_{H_2O_2} C_{HO\cdot} \quad (5.4)$$

$$R_{BPA}(x,t) = -r_{UV,BPA} - k_7 C_{BPA} C_{HO\cdot} \quad (5.5)$$

where, $R_i(x,t)$ (i = H_2O_2, BPA) are the local reaction rates; $C_{HO\cdot}$, $C_{H_2O_2}$, and C_{BPA} correspond to the hydroxyl radical, H_2O_2, and BPA concentrations, respectively; k_2 and k_7 are the second order kinetic rate constants defined in Table 5.1; $\Phi_{H_2O_2}$ is the quantum yield of H_2O_2 photolysis; and e_λ^a represents the local volumetric rate of photon absorption by H_2O_2 and BPA. The values for the constants are listed in Table 5.2.

Table 5.2 – Notations used for the parameters of the H_2O_2/UV process.

Parameter	Notation	Value	Reference
Quantum yield of H_2O_2 photolysis	$\Phi_{H_2O_2,254nm}$	0.5	(CRITTENDEN *et al.*, 1999)
Quantum yield of BPA	$\Phi_{BPA,254nm}$	0.0075	(ARAUJO *et al.*, 2017)
Molar absorption coefficient of H_2O_2	$\varepsilon_{H_2O_2,254\,nm}$	19.6 L mol^{-1} cm^{-1}	(OPPENLANDER, 2003)
Molar absorption coefficient of BPA	$\varepsilon_{BPA,254\,nm}$	912 L mol^{-1} cm^{-1}	(ARAUJO *et al.*, 2017)

5.2 Material balances

The general equation of component conservation is (BIRD *et al.*, 1960):

$$\left\{\begin{matrix}Mass\ entering\\ C.V.\end{matrix}\right\} - \left\{\begin{matrix}Mass\ leaving\\ C.V.\end{matrix}\right\} = \left\{\begin{matrix}Mass\ accumulation\\ C.V.\end{matrix}\right\} + \left\{\begin{matrix}Mass\ production\\ and\ consume\\ by\ homogeneous\\ reaction\ in\ C.V.\end{matrix}\right\} \quad (5.6)$$

Where C.V. is the control volume, in which the full experimental apparatus is considered, as shown previously in Figure 4.2.

For an infinitesimal control volume, Equation 5.6 becomes differential and it is given by the convection-diffusion equation:

$$\frac{\partial C_i(x,t)}{\partial t} + \underline{\nabla}.N_i(x,t) = R_i(x,t) \tag{5.7}$$

Where:

C_i: Concentration of the reacting species *i*;
N_i: Convection-diffusion flux of the reacting species *i*;
R_i: Homogeneous reaction rate of the reacting species *i*.

In this work, the reaction setup is as constant volume, isothermal, closed-loop, perfectly-mixed batch recirculation system, which can be approximated as discontinuous. Therefore, the second term on the left hand of Equation 5.7 ($\underline{\nabla}.N_i$) is considered zero. In this case,

$$\frac{\partial C_i(x,t)}{\partial t} = R_i(x,t) \tag{5.8}$$

Equation 5.8 was then integrated according to the Reynolds transport theorem, dividing the system volume in two terms. The volumes were named *V* for total volume, and V_r and V-V_r for the photoreactor and tank volumes, respectively. The following equation results:

$$\frac{d}{dt}\int_{V_r} C_i(\underline{x},t)dV + \frac{d}{dt}\int_{V-V_r} C_i(\underline{x},t)dV = \int_{V_r} R_i(\underline{x},t)dV + \int_{V-V_r} R_i^T(\underline{x},t)dV \tag{5.9}$$

On the grounds that the H_2O_2/UV process is dependent on irradiation, we considered that the chemical reactions only occurred in the irradiated volume (Equation 5.10). This consideration is valid, since the photochemical reactions are fast enough in such a way that they are not expected to occur outside the irradiated volume. In addition, dark chemical reactions outside the irradiated volume are unlikely or insignificant in comparison to photochemical reactions

$$\frac{d}{dt}\int_{V_r} C_i(\underline{x},t)dV + \frac{d}{dt}\int_{V-V_r} C_i(\underline{x},t)dV = \int_{V_r} R_i(\underline{x},t)dV \tag{5.10}$$

By applying volume averaging all terms of Equation 5.10 (OCHOA and WHITAKER, 1995), the following equations are obtained:

$$\langle C_i(\underline{x},t)\rangle_{V_r} = \frac{1}{V_r}\int_{V_r} C_i(\underline{x},t)dV \tag{5.11}$$

$$\langle C_i(\underline{x},t)\rangle_{V-V_r} = \frac{1}{V-V_r}\int_{V-V_r} C_i(\underline{x},t)dV \tag{5.12}$$

$$\langle R_i(\underline{x},t)\rangle_{V_r} = \frac{1}{V_r}\int_{V_r} R_i(\underline{x},t)dV \tag{5.13}$$

Substituting Equations 5.11-5.13 into Equation 5.10:

$$\frac{d}{dt}\left[\frac{V_r}{V}\langle C_i(\underline{x},t)\rangle_{V_r} + \frac{V-V_r}{V}\langle C_i(\underline{x},t)\rangle_{V-V_r}\right] = \frac{V_r}{V}\langle R_i(\underline{x},t)\rangle_{V_r} \tag{5.14}$$

The concentration of the species *i* (C_i) is considered uniform, since the system is assumed to be well mixed. In this case, $\langle C_i(\underline{x},t)\rangle_{V_r} = \langle C_i(\underline{x},t)\rangle_{V-V_r} = C_i(t)$, and the following molar balances can be written:

$$\frac{dC_i(t)}{dt} = \frac{V_R}{V}\langle R_i(x,t)\rangle_{V_R} \qquad i = BPA,\ H_2O_2, \tag{5.15}$$

With the initial conditions:

$$C_i(t_0) = C_i^0 \quad i = BPA, H_2O_2, \tag{5.16}$$

The reaction rates are given by Equations 5.4 and 5.5. Substituting both equations for the species (BPA and H_2O_2) into Equation 5.15:

$$\frac{dC_{H_2O_2}}{dt} = \frac{V_R}{V}\left(-\phi_{H_2O_2}\langle e^a_{H_2O_2}(x,t)\rangle_{254nm} - k_2 C_{H_2O_2} C_{HO\cdot}\right) \tag{5.17}$$

$$\frac{dC_{BPA}}{dt} = \frac{V_R}{V}(-\phi_{BPA}\langle e^a_{BPA}(x,t)\rangle_{254nm} - k_7 C_{BPA} C_{HO}\cdot) \quad (5.18)$$

5.3 Photoreactor modelling - Emission models in a homogeneous system

There is a considerable amount of research about photoreactor modeling, and various approaches have been proposed based on different photoreactor geometries and radiation sources.

It is worth observing that the model developed here is based on our work, i.e.: annular photoreactor; homogeneous solution; and the H_2O_2/UV process. Figure 5.1 illustrates the annular reactor used in this work. PERES *et al.* (2015) studied the same reactor configuration.

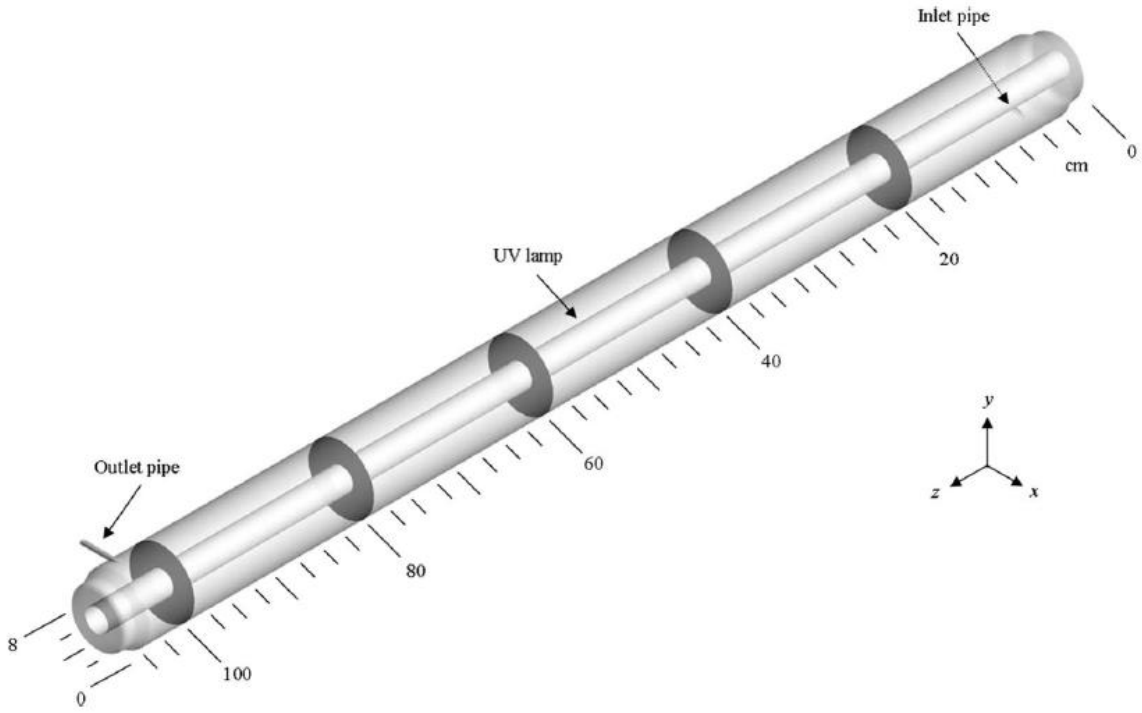

Figure 5.1 – Representation of the annular photoreactor.
Source: PERES *et al.* (2015)

The emission of the radiant energy from the lamp is usually described assuming that beams diverge radially from the linear source to parallel planes perpendicular to the lamp axis (LSPP model) or in all directions through the reaction space (LSSE model). In this work, the first approach was used. Photons propagation is expressed by bundles of rays and it is generally described by a fundamental property called spectral specific intensity $I_{\lambda,\Omega}$ (energy

per unit time, unit area, and unit solid angle on the direction or propagation) (CASSANO *et al.*, 1995). Figure 5.2 illustrates a characterization of the radiation field.

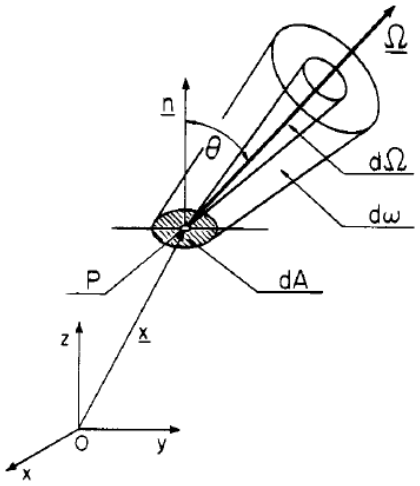

Figure 5.2 – Scheme of the radiation field.
Source: CASSANO *et al*. (1995)

Where d*A* is a small area on the *x* coordinate, *P* an arbitrary point in this area, and $\underline{n}$ the normal to the area at this point *P*. The radiation may be emitted, reflected or transmitted on this surface. By this draw line, one can consider the vector *Ω*. This vector originates an angle θ with the normal *n*. The vector *Ω* corresponds to the axis of a cone with solid angle d*Ω*. A truncated semi-infinite cone d*ω* is formed by elementary solid angles analogous to rays, and are parallel to *Ω* passing through d*A*.

By these definitions we can write the spectral specific intensity as follows (Equation 5.19) (CASSANO *et al.*, 1995):

$$I_\nu(x,\Omega,t,\nu) = \lim_{\mathrm{dA,d\Omega,dt,d\nu}\to 0}\left(\frac{\mathrm{d}E_\nu}{\mathrm{d}A\,\cos\theta\mathrm{d}\Omega\mathrm{dt}\,\mathrm{d}\nu}\right) \tag{5.19}$$

where I_ν is the spectral specific intensity (Einstein m^{-2} sr^{-1} unit frequency $^{-1}$ s^{-1}), dE_ν is radiative energy, *v* is radiation frequency, Ω is the solid angle and *t* is time.

The conservation equation applied on photons is given by Equation 5.20 (CASSANO *et al*. 1995).

$$\left|\begin{array}{c}\text{Inflow of}\\ \text{photons }\Omega,\nu\\ \text{into the volume}\\ \text{control}\end{array}\right| + \left|\begin{array}{c}\text{Outflow of}\\ \text{photons }\Omega,\nu\\ \text{out of the volume}\\ \text{control}\end{array}\right| = \left|\begin{array}{c}\text{Net gain of}\\ \Omega,\nu\text{ photons}\\ \text{owning to}\\ \text{photochemical}\\ \text{interactions}\end{array}\right| \tag{5.20}$$

The general form of the radiative transfer equation (RTE) considers how photons interact within the radiation field inside the photoreactor (OZISIK, 1973; CASSANO *et al.*, 1995; SIEGEL and HOWELL, 2002, MARUGÁN, 2008):

$$\frac{1}{c}\frac{\partial I_{\Omega,\nu}}{\partial x} + \nabla.\left(I_{\Omega,\nu}\Omega\right) = -\overbrace{W_{\Omega,\nu}^{a}}^{Absorption} + \overbrace{W_{\Omega,\nu}^{e}}^{Emission} + \overbrace{W_{\Omega,\nu}^{in-s}}^{In-Scattering} - \overbrace{W_{\Omega,\nu}^{out-s}}^{Out-Scattering} \quad (5.21)$$

where *c* is the speed of light, in meters per second.

As shown in Equation 5.21, the radiation field reaches its steady state instantaneously (first term at the left hand is very small). Nevertheless, *I* may change with time in case that the boundary condition associated with Equation 5.21 is time dependent. The processes related to absorption, emission, in-scattering or out-scattering may also change with time. Note that Equation 5.21 presents two source terms (absorption and emission) and two sink terms (in and out-scattering). Constitutive equations must be provided for each of these terms.

Some considerations were made:

i. The factor 1/*c* is too low, therefore the first member approaches to zero;
ii. Since the medium is optically homogeneous, there is no emission or scattering.

Thus, Equation 5.21 reduces to:

$$\nabla.\left(I_{\Omega,\nu}\Omega\right) = -W_{\Omega,\nu}^{a} = \frac{dI_{\nu}(s,\Omega,t)}{ds} \quad (5.22)$$

where $W_{\Omega,\nu}^{a}$ gives the contribution of photon absorption.

Note that without other contributions, the RTE (Equation 5.21) corresponds to the "Beer-Lambert-Bouguer Law". For the absorption contribution one can write:

$$W_{\Omega,\nu}^{a} = k_{\nu}(\underline{s},t)I_{\nu}(\underline{s},\Omega,t) \quad (5.23)$$

where $\kappa_\nu(\underline{s},t)$ is the absorption coefficient, representing the fraction of the incident radiation that is absorbed by the molecules, per unit length along the path of the beam; $\underline{s}$ is the spatial coordinate.

Including the definition of the absorption in Equation 5.23, the new equation reads:

$$\nabla.\left(I_{\Omega,\nu}\Omega\right) = -\kappa_\nu(\underline{s},t)I_\nu(\underline{s},\Omega,t) \tag{5.24}$$

By differentiating and integrating the last equation, we have:

$$I_\nu(s,\Omega,t) = Cexp\left[-\int_{\bar{s}=s_r}^{\bar{s}=s}\kappa_\nu(\bar{s},t)d\bar{s}\right] \tag{5.25}$$

The constant "C" from Equation (5.25) is obtained with the following boundary condition:

$$s = s_r \rightarrow I_\nu(s=s_r,\Omega,t) = I_\nu^0(\Omega,t) = I_\nu^0(\theta,\phi,t) = I_\nu^* = C \tag{5.26}$$

where s_r represents the point of radiation entry in the photoreactor reaction space, close to the quartz tube wall.

Upon application of the boundary condition, Equation (5.25) results:

$$I_\nu(s,\Omega,t) = I_\nu^* exp\left[-\int_{\bar{s}=s_r}^{\bar{s}=s}\kappa_\nu(\bar{s},t)ds\right] \tag{5.27}$$

Therefore, the equation that represents the radiation field profile in the photoreactor can be written as:

$$I_\nu(x,\theta,\phi,t) = I_\nu^0(\theta,\phi,t)exp\left[-\int_{\bar{s}=s_r(\theta,\phi)}^{\bar{s}=s(x,\theta,\phi)}\kappa_\nu(\bar{s},t)d\bar{s}\right] \tag{5.28}$$

One must obtain all the information to calculate the second term $I_\nu^0(\theta,\phi,t)$. Finally, with all those information, the LVRPA parameter (e^a) can be determined. Equation 5.29 describes this parameter as:

$$e_{\nu}^{a}(\underline{x},t) = \kappa_{\nu}(\underline{x},t) \times G_{\nu}(\underline{x},t) \tag{5.29}$$

where $G_{\nu}(x,t)$is another important photochemical property called spectral incident radiation (energy per unit time and unit area from all directions). This property can be calculated by integrating the spectral specific intensity over the entire photo-reactor volume. Therefore, $G_{\nu}(x,t)$ is mathematically defined as:

$$G_{\nu}(\underline{x},t) = \int_{\Omega} I_{\nu} d\Omega \tag{5.30}$$

The solid angle (Ω) can be written as:

$$d\Omega = sin\theta d\theta d\phi \tag{5.31}$$

In spherical coordinates and by substituting Equation 5.31 into Equation 5.30:

$$G_{\nu} = \int_{\theta_1}^{\theta_2} \int_{\phi_1}^{\phi_2} I_{\nu} sin\theta d\phi d\theta \tag{5.32}$$

Note that Equation 5.32 is valid only for monochromatic radiation.

Now, with the expressions for $G_{\nu}(x,t)$, Equation 5.29 reads:

$$e_{\nu}^{a}(\underline{x},t) = \kappa_{\nu}(\underline{x},t) \int_{\theta_1}^{\theta_2} \int_{\phi_1}^{\phi_2} I_{\nu} sin\theta d\phi d\theta \tag{5.33}$$

I_{ν} was defined previously in Equation 5.28; therefore, Equation 5.33 can be rewritten as:

$$e_{\nu}^{a}(\underline{x},t) = \kappa_{\nu}(\underline{x},t) \int_{\phi_1}^{\phi_2} d\phi \int_{\theta_1}^{\theta_2} I_{\nu}^{*} exp\left[- \int_{\bar{s}=s_r}^{\bar{s}=s(x,\theta,\phi)} \kappa_{\nu}(\bar{s},t) \right] sin\theta d\theta \tag{5.34}$$

where I_v* is the energy transferred from the wall of the quartz tube to the reaction medium and it is obtained by an emission model. The term I_v* is initially written as:

$$I_v^*(\theta, \phi, t) = f[lamp\ caractheristics; reactor\ geometry] \tag{5.35}$$

This equation provides the boundary condition in the reactor entry. Note that the process of radiation emission is considered stationary.

5.3.1 LSPP MODEL

The e^a for the LSPP model was previously given (Equation 3.19), and its average value for our experimental setup is given by:

$$\langle e^a(x)\rangle_{V_r} = \frac{1}{V}\kappa_i r_i q_i \int_{ri}^{re} \frac{e^{-\kappa_i(r-ri)}}{r} 2\pi r dr dz \tag{5.36}$$

where $\langle e^a(x)\rangle_{V_r}$ is a volumetric average value and κ_i is the volumetric absorption coefficient of the reacting species (H_2O_2 and BPA), which can be expressed as:

$$\kappa_{i,\lambda} = \alpha_{i,254nm} \times C_i \tag{5.37}$$

where $\kappa_{i,\lambda}$ is the molar absorptivity of the absorbing species, which is a function of the wavelength λ (254 nm in the present work).

By integrating Equation 5.36 and substituting "q_i" by Equation 3.20, we obtained the expression for the radiation field for our system by means of the LSPP model:

$$\langle e^a(x)\rangle_{V_r} = \frac{P}{V} \times [1 - exp(-b(\kappa_{H_2O_2} + \kappa_{BPA}))] \tag{5.38}$$

where the first term of the right hand side of the expression is the specific rate of photons emission ($P/V = E_{P,0}$) and b is the path length.

With the expression for the radiation field, we can obtain the final equations for our system by substituting Equations 5.17 and 5.18 into Equation 5.38:

$$\frac{dC_{H_2O_2}}{dt} = \frac{V_R}{V}\left(-\phi_{H_2O_2}\frac{P}{V}\times[1-exp(-b(\kappa_{H_2O_2}+\kappa_{BPA}))]-k_2C_{H_2O_2}C_{HO}\cdot\right) \quad (5.39)$$

$$\frac{dC_{BPA}}{dt} = \frac{V_R}{V}(-\phi_{BPA}\frac{P}{V}\times[1-exp(-b(\kappa_{H_2O_2}+\kappa_{BPA}))]-k_7C_{BPA}C_{HO}\cdot) \quad (5.40)$$

6. RESULTS AND DISCUSSION

This section is organized as follows. The first part details the determination of the spectral molar absorption coefficient (ε) of BPA, as well as the results of the H_2O_2/UV experiments in terms of BPA, H_2O_2, TOC, and pH behaviors over time. A discussion is also presented, comparing and relating the results as regards the literature whenever possible. In the second part, the effects of each independent variable (H_2O_2 and $E_{P,0}$) on BPA degradation by the H_2O_2/UV process is discussed according to the response surface analysis, for each experimental response (apparent first-order BPA degradation rate constant, BPA degradation after 15 min, and TOC removal after 120 min). The third and last part presents the results obtained by the kinetic study and mathematical modelling, comparing predicted and experimental values of BPA and H_2O_2 concentrations as a function of reaction time.

6.1 Experimental results

6.1.1 DETERMINATION OF THE SPECTRAL MOLAR ABSORPTION COEFFICIENT (ε)

The molar absorption coefficient of BPA was determined as a function of wavelength. Figure 6.1 shows the absorption spectrum.

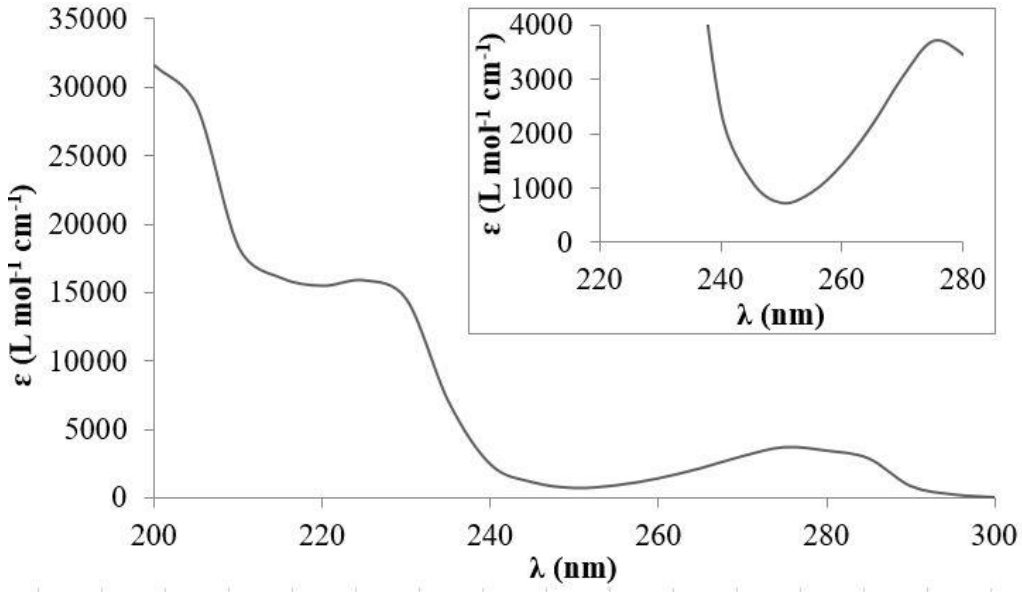

Figure 6.1 – UV-Vis absorption spectrum of BPA in aqueous solution.

Figure 6.1 shows that BPA absorbs UV radiation in the range of 200-300 nm and two main peaks are seen, at 230 nm and 280 nm. The photolysis efficiency relies on the decadic molar absorption coefficient of the compound at these wavelengths. The most relevant value for this coefficient is at 254 nm, since the lamp used in the experiments emits at this wavelength. Figure 6.1 also highlights the molar absorption coefficient in a shorter range of 220-280 nm for λ and 0-4000 L mol^{-1} cm^{-1} for ε. According to these results, ε is approximately 840 L mol^{-1} cm^{-1} at 254 nm at pH 7, which is slightly different to the value obtained by BAEZA and KNAPPE (2011), 750 L mol^{-1} cm^{-1} at 254 nm and pH 7.85. In addition, the value found for the molar absorption of BPA is much higher than that of H_2O_2, which has a direct impact on BPA degradation during the H_2O_2/UV process, as discussed later.

6.1.2 BPA DEGRADATION BY THE H_2O_2/UV PROCESS

Figure 6.2 illustrates BPA concentration over time during the H_2O_2/UV process under different conditions.

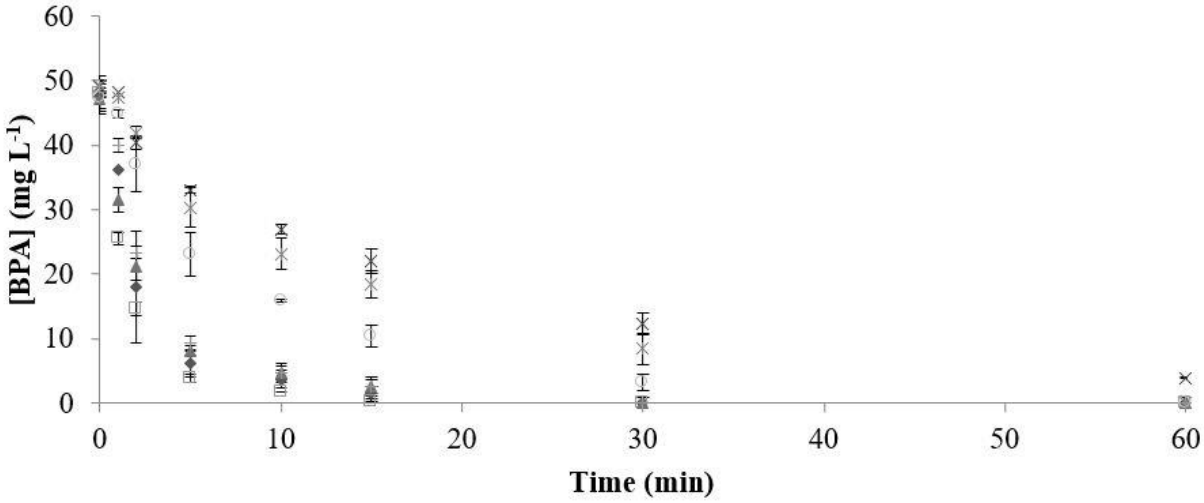

Figure 6.2 – BPA degradation during the H_2O_2/UV experiments for different H_2O_2 initial concentrations and specific photon emission rates. $[BPA]_0$ = 48.2 ± 0.9 mg L^{-1}. Conditions ($[H_2O_2]_0$, mmol L^{-1} – $E_{P,0}$, × 10^{18} photons·L^{-1} s^{-1}): ▲ Exp 1 (3.6 – 3.6); □ Exp 2 (7.6 – 3.6); ◆ Exp 3 (9.6 – 1.4); ○ Exp 4 (7.6 – 0.87); ✳ Exp 5 (3.6 – 0.87); ✕ Exp 6 (1.6 – 1.4); + Exp7 (5.6 – 1.4). Experiments run in duplicate.

All the BPA concentrations were below the detection limit after 80 min of irradiation. However, the experiments signalled contrasting BPA degradation extents. Experiments 1, 2, 3, and 7 resulted in BPA degradations of 97, 99, 94, and 95%, respectively, after 15 min. On the contrary, in experiments 4, 5, and 6 lower degradations were achieved (55, 62, and 78%, respectively) at the same reaction time. These data suggest a higher importance of the specific photon emission rate compared to the effect of hydrogen peroxide, since a higher initial oxidant concentration (experiment 6, $[H_2O_2]_0$ = 7.6 mmol L^{-1}) resulted in lower pollutant removal after 15 min. Moreover, the results indicate that BPA degradation followed apparent first-order decay for all the experimental conditions, with high values of the determination coefficients (R^2) shown by the curves of ln($[BPA]/[BPA]_0$) × time, for all the experiments (0.932, 0.967, 0.933, 0.989, 0.981, 0.985, and 0.944, respectively).

The results in Table 6.1 show that experiment 2 ($[H_2O_2]_0$ = 7.6 mmol L^{-1}; $E_{P,0}$ = 3.6 × 10^{18} photons L^{-1} s^{-1}) signalled the highest values of the specific BPA degradation rate and BPA degradation after 15 min, and the second highest TOC removal. It is worth observing that the value of $[H_2O_2]_0$ for experiment 2 was close to the theoretical stoichiometric concentration (8 mmol L^{-1}) estimated for the initial BPA concentration adopted (50 mg L^{-1}). In this case, BPA degradation in experiment 2 was about 70% after only two min. FELIS *et al.* (2010) obtained about 60% BPA degradation after five min, using 3 × 10^{-1} mmol L^{-1} H_2O_2 and 9.8 mg L^{-1} initial BPA concentration.

Table 6.1 – Conditions and results of the H_2O_2/UV experiments. Y_1: apparent first-order specific BPA degradation rate; Y_2: BPA degradation after 15 min; Y_3: TOC removal after 120 min. $[BPA]_0$ = 48.2 ± 0.9 mg L^{-1}; $[TOC]_0$ = 38.7 ± 0.9 mg L^{-1}. The Y values are the average of the results of duplicate runs.

Exp	**$[H_2O_2]_0$; $E_{P,0}$**	**Y_1**	**Y_2**	**Y_3**
	(mmol L^{-1}; × 10^{18} photons $L^{-1}s^{-1}$)	(min^{-1})	(%)	(%)
1	3.6; 3.6	0.223	96.9	94.9
2	7.6; 3.6	0.305	99.3	91.5
3	9.6; 1.4	0.187	97.7	43.8
4	7.6; 0.87	0.041	91.9	11.3
5	3.6; 0.87	0.058	62.5	15.6
6	1.6; 1.4	0.089	93.0	34.4
7	5.6; 1.4	0.196	94.7	50.9

A closer look at the data indicates that experiment 4 ($[H_2O_2]_0$ = 7.6 mmol L^{-1} and $E_{P,0}$ = 0.87 × 10^{18} photons $L^{-1}s^{-1}$) recorded a low value of the specific BPA degradation rate Y_1, even though a high H_2O_2 concentration was employed. In contrast, an improvement was observed when $E_{P,0}$ was kept at 3.6 × 10^{18} photons $L^{-1}s^{-1}$, and $[H_2O_2]_0$ moved to 3.6 mmol L^{-1} (experiment 1), suggesting that the effect of the photon emission rate would be more relevant upon the BPA removal.

There is an additional aspect that should be considered regarding the effect of H_2O_2 concentration, namely the competition of H_2O_2 and BPA molecules for incident photons. In fact, the molar absorption coefficient of BPA at 254 nm (840 L mol^{-1} cm^{-1}) is much higher than that of hydrogen peroxide (19 L mol^{-1} cm^{-1}, according to OPPENLÄNDER, 2003). Therefore, for our experiments the fraction of UV radiation absorbed at time zero by H_2O_2 in comparison with BPA molecules would be between 15% to 50% for $[H_2O_2]_0$ = 1.6 and 9.6 mmol L^{-1}, respectively, varying with time as both H_2O_2 and BPA concentrations decrease (for simplification, the effect of unknown absorbing intermediate compounds is not considered). Nevertheless, the quantum yield of BPA photolysis is quite low (0.0075 mol BPA mol $photons^{-1}$), in such a way that the contribution of BPA photolysis could be neglected during the H_2O_2/UV process, particularly for the lowest H_2O_2 concentration levels.

The degree of total mineralization is usually determined by measuring the difference between the initial and final concentrations of the total organic carbon (TOC). TOC removal for each condition was analyzed within 180 min (Figure 6.3).

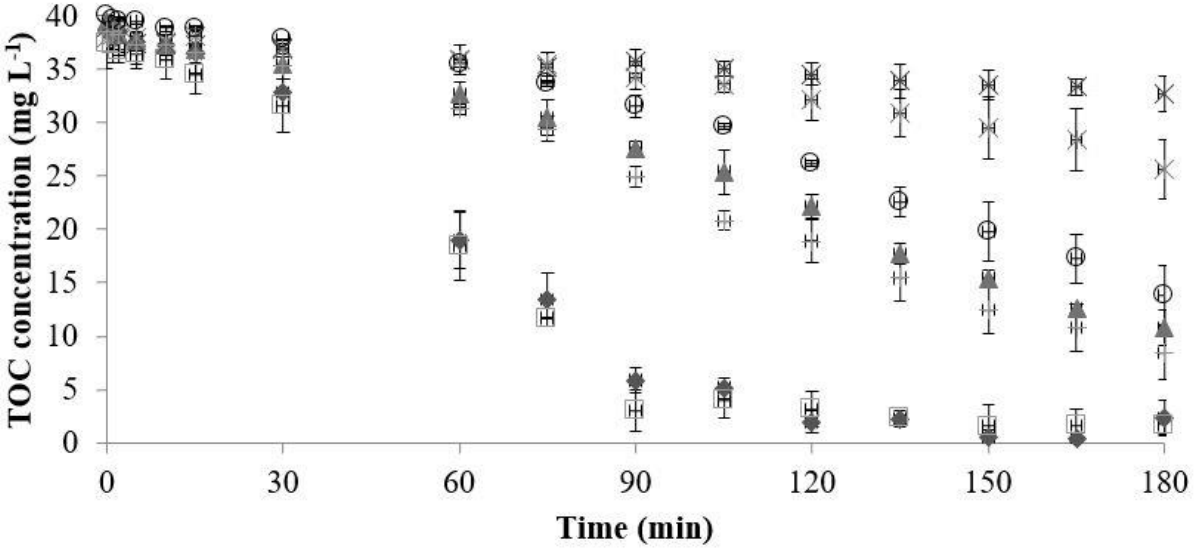

Figure 6.3 – Total organic carbon removal during the H_2O_2/UV experiments for different H_2O_2 initial concentrations and specific photon emission rates. $[TOC]_0$ = 38.7 ± 0.9 mg L^{-1}. Conditions ($[H_2O_2]_0$, mmol L^{-1} – $E_{P,0}$, ×10^{18} photons L^{-1} s^{-1}): ▲ Exp 1 (3.6 – 3.6); □ Exp 2 (7.6 – 3.6); ◆ Exp 3 (9.6 – 1.4); ○ Exp 4 (7.6 – 0.87); ✳ Exp 5 (3.6 – 0.87); ✕ Exp 6 (1.6 – 1.4); + Exp 7 (5.6 – 1.4). Experiments run in duplicate.

Experiments yielded different TOC removals, with the most relevant mineralization achieved in experiments 3 ($[H_2O_2]_0$ = 9.6 mmol L^{-1}; $E_{P,0}$ = 1.4 × 10^{18} photons L^{-1} s^{-1}) and 2 ($[H_2O_2]_0$ = 7.6 mmol L^{-1}; $E_{P,0}$ = 3.6 × 10^{18} photons L^{-1} s^{-1}); the TOC removals for these experiments were 94 and 95 %, respectively. Conversely, the TOC removals for experiments 1, 4, 5, 6, and 7 after 180 min were notably lower (73, 16, 33, 65, and 78 %, respectively). Generally, an extended degradation time is required to accomplish complete mineralization after the removal of the target compound (COMNINELLIS *et al.*, 2008). These results suggest that experiment 2 records the best conditions for BPA degradation, with high values of the specific BPA degradation rate (0.305 min^{-1}), BPA degradation after 15 min (99.3%), and TOC removal of 91.5% (120 min).

Figure 6.4 shows that most H_2O_2 concentrations were below the detection limit after 150 min of irradiation. However, experiments 4 and 5 presented significant remaining amounts of the oxidant at the end of reaction time, even starting with low initial H_2O_2 concentrations. Note that these same experiments resulted in lower TOC removals, as shown previously. The low initial H_2O_2 concentrations (1.6 and 3.6 mmol L^{-1}, respectively) associated with lower specific photon emission rates (1.4 and 0.87 × 10^{18} photons L^{-1} s^{-1}, respectively) are insufficient to degrade BPA degradation products formed, even with the presence of H_2O_2 during all the reaction time.

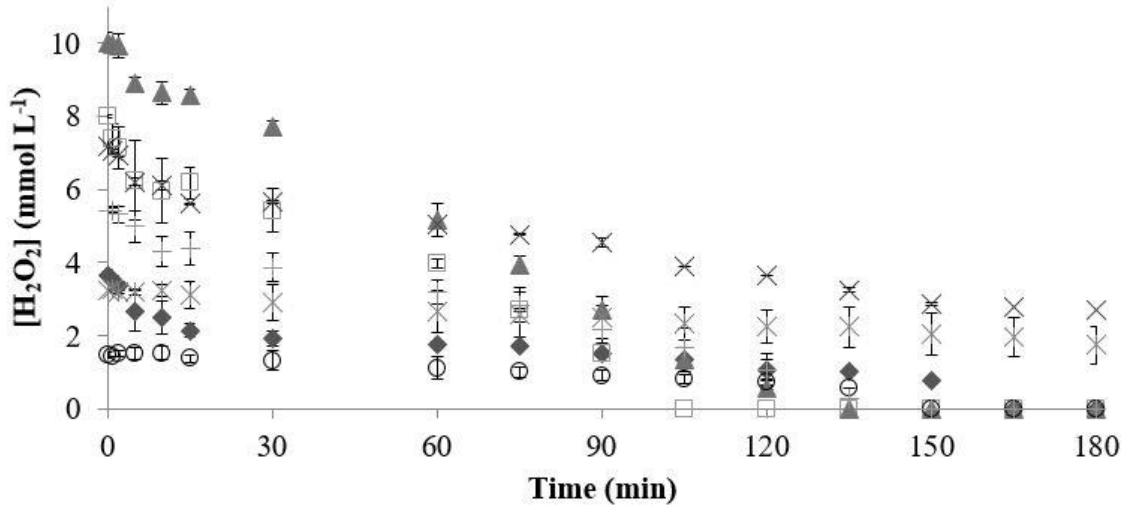

Figure 6.4 – Time profiles of hydrogen peroxide concentrations during the H_2O_2/UV experiments. Conditions ($[H_2O_2]_0$, mmol L^{-1} – $E_{P,0}$, × 10^{18} photons L^{-1} s^{-1}): ▲ Exp 1 (3.6 – 3.6); □ Exp 2 (7.6 – 3.6); ◆ Exp 3 (9.6 – 1.4); ○ Exp 4 (7.6 – 0.87); ✳ Exp 5 (3.6 – 0.87); × Exp 6 (1.6 – 1.4); + Exp 7 (5.6 – 1.4). Experiments run in duplicate.

Figure 6.5 shows the time evolution of pH during the H_2O_2/UV experiments. For experiments 2 and 3, pH decreased from 7 to 3 in the first 70 min, followed by an increase to about pH 5 until the end of the experiments. Interestingly, experiments 1, 4, 5, 6, and 7 showed the same initial behaviour observed in experiments 2 and 3, whereas no substantial pH increase was observed therein. The literature on this topic reports the formation of oxalic, succinic, and fumaric acids from BPA degradation under the H_2O_2/UV process (OLMEZ-HANCI *et al.*, 2015). As soon as these acids are formed, they are also degraded and mineralized to CO_2 and H_2O, resulting in pH increase. This is in agreement with the time-evolution of TOC shown in Figure 6.3, which clearly indicates nearly total BPA mineralization after 150 min.

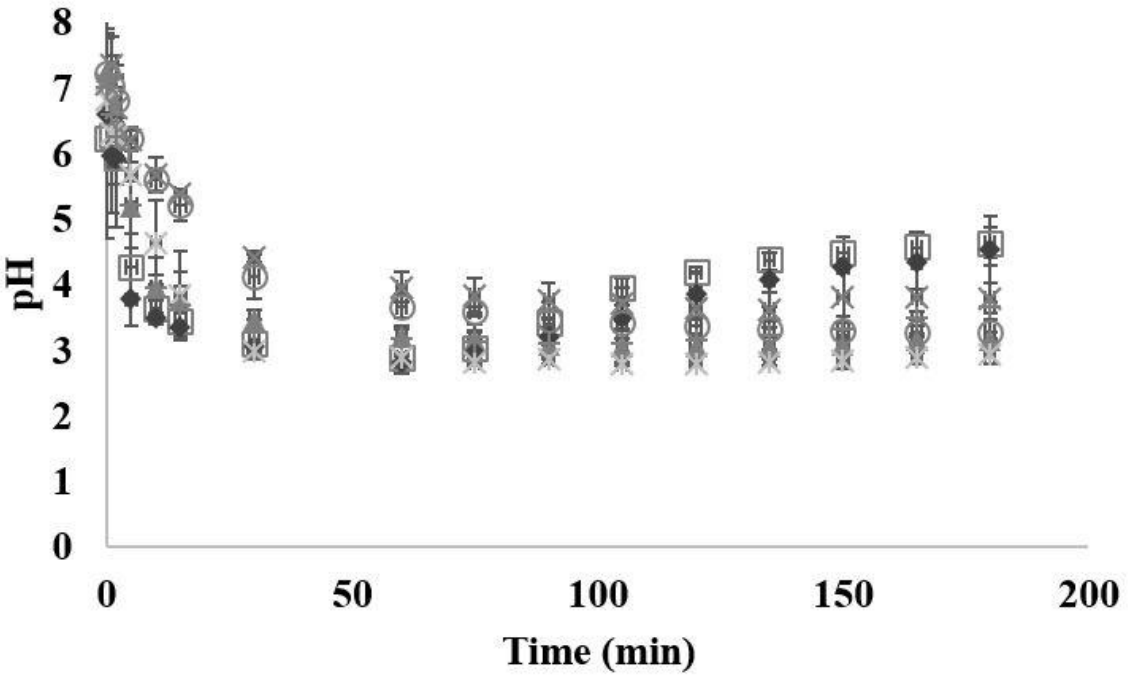

Figure 6.5 – Time profiles of pH during the H_2O_2/UV experiments.pH_0 = 7.08 ± 0.47. Conditions ($[H_2O_2]_0$, mmol L^{-1} – $E_{P,0}$, $\times 10^{18}$ photons L^{-1} s^{-1}): ▲ Exp 1 (3.6 – 3.6); □ Exp 2 (7.6 – 3.6); ◆ Exp 3 (9.6 – 1.4); ○ Exp 4 (7.6 – 0.87); ✳ Exp 5 (3.6 – 0.87); ✕ Exp 6 (1.6 – 1.4); + Exp 7 (5.6 – 1.4). Experiments run in duplicate.

6.2 Statistical analysis - results of the Doehlert experimental design

Response surface models were considered, in order to find the best conditions for BPA degradation by the H_2O_2/UV process. As stated in Section 4.2.3, the dependent variables (responses) evaluated were the apparent first-order BPA degradation rate constant (Y_1, min^{-1}), BPA degradation after 15 min (Y_2, %), and TOC removal after 120 min (Y_3, %). Table 6.1 lists these responses for each experimental condition ($[H_2O_2]_0$ and $E_{P,0}$). Table 6.2 lists the corresponding values of the fitted coefficients of the response surface models.

Table 6.2 – Response surface models obtained for the H_2O_2/UV process. Y_1: apparent first-order specific BPA degradation rate; Y_2: BPA degradation after 15 min; Y_3: TOC removal after 120 min. Codified variables X_1 and X_2 refer to $[H_2O_2]_0$ and $E_{P,0}$, respectively. See Table 6.1 for the codified values of the Doehlert design, corresponding to $[H_2O_2]_0$ (initial hydrogen peroxide concentration) and $E_{P,0}$ (specific photon emission rate).

Model Equations
Y_1 (min^{-1}) = 0.19 + 0.09X_1 + 0.10X_2 – 0.06X_1^2 + 0.07X_1X_2 – 0.03X_2^2 (I)
Y_2 (%, 15 min) = 94.61 + 16.84X_1 + 14.46X_2 – 16.63X_1^2 – 3.90X_1X_2 – 8.01X_2^2 (II)
Y_3 (%, 120 min) = 51.58 + 37.19X_1 + 23.95X_2 + 0.46X_1^2 + 11.90X_1X_2 – 9.60X_2^2 (III)

The ANOVA (Table 6.3 to Table 6.5) and the Pareto charts (Figure 6.6) indicate significant effects of the independent variables on Y_1, Y_2, and Y_3 at the 95% confidence level (p-values < 0.05).

Table 6.3 – Analysis of variance (ANOVA) for the apparent first-order specific BPA degradation rate (Y_1, min^{-1}). Fisher F for 95 % confidence level. X_1 and X_2 are the codified independent variables corresponding to $[H_2O_2]_0$ and $E_{P,0}$, respectively.

Variables and interactions	Sum of squares	Degrees of freedom	Mean square	*F*-ratio	*p*-value
A: X_1	0.048289	1	0.048289	38.74	0.0003
B: X_2	0.05838	1	0.05838	46.84	0.0001
AA	0.00633363	1	0.00633363	5.08	0.0542
AB	0.00795727	1	0.00795727	6.38	0.0354
BB	0.00107985	1	0.00107985	0.87	0.3792
Total error	0.00997156	8	0.00124644		
Total (corr.)	0.134681	13			
R^2	0.9560				

Table 6.4 − Analysis of variance (ANOVA) for BPA degradation after 15 minutes (Y_2, %). Fisher F for 95 % confidence level. X_1 and X_2 are the codified independent variables corresponding to $[H_2O_2]_0$ and $E_{P,0}$, respectively.

Variables and interactions	Sum of squares	Degrees of freedom	Mean square	*F*-ratio	*p*-value
A: X_1	1714.71	1	1714.71	49.79	0.0001
B: X_2	1224.54	1	1224.54	35.56	0.0003
AA	476.614	1	476.614	13.84	0.0059
AB	26.0841	1	26.0841	0.76	0.4095
BB	85.5898	1	85.5898	2.49	0.1536
Total error	275.512	8	34.439		
Total (corr.)	3984.95	13			
R^2	0.9308				

Table 6.5 − Analysis of variance (ANOVA) for TOC removal after 120 minutes (Y_3, %). Fisher F for 95 % confidence level. X_1 and X_2 are the codified independent variables corresponding to $[H_2O_2]_0$ and $E_{P,0}$, respectively.

Variables and interactions	Sum of squares	Degrees of freedom	Mean square	*F*-ratio	*p*-value
A: X_1	9507.99	1	9507.99	742.43	0.0000
B: X_2	3522.46	1	3522.46	275.05	0.0000
AA	0.3631118	1	0.363118	0.03	0.8705
AB	242.344	1	242.344	18.92	0.0024
BB	122.856	1	122.856	9.59	0.0147
Total error	102.452	8	12.8066		
Total (corr.)	14237.0	13			
R^2	0.9928				

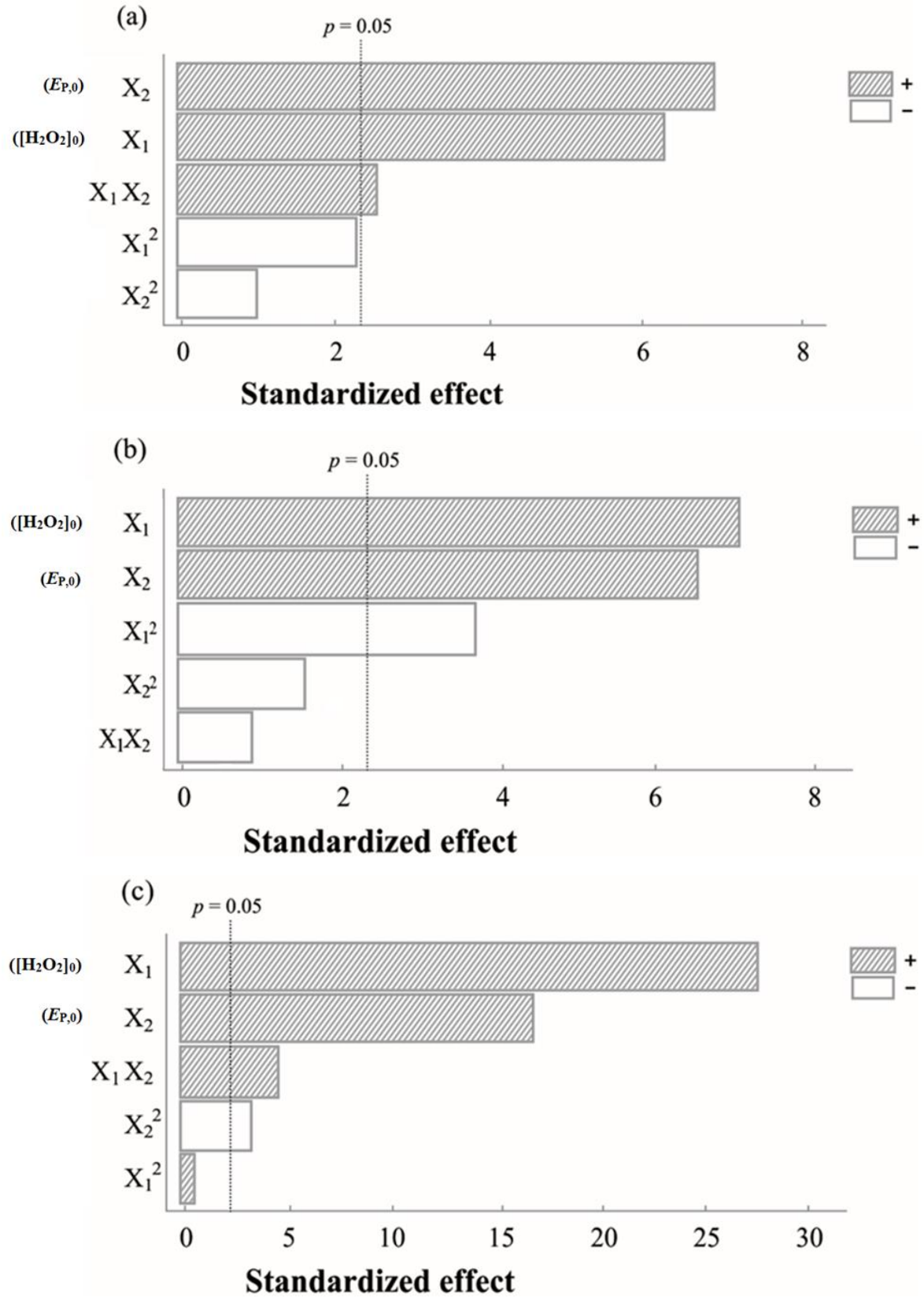

Figure 6.6 – Pareto charts for the responses. Degrees of freedom = 8 (t = 2.31). Fisher F for 95% confidence level. (a) Y_1, apparent first-order specific BPA degradation rate (min^{-1}). (b) Y_2, BPA degradation after 15 min (%). (c) Y_3, TOC removal after 120 min (%). X_1 and X_2 are the codified independent variables corresponding to $[H_2O_2]_0$ and $E_{P,0}$, respectively.

For the specific BPA degradation rate (Y_1, min^{-1}), the positive significant effects of X_2 ($E_{P,0}$), X_1 (initial H_2O_2 concentration), and interaction of these two variables, X_2X_1, are observed (Figure 6.6a); the determination coefficient (R^2) indicates that the model as fitted explains 95.6% of the variability of Y_1 (Table 6.3). Figure 6.6b indicates significant positive effects of X_1 and X_2, and the significant negative quadratic effect X_1^2 on Y_2 (BPA % degradation after 15 min) at the 95% confidence level; R^2 indicates that the model (Table 6.4) as fitted explains 93.1% of the variability of the response. For the response Y_3 (TOC removal after 120 min), Figure 6.6c shows significant positive effects of X_1, X_2 and X_1X_2, and the significant negative quadratic effect X_2^2 on Y_3 (% TOC removal after 120 min), and R^2 confirms that the model as fitted (Table 6.5) explains 99.3% of the variability of this response. In all cases, the residuals were randomly distributed around residue zero with zero mean (Figure 6.7).

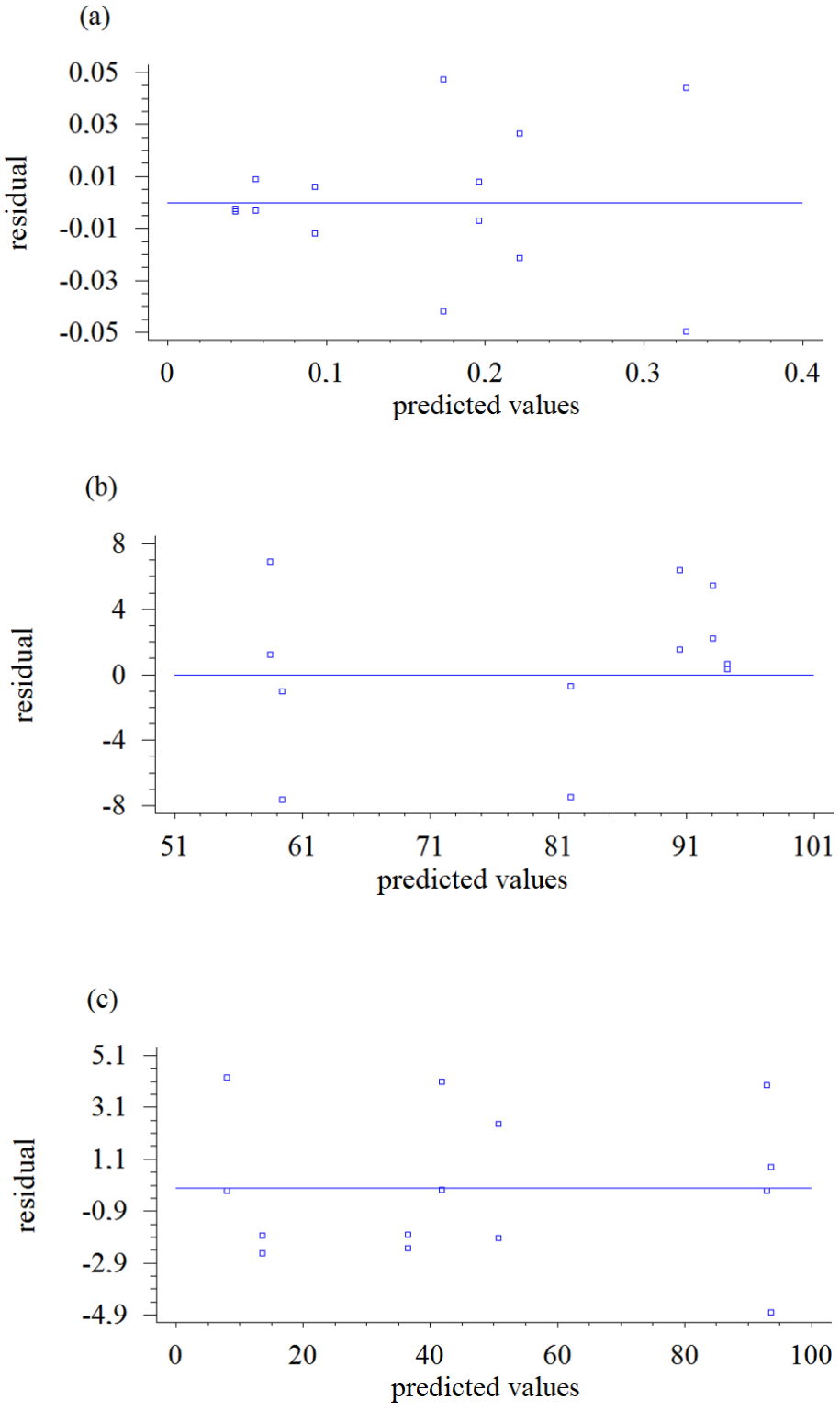

Figure 6.7 – Distribution of residuals as a function of the predicted values. (a) Y_1, apparent first-order specific BPA degradation rate (min^{-1}). (b) Y_2, BPA degradation after 15 min (%). (c) Y_3, TOC removal after 120 min (%). X_1 and X_2 are the codified independent variables corresponding to $[H_2O_2]_0$ and $E_{P,0}$, respectively.

Figures 6.8, 6.9 and 6.10 show the two-dimensional contour plots and the response surface for Y_1, Y_2 and Y_3, respectively. They were designed using the data provided in Table 6.2.

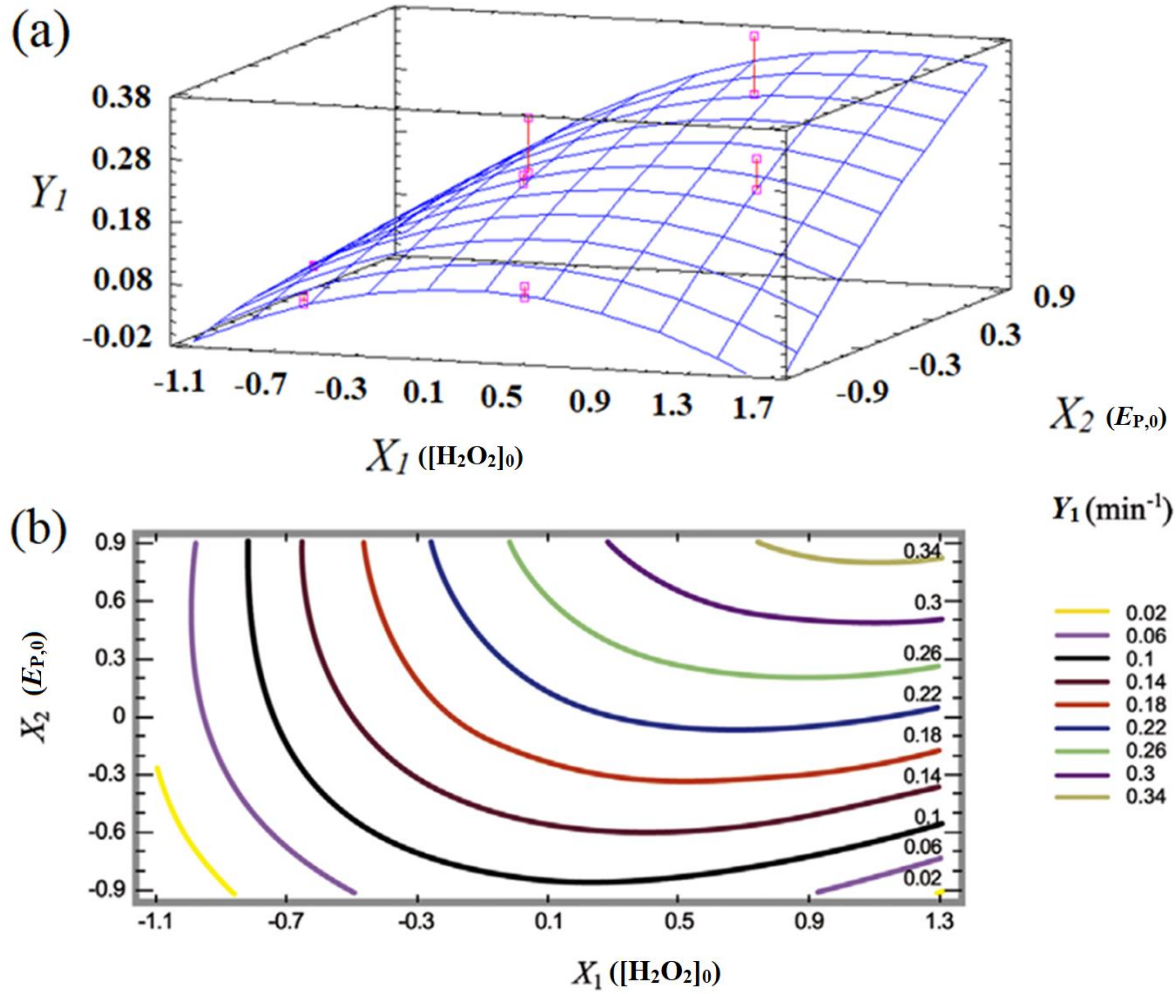

Figure 6.8 – (a) Response surface for Y_1 (apparent first-order specific BPA degradation rate, min^{-1}), described by Equation I in Table 6.2. (b) Contour plots. X_1 and X_2 are the codified independent variables corresponding to $[H_2O_2]_0$ and $E_{P,0}$, respectively.

The response surface suggests a highest value for Y_1, which is 0.35 min^{-1}. The combination of factor levels which maximizes Y_1 over the indicated region is 1.0975 and 0.866 for X_1 and X_2, respectively. The real values of the variables: U_1 (initial H_2O_2 concentration) and U_2 (specific rate of photons emission) are 9.6 mmol L^{-1} and 3.6×10^{18} photons $L^{-1}s^{-1}$, respectively. A fast increase in the specific BPA degradation rate (response Y_1) with increasing H_2O_2 concentration (X_1) and specific photon emission rate (X_2) is observed. The upper line corresponds to Y_1 = 0.34 min^{-1}, for X_1 from about 0.8 to 1.3 (8.88 to 11.64

mmol L^{-1}) and X_2 from about 0.8 to 0.9 (3.32 to 3.46 × 10^{18} photons L^{-1} s^{-1}). On the other hand, when only one of the variables is at its highest level, low values of Y_1 are observed.

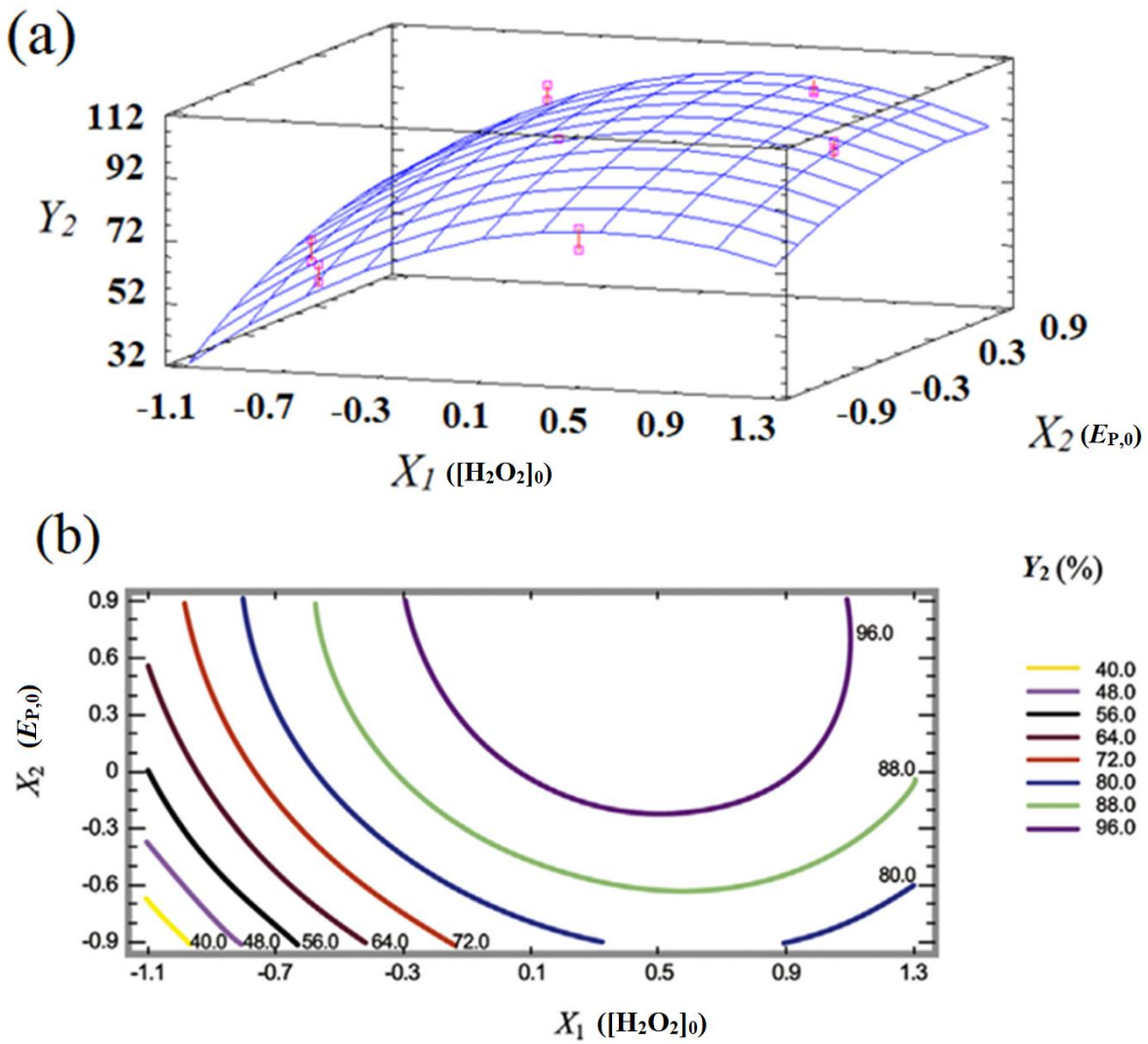

Figure 6.9 – (a) Response surface for Y_2 (BPA degradation after 15 min, %), described by Equation II in Table 6.2. (b) Contour plots. X_1 and X_2 are the codified independent variables corresponding to $[H_2O_2]_0$ and $E_{P,0}$, respectively.

Figure 6.9a revealed a maximum value for Y_2, which is ~100%. The combination of factor levels which maximizes Y_2 over the indicated region is 0.412 and 0.802 for X_1 and X_2, respectively. The corresponding real values of the variables: U_1 (initial H_2O_2 concentration) and U_2 (specific rate of photons emission) are 7.23 mmol L^{-1} and 3.32 × 10^{18} photons $L^{-1}s^{-1}$, respectively. It is interesting to note that the H_2O_2 concentration considered as optimum was close to the theoretical stoichiometric concentration (8 mmol L^{-1}) estimated for the initial BPA concentration adopted (50 mg L^{-1}). An increase in the efficiency of the oxidation process with increasing X_1 and X_2 is also observed, whereas in this case a region of maximum is

clearly distinguished, with nearly 100% BPA removal at X_1 = 0.412 and X_2 = 0.802; these codified variables correspond to $[H_2O_2]_0$ = 6.75 mmol L^{-1} and $E_{P,0}$ = 3.33 × 10^{18} photons L^{-1} s^{-1}, respectively. Note that these results are quite similar to those observed in experiment 2, whose conditions ($[H_2O_2]_0$ = 7.6 mmol L^{-1} and $E_{P,0}$ = 3.6 × 10^{18} photons L^{-1} s^{-1}) were previously suggested as the most adequate for BPA degradation. This behaviour indicates the effects of hydrogen peroxide, also acting as an efficient hydroxyl radical scavenger, producing water and hydroperoxyl radicals (HO_2•), which are less reactive than hydroxyl radicals

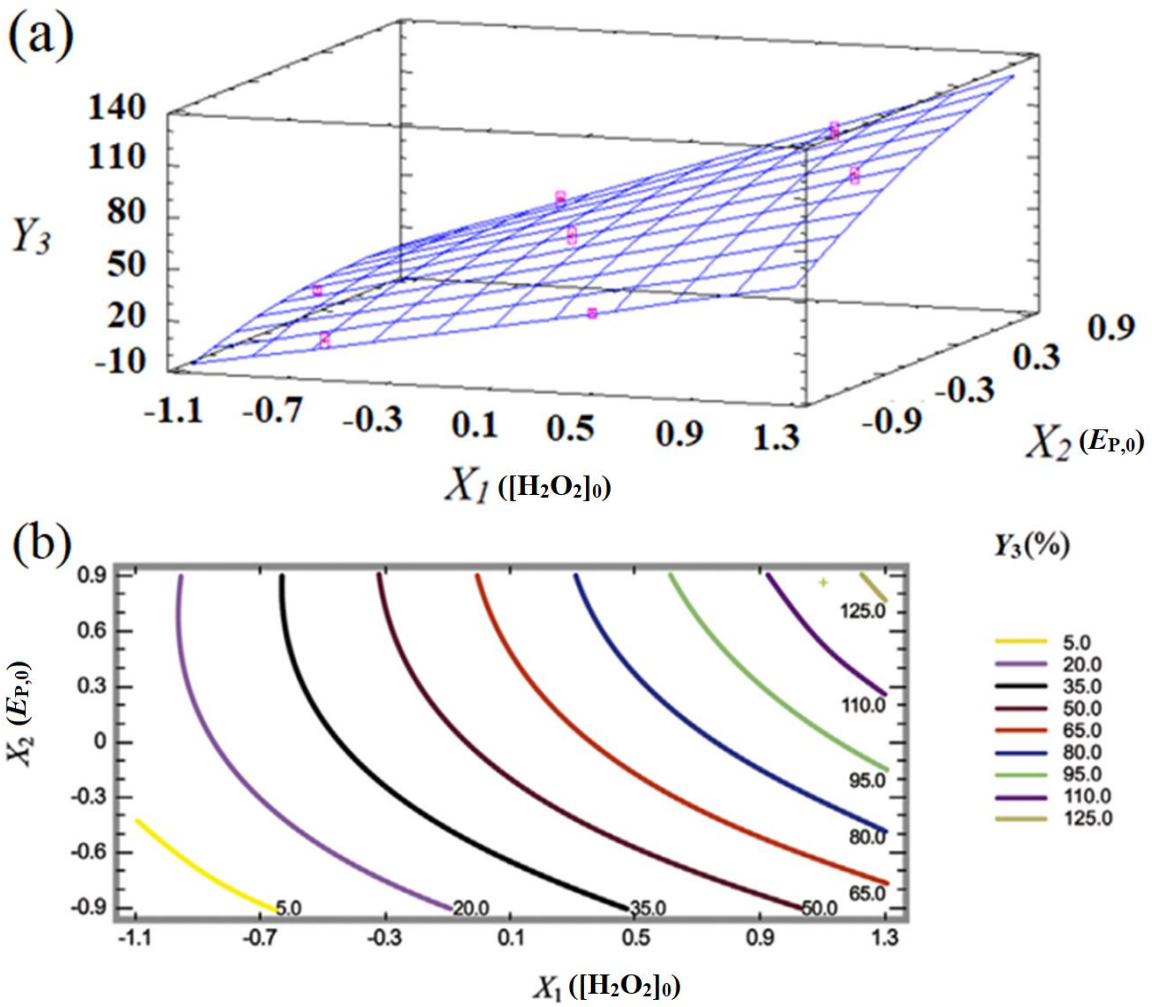

Figure 6.10 – (a) Response surface for Y_3 (TOC removal after 120 min, %), described by Equation III in Table 6.2. (b) Contour plots. X_1 and X_2 are the codified independent variables corresponding to $[H_2O_2]_0$ and $E_{P,0}$, respectively.

Figure 6.10a does not indicate any clear region of maximum response for Y_3. Finally, Figure 6.10b illustrates the behaviour of TOC removal after 120 min (Y_3), which also increases for increasing $[H_2O_2]_0$ and $E_{P,0}$. The line corresponding to 20% TOC removal is

found for X_1 from about −0.9 to −0.1, and that of 95% for X_1 from about 0.6 to 1.3. For this response, the effect of $E_{P,0}$ seems to be less significant, since high TOC removals are also observed for lower levels of X_2, as suggested by most lines (5 to 65%).

6.3 Kinetic modelling

As mentioned previously, two models that describe the lamp and its emission into the radiation field were evaluated for our system. Each model will be discussed as regards our experiments. Therefore, this section is divided in two. The first one is dedicated to the LSPP model, and the second one to the LSSE model. A brief conclusion will be presented after these both sections, stating our perceptions for each model. These sub-sections will also present the average values for the LVRPA ($\langle e_\lambda^a \rangle_{V_r}$) and the rate constants for each model.

6.3.1 PARAMETERS ESTIMATION – LSPP MODEL

A nonlinear least-square objective function minimized with the Neld-Mead simplex algorithm (fminsearch) was applied to estimate the kinetic parameters k_2 and k_7, which correspond to the reactions $H_2O_2 + HO^\bullet \xrightarrow{k_2} HO_2^\bullet + H_2O$ and $BPA + HO^\bullet \xrightarrow{k_7} product$, respectively. This procedure searched for values that minimize the sum of squared differences between predicted and experimental BPA and H_2O_2 concentrations (Equation 6.1).

Minimize,

$$f = \sum [\left(BPA_{predicted} - BPA_{experiment}\right)^2 + (H_2O_{2_{predicted}} - H_2O_{2_{experiment}})^2] \quad (6.1)$$

Subject to: $\frac{dC_i}{dt} = R_i(x,t) \qquad (i = H_2O_2 \; or \; BPA)$

k_2 and $k_7 > 0$

Relative H_2O_2 and BPA concentrations were used in order to overcome possible drawbacks during the optimization procedure, owing to the different magnitudes of their real values. The system of equations representing the batch reactor (Equations 5.39 and 5.40) was implemented in MatLab® in order to gather the calculated concentrations. The mathematical

solution was provided by solving stiff differential equations based on Gear's method (*ode15s*).

For the numerical solution, the following information was needed:

i. The initial guesses of the kinetic constants k_2 and k_7 were gathered from SIMUNOVIC *et al*. (2011) and FELIS *et al.* (2011);

ii. As previously mentioned in Section 4 – *Materials and Methods*, the specific rate of photon absorption $E_{P,0}$ was obtained by ferrioxalate actinometry and the values were 1.44×10^{-3}, 2.32×10^{-3}, and 5.98×10^{-3} Einstein m^{-3} s^{-1};

iii. The molar absorption coefficient of H_2O_2 and its photolysis quantum yield ($\varepsilon_{H_2O_2}, \Phi_{H_2O_2,254nm}$) were obtained from the literature (Table 5.2). The corresponding values for BPA ($\varepsilon_{BPA}, \Phi_{BPA,254nm}$) were obtained from a previous work (GOULART DE ARAUJO *et al.*, 2017).

iv. The time period evaluated for the kinetic study was the first 15 min of irradiation, since in most cases the H_2O_2 concentrations were below the limit of detection after the mentioned time.

By using BPA and H_2O_2 concentrations versus time data, along with the nonlinear regression algorithm described above, two parameters were adjusted (k_2 and k_7) and are shown in Table 6.6.

Table 6.6 – Comparison between estimated and reported values of the kinetic constants k_2 and k_7.

Parameters	**Estimated values**	**Literature values**
k_2	3.4×10^7 L mol^{-1} s^{-1}	$1.2 – 4.5 \times 10^7$ L mol^{-1} s^{-1} (SIMUNOVIC *et al.*, 2011)
K_7	1.84×10^9 L mol^{-1} s^{-1}	3.3×10^9 L mol^{-1} s^{-1} (FELIS *et al.*, 2011)

The estimated value of k_2 falls within the range of measurements reported by SIMUNOVIC *et al*. (2011). On the other hand, there are very few studies that have calculated the reaction constant between BPA and the hydroxyl radical (k_7), which makes it difficult to search for intervals for this constant. However, our estimated value is of the same order of magnitude as that calculated by FELIS *et al.* (2011). Figure 6. compares experimental versus predicted values of BPA and H_2O_2 concentrations for all experiments.

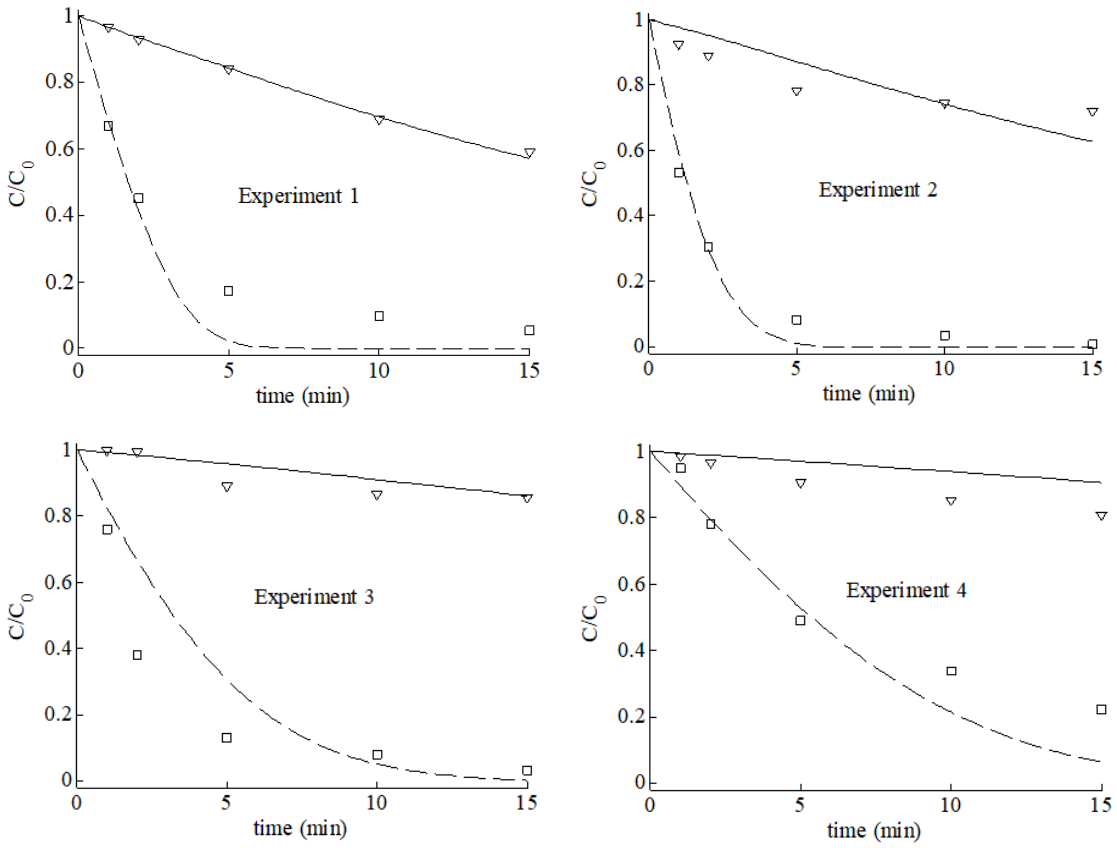

Figure 6.11 – Experimental and predicted normalized BPA (□, dashed line) and H_2O_2 (▽, solid line) concentrations over time for all experimental conditions. Conditions ($[H_2O_2]_0$, mmol L^{-1} – $E_{P,0}$, $\times 10^{18}$ photons L^{-1} s^{-1}): Exp 1 (3.6 – 3.6); Exp 2 (7.6 – 3.6); Exp 3 (9.6 – 1.4); Exp 4 (7.6 – 0.87). Experiments run in duplicate.

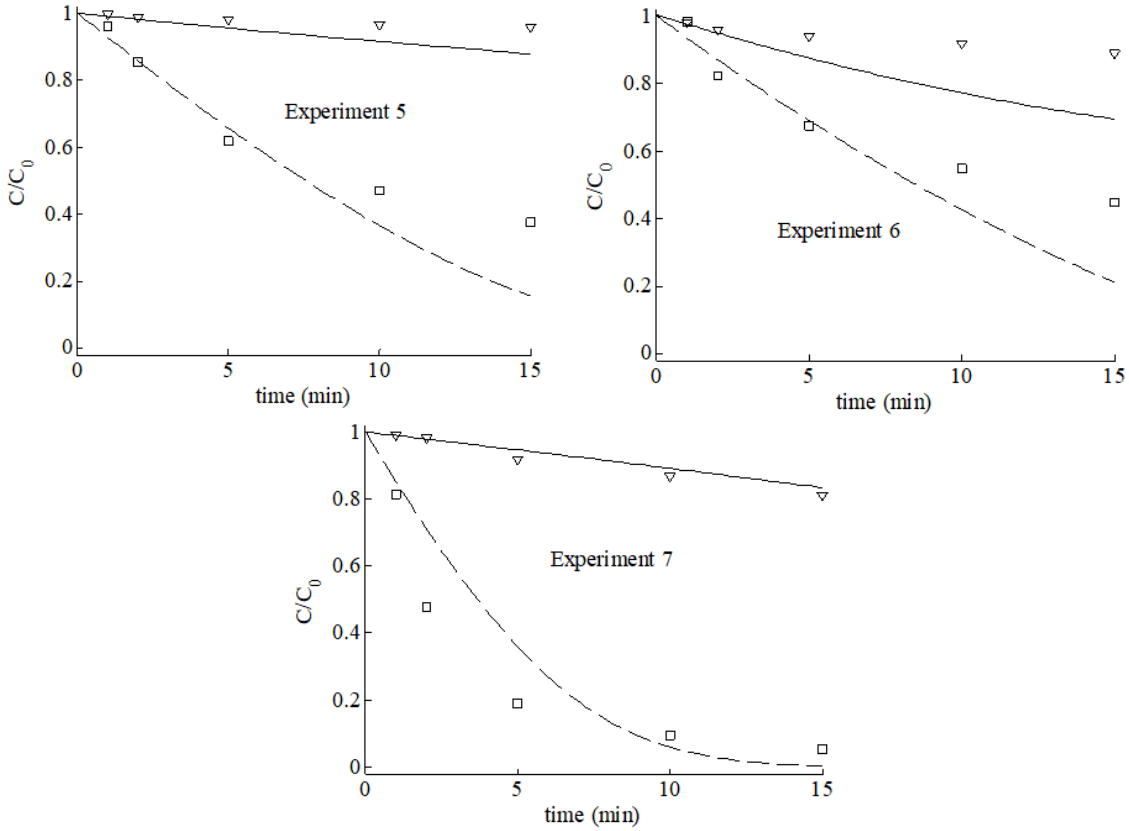

Figure 6.11 (Cont.) – Experimental and predicted normalized BPA (□, dashed line) and H_2O_2 (▽, solid line) concentrations over time for all experimental conditions. Conditions ($[H_2O_2]_0$, mmol L^{-1} – $E_{P,0}$, $\times 10^{18}$ photons L^{-1} s^{-1}): Exp 5 (3.6 – 0.87); Exp 6 (1.6 – 1.4); Exp 7 (5.6 – 1.4). Experiments run in duplicate.

As highlighted in Figure 6.11, a good fit of experimental data for both BPA and H_2O_2 concentrations over time was obtained for experiments 1, 2, 4, and 7. In such cases, the optimized two reaction rate constants were adequate. However, for the other experiments (3, 5, and 6) the results predicted by the kinetic model were unsatisfactory, particularly when the lowest H_2O_2 was employed (Exp 6). This remark indicated that the fitted model is not suitable for the entire range of initial H_2O_2 concentrations.

Some considerations are made regarding these differences:

i. The initial conditions for each experiment were different. Therefore, the predicted model will privilege some experimental runs at the expense of others; in this case, the most impaired experimental runs were performed at either low initial hydrogen peroxide concentration (Exp 6, $[H_2O_2]_0$ = 1.6 mmol L^{-1}), or low specific photon emission rate (Exp 4, $E_{P,0}$ = 1.44 ×10^{-3} Einstein m^{-3} s^{-1}) or both variables at low values (Exp 5, $[H_2O_2]_0$ = 3.6 mmol L^{-1} and $E_{P,0}$ = 1.44 ×10^{-3} Einstein m^{-3} s^{-1});
ii. The LSPP model considers the radiation field as uniform in the axial direction, which may result in errors.

The root mean square error (RMSE) was used to evaluate the accuracy of the model and it was obtained for both BPA and H_2O_2 concentrations. The root mean square errors (RMSE) are 2.92 × 10^{-1} and 2.16 × 10^{-2} mmol L^{-1}, for H_2O_2 and BPA concentrations, respectively.

7. CONCLUSIONS AND FUTURE WORK

Bisphenol A (BPA) degradation in aqueous solution by the H_2O_2/UV process at 254 nm was investigated in this Thesis. Two main original contributions were accomplished. The first is a systematic investigation on the influence of the initial H_2O_2 concentration ($[H_2O_2]_0$) and specific rate of photons emission ($E_{P,0}$) on the apparent first-order specific BPA degradation rate, BPA degradation after 15 min, and TOC removal after 180 min. With this aim, a detailed approach based on a Doehlert experimental design and response surface methodology was used. The second contribution is the proposal of a rigorous kinetic model for the H_2O_2/UV-driven BPA degradation process. In this case, as far as we know, no previous studies had employed the local volumetric rate of photons absorption explicitly in a kinetic model.

As regards the first contribution, we found that the best conditions for BPA degradation by the H_2O_2/UV process were $[H_2O_2]_0$ = 7.6 mmol L^{-1} and $E_{P,0}$ = 3.6 × 10^{18} photons L^{-1} s^{-1}. These conditions resulted in the highest apparent first-order specific BPA degradation rate and BPA degradation after 15 min, and the second highest TOC removal after 180 min. Nevertheless, despite the very good results regarding BPA degradation, in most cases less than 75% TOC removals were achieved after 180 min, with nearly 95% mineralization observed only for the highest $[H_2O_2]_0$ and $E_{P,0}$ used.

Moreover, the lowest initial H_2O_2 concentrations (1.6 and 3.6 mmol L^{-1}, respectively), associated with low specific photon emission rates (1.4 and 0.87 × 10^{18} photons L^{-1} s^{-1}, respectively) were found to be insufficient to degrade the transformation products formed, even in the presence of H_2O_2 during all the reaction time. In addition, roughly the same time behaviour of pH was observed in all experiments, i.e., a decrease from 7 to about 3 in the first 70 min. In only two experiments pH 5 increased from about 3 to 5 until the end of the reaction. This behaviour is well known in the field of AOPs. In fact, the formation of acidic intermediates results in pH decrease, which under some conditions increases as a result of BPA by-products mineralization to CO_2 and H_2O.

Finally, the experimental design based on the Doehlert matrix showed to be adequate for evaluating the main effects of process variables (initial H_2O_2 concentrations, specific photon emission rate) along with their interactions. Combined with the response surface methodology, the Doehlert design enabled the determination of the most adequate conditions for BPA degradation by the H_2O_2/UV process.

Regarding the second original contribution, a rigorous kinetic model for BPA degradation by the H_2O_2/UV process in an annular photochemical reactor in batch recirculation mode was developed, based on the line source with parallel plane emission (LSPP) approach, in combination with the radiative transfer equation (RTE) and mass balances. The steady-state approximation (SSA) was applied for highly reactive intermediates, such as $HO^{\bullet}$ and $HO_2^{\bullet}$ radicals, which is an adequate simplification. Two main reaction rate constants were optimized and the values were considered adequate. By comparing predicted and experimental data, a good representation of the BPA and H_2O_2 concentrations over treatment time was obtained.

The H_2O_2/UV process showed to be a good alternative for the treatment of aqueous streams containing BPA. On the other hand, the optimal conditions may vary depending on the matrix of interest, such as different types of effluents. However, this study may serve as first guidelines for process conditions in a pilot-plant or even industrial projects. It is worth mentioning that our kinetic study may provide useful information for studying the process variables and consequently the system optimization and the determination of the best parameters for process design and scaling-up. It is worth mentioning that the process could be employed directly in BPA production sites. This could avoid high BPA concentrations in the final industrial waste, where its treatment by H_2O_2/UV would be more difficult, since more absorbent or higher concentration species may be present. In light of this, the kinetic model proposed in this study can be appropriately applied in practice, taking into account that no other species is being considered but only those that are particular to the H_2O_2/UV process and to BPA.

Finally, further work is required. At first, other lamp emission models, such as LSSE or ESVE, can be employed and compared with the LSPP model used in this Thesis, to check whether they provide better fits of the experimental data. Other information that is crucial for a complete kinetic model is the identification of intermediate by-products, which is usually provided by detailed liquid chromatography-mass spectrometry work, in combination with total organic carbon measurements. This helps propose degradation pathways, resulting in extra reactions and reaction rate constants to be included in the mathematical model and optimized. Finally, the determination of residual toxicity and endocrine activity of treated solutions is necessary, in order to prove the applicability of the photo-oxidative process for real water and wastewater treatment before their release to the environment.

8. REFERENCES

AGENSON, K. O.; URASE, T. Change in membrane performance due to organic fouling in nanofiltration (NF)/reverse osmosis (RO) applications. **Separation and Purification Technology**, v. 55, n. 2, p. 147-156, 2007.

AGRAWAL, R.; SUMAN, A. **Production of Bisphenol A**. Bachelor of Technology in Chemical Engineering at Jaypee University of Engineering and Technology, India, 2012.

ALFANO, O. M.; ROMERO, R. L.; CASSANO, A. E. A cylindrical photoreactor irradiated from the bottom - I. Radiation flux density generated by a tubular source and a parabolic reflector. **Chemical Engineering Science**, v. 40, n. 11, p. 2119-2127, 1985.

ALFANO, O. M.; ROMERO, R. L.; CASSANO, A. E. A cylindrical photoreactor irradiated from the bottom - II. Models for the local volumetric rate of energy absorption with polychromatic radiation and their evaluation. **Chemical Engineering Science**, v. 41, n. 5, p. 1155-1161, 1986a.

ALFANO, O. M.; ROMERO, R. L.; CASSANO, A. E. Radiation field modelling in photoreactors - I. Homogeneous media. **Chemical Engineering Science**, v. 41, n. 3, p. 421-444, 1986.

ALFANO, O. M.; ROMERO, R. L.; NEGRO, A. C.; CASSANO, A. E. A cylindrical photoreactor irradiated from the bottom. III. Measurement of absolute values of the local volumetric rate of energy absorption. Experiments with polychromatic radiation. **Chemical Engineering Science**, v. 41, n. 5, p. 1163-1169, 1986.

ALNAIZY, R.; AKGERMAN, A. Advanced oxidation of phenolic compounds. **Advances in Environmental Research**, v. 4, n. 3, p. 233-244, 2000.

ALUM, A.; YOON, Y.; WESTERHOFF, P.; ABBASZADEGAN, M. Oxidation of bisphenol A, 17β-estradiol, and 17α-ethynylestradiol and by product estrogenicity. **Environmental Toxicology**, v. 19, n. 3, p. 257-264, 2004.

ANDREOZZI, R., CAPRIO, V., INSOLA, A., MAROTTA, R. Advanced oxidation processes (AOP) for water purification and recovery. **Catalysis Today**, v. 53, n. 1, p. 51-59, 1999.

ANDREOZZI, R.; CAPRIO, V.; INSOLA, A.; MAROTTA, R.; SANCHIRICO, R. Advanced oxidation processes for the treatment of mineral oil-contaminated wastewaters. **Water Research**, v. 34, n. 2, p. 620-628, 2000.

ARAUJO, L. G.; SANTOS, F. S.; TEIXEIRA, A. C. S. C. Degradation of bisphenol A by the UV and UV/H_2O_2 processes: Evaluation of process variables through experimental design. **The Canadian Journal of Chemical Engineering**, v. 95, n. 12, p. 2278-2285, 2017.

ARP, H. P. Compilation of Norwegian screening data for selected contaminants (2002–2012). **Oslo, Norwegian Climate and Pollution Agency (Statlig program for forurensningsovervåking.** Rapport n. 1133/2012. TA-2982/2012).

ASAKURA, H.; MATSUTO, T.; TANAKA, N. Behavior of endocrine-disrupting chemicals in leachate from MSW landfill sites in Japan. **Waste Management**, v. 24, n. 6, p. 613-622, 2004.

BAEZA, C.; KNAPPE, D. R. Transformation kinetics of biochemically active compounds in low-pressure UV photolysis and H2O2/UV advanced oxidation processes. **Water Research**, v. 45, n. 15, p. 4531-4543, 2011.

BENZAQUÉN, T. B.; ISLA, M. A.; ALFANO, O. M. Fenton and photo-Fenton processes for the degradation of atrazine: a kinetic study. **Journal of Chemical Technology and Biotechnology**, v. 90, n. 3, p. 459-467, 2015.

BENZAQUÉN, T. B.; ISLA, M. A.; ALFANO, O. M. Quantum efficiencies of the photo-Fenton degradation of atrazine in water. **Water Science and Technology**, v. 66, n. 10, p. 2209-2216, 2012.

BIELSKI, B. H.; CABELLI, D. E.; ARUDI, R. L.; ROSS, A. B. Reactivity of HO_2/O_2^- radicals in aqueous solution. **Journal of Physical and Chemical Reference Data**, v. 14, n. 4, p. 1041-1100, 1985.

BIRD, R. B.; STEWART, W. E.; LIGHTFOOT, E. N. **Transport Phenomena**. 1960. Madison, USA, 1960.

BRAUN, A. M.; JAKOB, L.; OLIVEROS, E.; NASCIMENTO, C. A. O. D. Up-scaling photochemical reactions. **Advances in Photochemistry**, v. 18, p. 235-314, 1993.

BRAUN, A. M.; MAURETTE, M. T.; OLIVEROS, E. **Photochemical Technology**. John Wiley & Son Ltd, 1991.

BROTONS, J. A.; OLEA-SERRANO, M. F.; VILLALOBOS, M.; PEDRAZA, V.; OLEA, N. Xenoestrogens released from lacquer coatings in food cans. **Environmental Health Perspectives**, v. 103, n. 6, p. 608-612, 1995.

BUXTON, G. V.; GREENSTOCK, C. L.; HELMAN, W. P.; ROSS, A. B. Critical review of rate constants for reactions of hydrated electrons, hydrogen atoms and hydroxyl radicals ($^{\bullet}OH/^{\bullet}O^{-}$) in aqueous solution. **Journal of Physical and Chemical Reference Data**, v. 17, n. 2, p. 513-886, 1988.

CALAFAT, A. M.; KUKLENYIK, Z.; REIDY, J. A.; CAUDILL, S. P.; EKONG, J.; NEEDHAM, L. L. Urinary concentrations of bisphenol A and 4-nonylphenol in a human reference population. **Environmental Health Perspectives**, v. 113, n. 4, p. 391-395, 2005.

CAMPAÑA, A. G.; RODRÍGUEZ, L. C.; GONZÁLEZ, A. L.; BARRERO, F. A.; CEBA, M. R. Sequential response surface methodology for multi optimization in analytical chemistry with three-variable Doehlert designs. **Analytica Chimica Acta**, v. 348, n. 1, p. 237-246, 1997.

CASSANO, A. E.; MARTIN, C. A.; BRANDI, R. J.; ALFANO, O. M. Photoreactor analysis and design: fundamentals and applications. **Industrial & Engineering Chemistry Research**, v. 34, n. 7, p. 2155-2201, 1995.

CERDA, J.; MARCHETTI, J. L.; CASSANO, A. E. The use of simple radiation models for the case of direct irradiation of photochemical reactors. **Latin America Journal of Chemical Engineering and Applied Chemistry**, v. 8, p. 15-25, 1978.

CHEN, M. Y.; IKE, M.; FUJITA, M. Acute toxicity, mutagenicity, and estrogenicity of bisphenol-A and other bisphenols. **Environmental Toxicology**, v. 17, n. 1, p. 80-86, 2002.

CHEN, P. J.; LINDEN, K. G.; HINTON, D. E.; KASHIWADA, S.; ROSENFELDT, E. J.; KULLMAN, S. W. Biological assessment of bisphenol A degradation in water following direct photolysis and UV advanced oxidation. **Chemosphere**, v. 65, n. 7, p. 1094-1102, 2006.

CHEN, P. J.; ROSENFELDT, E. J.; KULLMAN, S. W.; HINTON, D. E.; LINDEN, K. G. Biological assessments of a mixture of endocrine disruptors at environmentally relevant concentrations in water following H_2O_2/UV oxidation. **Science of the Total Environment**, v. 376, n. 1, p. 18-26, 2007.

CHENG, M.; ZENG, G.; HUANG, D.; LAI, C.; XU, P.; ZHANG, C.; LIU, Y. Hydroxyl radicals based advanced oxidation processes (AOPs) for remediation of soils contaminated with organic compounds: a review. **Chemical Engineering Journal**, v. 284, p. 582-598, 2016.

COMNINELLIS, C.; KAPALKA, A.; MALATO, S.; PARSONS, S. A.; POULIOS, I.; MANTZAVINOS, D. Advanced oxidation processes for water treatment: advances and trends for R&D. **Journal of Chemical Technology and Biotechnology**, v. 83, n. 6, p. 769-776, 2008.

CONTRERAS, S.; RODRIGUEZ, M.; AL MOMANI, F.; SANS, C.; ESPLUGAS, S. Contribution of the ozonation pre-treatment to the biodegradation of aqueous solutions of 2, 4-dichlorophenol. **Water Research**, v. 37, n. 13, p. 3164-3171, 2003.

COORS, A.; JONES, P. D.; GIESY, J. P.; RATTE, H. T. Removal of estrogenic activity from municipal waste landfill leachate assessed with a bioassay based on reporter gene expression. **Environmental Science & Technology**, v. 37, n. 15, p. 3430-3434, 2003.

CRITTENDEN, J. C.; HUA, S.; HAND, D. W.; GREEN, S. A. A kinetic model for H_2O_2/UV process in a completely mixed batch reactor. **Water Research**, v. 33, n. 10, p. 2315-2328. 1999.

DE LAAT, J.; GALLARD, H.; ANCELIN, S.; LEGUBE, B. Comparative study of the oxidation of atrazine and acetone by H_2O_2/UV, Fe (III)/UV, Fe (III)/H_2O_2/UV and Fe (II) or Fe (III)/H_2O_2. **Chemosphere**, v. 39, n. 15, p. 2693-2706, 1999.

DIAMANTI-KANDARAKIS, E.; BOURGUIGNON, J. P.; GIUDICE, L. C.; HAUSER, R.; PRINS, G. S.; SOTO, A. M.; ZOELLER, R. T.; GORE, A. C. Endocrine-disrupting chemicals: an Endocrine Society scientific statement. **Endocrine Reviews**, v. 30, n. 4, p. 293-342, 2009.

DODDS, E. C.; LAWSON, W. Synthetic estrogenic agents without the phenanthrene nucleus. **Nature**, v. 137, n. 3476, p. 996, 1936.

DOMÈNECH, X.; JARDIM, W. F.; LITTER, M. I. Procesos avanzados de oxidación para la eliminación de contaminantes. **Eliminación de Contaminantes por Fotocatálisis Heterogénea, cap**, v. 1, 2001.

DORN, P. B.; CHOU, C. S.; GENTEMPO, J. J. Degradation of bisphenol A in natural waters. **Chemosphere**, v. 16, n. 7, p. 1501-1507, 1987.

EDALATMANESH, M.; DHIB, R.; MEHRVAR, M.. Kinetic modeling of aqueous phenol degradation by H_2O_2/UV process. **International Journal of Chemical Kinetics**, v. 40, n. 1, p. 34-43, 2008.

EPA, U. S. **Special report on Environmental endocrine disruption: An effects assessment and analysis office of research and development**. REPA/630/R-96/012. In: Washington DC, 1997.

ERICKSON, M. L. **Steroidal hormones and other endocrine active compounds in shallow groundwater in nonagricultural areas of Minnesota - Study design, methods, and data**, 2012. 2009–10: U.S. Geological Survey Data Series 663, p. 9. https://pubs.usgs.gov/ds/663/pdf/ds663.pdf.

ERICKSON, M. L.; LANGER, S. K.; ROTH, J. L.; KROENING, S. E. **Contaminants of emerging concern in ambient groundwater in urbanized areas of Minnesota**, 2014. 2009–12 (ver. 1.2, September 2014): U.S. Geological Survey Scientific Investigations Report 2014–5096, p. 38, with appendix, http://dx.doi.org/10.3133/sir20145096

EUROPEAN UNION, Risk Assessment Report, CAS: 80-05-7 EINECS No: 201-245-8, Environment Addendum of April 2008, **4,4'-ISOPROPYLIDENEDIPHENOL (Bisphenol-A), Part 1 Environment**, 2012.

FELIS, E.; LEDAKOWICZ, S.; MILLER, J. S. Degradation of bisphenol A using UV and H_2O_2/UV processes. **Water Environment Research**, v. 83, n. 12, p. 2154-2158, 2011.

FENT, G.; HEIN, W. J.; MOENDEL, M. J.; KUBIAK, R. Fate of 14 C-bisphenol A in soils. **Chemosphere**, v. 51, n. 8, p. 735-746, 2003.

FROMME, H.; KÜCHLER, T.; OTTO, T.; PILZ, K.; MÜLLER, J.; WENZEL, A. Occurrence of phthalates and bisphenol A and F in the environment. **Water Research**, v. 36, n. 6, p. 1429-1438, 2002.

FÜRHACKER, M.; SCHARF, S.; WEBER, H. Bisphenol A: emissions from point sources. **Chemosphere**, v. 41, n. 5, p. 751-756, 2000.

GAERTNER, R. F.; KENT, J. A. Conversion in a continuous photochemical reactor. **Industrial & Engineering Chemistry**, v. 50, n. 9, p. 1223-1226, 1958.

GATIDOU, G.; THOMAIDIS, N. S.; STASINAKIS, A. S.; LEKKAS, T. D. Simultaneous determination of the endocrine disrupting compounds nonylphenol, nonylphenolethoxylates, triclosan and bisphenol A in wastewater and sewage sludge by gas chromatography–mass spectrometry. **Journal of Chromatography A**, v. 1138, n. 1, p. 32-41, 2007.

GUNNARSSON, L.; JAUHIAINEN, A.; KRISTIANSSON, E.; NERMAN, O.; LARSSON, D. J. Evolutionary conservation of human drug targets in organisms used for environmental risk assessments. **Environmental Science & Technology**, v. 42, n. 15, p. 5807-5813, 2008.

HAGER, D. G. UV-catalyzed hydrogen peroxide chemical oxidation of organic contaminants in water. **IN: Innovative Hazardous Waste Treatment Technology Series.**, v. 2, 1990.

HARRIS, P. R.; DRANOFF, J. S. A study of perfectly mixed photochemical reactors. **AIChE Journal**, v. 11, n. 3, p. 497-502, 1965.

HAYNES, William M. (Ed.). **CRC handbook of chemistry and physics**. CRC press, 2014.

HUANG, C. R.; SHU, H. Y. The reaction kinetics, decomposition pathways and intermediate formations of phenol in ozonation, UV/O_3 and H_2O_2/UV processes. **Journal of Hazardous Materials**, v. 41, n. 1, p. 47-64, 1995.

IJPELAAR, G. F.; HARMSEN, D. J.; BEERENDONK, E. F.; VAN LEERDAM, R. C.; METZ, D. H.; KNOL, A. H.; FULMER, A.; KRIJNEN, S. Comparison of low pressure and medium pressure UV lamps for H_2O_2/UV treatment of natural waters containing micro pollutants. **Ozone: Science & Engineering,** v. 32, n. 5, p. 329-337, 2010.

IKEZUKI, Y.; TSUTSUMI, O.; TAKAI, Y.; KAMEI, Y.; TAKETANI, Y. Determination of bisphenol A concentrations in human biological fluids reveals significant early prenatal exposure. **Human Reproduction**, v. 17, n. 11, p. 2839-2841, 2002.

IMOBERDORF, G. E.; IRAZOQUI, H. A.; ALFANO, O. M.; CASSANO, A. E. Scaling-up from first principles of a photocatalytic reactor for air pollution remediation. **Chemical Engineering Science**, v. 62, n. 3, p. 793-804, 2007.

INGERSLEV, F.; HALLING-SØRENSEN, B. **Evaluation of analytical chemical methods for detection of estrogens in the environment**. Danish Ministry of the Environment, Danish Environmental Protection Agency, 2003.

IRAZOQUI, H. A.; CERDÁ, J.; CASSANO, A. E. Radiation profiles in an empty annular photoreactor with a source of finite spatial dimensions. **AICHE Journal**, v. 19, n. 3, p. 460-467, 1973.

JACOB, S. M; DRANOFF, J. S. Design and analysis of perfectly mixed photochemical reactors. **Chemical Engineering Progress Symposium Series**, v. 89, p. 47-63, 1966.

JAMIL, T. S.; ROLAND, H.; MICHAEL, H.; JENS-UWE, R. Homogeneous photocatalytic processes for degradation of some endocrine disturbing chemicals under UV irradiation. **Journal of Water Process Engineering**, v. 18, p. 159-168, 2017.

KANG, N.; LEE, D. S.; YOON, J. Kinetic modeling of Fenton oxidation of phenol and monochlorophenols. **Chemosphere**, v. 47, n. 9, p. 915-924, 2002.

KATSUMATA, H.; KAWABE, S.; KANECO, S.; SUZUKI, T.; OHTA, K. Degradation of bisphenol A in water by the photo-Fenton reaction. **Journal of Photochemistry and Photobiology A: Chemistry**, v. 162, n. 2, p. 297-305, 2004.

KAWAGOSHI, Y.; FUJITA, Y.; KISHI, I.; FUKUNAGA, I. Estrogenic chemicals and estrogenic activity in leachate from municipal waste landfill determined by yeast two-hybrid assay. **Journal of Environmental Monitoring**, v. 5, n. 2, p. 269-274, 2003.

KIM, Y. H.; KIM, C. S.; PARK, S.; HAN, S. Y.; PYO, M. Y.; YANG, M. Gender differences in the levels of bisphenol A metabolites in urine. **Biochemical and Biophysical Research Communications**, v. 312, n. 2, p. 441-448, 2003.

KLEČKA, G. M.; STAPLES, C. A.; CLARK, K. E.; VAN DER HOEVEN, N.; THOMAS, D. E.; HENTGES, S. G. Exposure analysis of bisphenol A in surface water systems in North America and Europe. **Environmental Science & Technology**, v. 43, n. 16, p. 6145-6150, 2009.

KOLPIN, D. W.; FURLONG, E. T.; MEYER, M. T.; THURMAN, E. M.; ZAUGG, S. D.; BARBER, L. B.; BUXTON, H. T. Pharmaceuticals, hormones, and other organic wastewater contaminants in US streams, 1999-2000: A national reconnaissance. **Environmental Science & Technology**, v. 36, n. 6, p. 1202-1211, 2002.

KOMESLI, O. T.; MUZ, M.; AK, M. S.; BAKIRDERE, S.; GOKCAY, C. F. Occurrence, fate and removal of endocrine disrupting compounds (EDCs) in Turkish wastewater treatment plants. **Chemical Engineering Journal**, v. 277, p. 202-208, 2015.

KURATA, Y.; ONO, Y.; ONO, Y. Occurrence of phenols in leachates from municipal solid waste landfill sites in Japan. **Journal of Material Cycles and Waste Management**, v. 10, n. 2, p. 144-152, 2008.

KUSVURAN, E.; YILDIRIM, D. Degradation of bisphenol A by ozonation and determination of degradation intermediates by gas chromatography–mass spectrometry and liquid chromatography–mass spectrometry. **Chemical Engineering Journal**, v. 220, p. 6-14, 2013.

LAU, T. K.; CHU, W.; GRAHAM, N. J. The aqueous degradation of butylated hydroxyanisole by UV/$S_2O_8^{2-}$: study of reaction mechanisms via dimerization and mineralization. **Environmental Science & Technology**, v. 41, n. 2, p. 613-619, 2007.

LEE K. E.; SCHOENFUSS H. L.; BARBER L. B.; WRITER J. H.; BLAZER V. S.; KIESLING R. L.; FERREY M. L. Endocrine active chemicals and endocrine disruption in Minnesota streams and lakes - implications for aquatic resources, 1994-2008. 2010. U.S. Geological Survey Scientific Investigations Report 2010–5107, 47 p. with Appendixes, https://pubs.usgs.gov/sir/2010/5107/pdf/sir2010-5107.pdf.(2007)

LEE, K. E.; LANGER, S. K.; BARBER, L. B.; WRITER, J. H.; FERREY, M. L.; SCHOENFUSS, H. L.; FURLONG, E. T.; FOREMAN, W. T.; GRAY, J. L.; REVELLO, R. C.; MARTINOVIC, D.; WOODRUFF, O. P.; KEEFE, S. H.; BROWN, G. K.; TAYLOR, H.

E.; FERRER, I.; THURMAN, E. M. **Endocrine active chemicals, pharmaceuticals, and other chemicals of concern in surface water, wastewater-treatment plant effluent, and bed sediment, and biological characteristics in selected streams**. Minnesota - design, methods, and data, 2011. 2009: U.S. Geological Survey Data Series 575, p. 54, with appendixes, https://pubs.usgs.gov/ds/575/pdf/ds575.pdf.

LEGRINI, O.; OLIVEROS, E.; BRAUN, A. M. Photochemical processes for water treatment. **Chemical Reviews**, v. 93, n. 2, p. 671-698, 1993.

LI, Y. M.; ZENG, Q. L.; YANG, S. J. Removal and fate of estrogens in an anaerobic-anoxic-oxic activated sludge system. **Water Science and Technology**, v. 63, n. 1, p. 51-56, 2011.

LIU, Z. H.; KANJO, Y.; MIZUTANI, S. Removal mechanisms for endocrine disrupting compounds (EDCs) in wastewater treatment - physical means, biodegradation, and chemical advanced oxidation: a review. **Science of the Total Environment**, v. 407, n. 2, p. 731-748, 2009.

MAJCEN-LE MARECHAL, A.; SLOKAR, Y. M.; TAUFER, T. Decoloration of chlorotriazine reactive azo dyes with H_2O_2/UV. **Dyes and Pigments**, v. 33, n. 4, p. 281-298. 1997.

MCGROUP. Bisphenol A (BPA): 2015 World Market Outlook and Forecast up to 2019. July, 2015, accessed on 7 September 2015, http://mcgroup.co.uk/news/20131108/bpa-production-grew-372000-tonnes.html.

MOHAJERANI, M.; MEHRVAR, M.; EIN-MOZAFFARI, F. Computational Fluid Dynamics (CFD) Modeling of Photochemical Reactors. In: **Applied Computational Fluid Dynamics**. InTech, 2012.

MOHAPATRA, D. P.; BRAR, S. K.; TYAGI, R. D.; SURAMPALLI, R. Y. Concomitant degradation of bisphenol A during ultrasonication and Fenton oxidation and production of biofertilizer from wastewater sludge. **Ultrasonics Sonochemistry**, v. 18, n. 5, p. 1018-1027, 2011.

MORIN, N.; ARP, H. P. H.; HALE, S. E. Bisphenol A in solid waste materials, leachate water, and air particles from Norwegian waste-handling facilities: presence and partitioning behavior. **Environmental Science & Technology**, v. 49, n. 13, p. 7675-7683, 2015.

NAKASHIMA, T.; OHKO, Y.; KUBOTA, Y.; FUJISHIMA, A. Photocatalytic decomposition of estrogens in aquatic environment by reciprocating immersion of TiO_2-modified polytetrafluoroethylene mesh sheets. **Journal of Photochemistry and Photobiology A: Chemistry**, v. 160, n. 1, p. 115-120, 2003.

NICK, K.; SCHÖLER, H. F.; MARK, G.; SÖYLEMEZ, T.; AKHLAQ, M. S.; SCHUCHMANN, H. P.; VON SONNTAG, C. Degradation of some triazine herbicides by UV radiation such as used in the UV disinfection of drinking water. **Aqua - Journal of Water Supply: Research and Technology**, v. 41, n. 2, p. 82-87, 1992.

OCHOA, T. J. A.; WHITAKER, S. El Método del promedio volumétrico para el estudio de difusión en sistemas de varias componentes. **Revista Mexicana de Física**, v. 41, n. 3, p. 451-470, 1995.

OLEA, N.; PULGAR, R.; PÉREZ, P.; OLEA-SERRANO, F.; RIVAS, A.; NOVILLO-FERTRELL, A.; PEDRAZA, V.; SOTO, A. M.; SONNENSCHEIN, C. Estrogenicity of resin-based composites and sealants used in dentistry. **Environmental Health Perspectives**, v. 104, n. 3, p. 298-305, 1996.

OLMEZ-HANCI, T.; DURSUN, D.; AYDIN, E.; ARSLAN-ALATON, I.; GIRIT, B., MITA, L.; DIANO, N.; MITA, D. G.; GUIDA, M. $S_2O_8^{2-}$/UV-C and H_2O_2/UV-C treatment of Bisphenol A: Assessment of toxicity, estrogenic activity, degradation products and results in real water. **Chemosphere**, v. 119, p. S115-S123, 2015.

OPPENLÄNDER, T. **Photochemical purification of water and air: advanced oxidation processes (AOPs)-principles, reaction mechanisms, reactor concepts**. John Wiley & Sons, 2003.

ÖZIŞIK, M. N. **Radiative transfer and interactions with conduction and convection**. Werbel & Peck, 1973.

PARK, C. G.; CHOI, E. S.; JEON, H. W.; LEE, J. H.; SUNG, B. W.; CHO, Y. H.; KO, K. B. Effect of nitrate on the degradation of bisphenol A by H_2O_2/UV and ozone/H_2O_2 oxidation in aqueous solution. **Desalination and Water Treatment**, v. 52, n. 4-6, p. 797-804, 2014.

PARSONS, S. (Ed.). **Advanced oxidation processes for water and wastewater treatment**. IWA publishing, 2004.

PERA-TITUS, M.; GARCÍA-MOLINA, V.; BAÑOS, M. A.; GIMÉNEZ, J.; ESPLUGAS, S. Degradation of chlorophenols by means of advanced oxidation processes: a general review. **Applied Catalysis B: Environmental**, v. 47, n. 4, p. 219-256, 2004.

PERES, J. C. G.; SILVIO, U. D.; TEIXEIRA, A. C. S.; GUARDANI, R. Study of an Annular Photoreactor with Tangential Inlet and Outlet: I. Fluid Dynamics. **Chemical Engineering & Technology**, v. 38, n. 2, p. 311-318, 2015.

PLANT, L.; JEFF, M. Hydrogen peroxide: a potent force to destroy organics in wastewater. **Chemical Engineering**, p. EE16, 1994.

POLYCARBONATE/BPA GLOBAL GROUP, **About Bisphenol A, *Bisphenol A***, 2003, accessed on 9 September 2017, http://www.bisphenol-a.org/about/bpa-info/bpa-synthesis.html.

PUMA, G. L.; PUDDU, V.; TSANG, H. K.; GORA, A.; TOEPFER, B. Photocatalytic oxidation of multicomponent mixtures of estrogens (estrone (E1), 17β-estradiol (E2), 17α-ethynylestradiol (EE2) and estriol (E3)) under UVA and UVC radiation: photon absorption, quantum yields and rate constants independent of photon absorption. **Applied Catalysis B: Environmental**, v. 99, n. 3, p. 388-397, 2010.

QUAN, Y.; PEHKONEN, S. O.; RAY, M. B. Evaluation of three different lamp emission models using novel application of potassium ferrioxalate actinometry. **Industrial & Engineering Chemistry Research**, v. 43, n. 4, p. 948-955, 2004.

RDC RESOLUTION n. 41/2011. Ministério da Saúde. ANVISA, 16 September 2011. Dispõe sobre a proibição de uso de bisfenol A em mamadeiras destinadas a alimentação de lactentes e dá outras providências, 2011, accessed in 10 September 2017, http://bvsms.saude.gov.br/bvs/saudelegis/anvisa/2011/res0041_16_09_2011.html. (In Portuguese)

RODRÍGUEZ, E. M.; FERNÁNDEZ, G.; KLAMERTH, N.; MALDONADO, M. I.; ÁLVAREZ, P. M.; MALATO, S. Efficiency of different solar advanced oxidation processes on the oxidation of bisphenol A in water. **Applied Catalysis B: Environmental**, v. 95, n. 3, p. 228-237, 2010.

ROMERO, R. L.; ALFANO, O. M.; MARCHETTI, J. L.; CASSANO, A. E. Modelling and parametric sensitivity of an annular photoreactor with complex kinetics. **Chemical Engineering Science**, v. 38, n. 9, p. 1593-1605, 1983.

ROSENFELDT, E. J.; CHEN, P. J.; KULLMAN, S.; LINDEN, K. G. Destruction of estrogenic activity in water using UV advanced oxidation. **Science of the Total Environment**, v. 377, n. 1, p. 105-113, 2007.

ROSENFELDT, E. J.; LINDEN, K. G. Degradation of endocrine disrupting chemicals bisphenol A, ethinylestradiol, and estradiol during UV photolysis and advanced oxidation processes. **Environmental Science & Technology**, v. 38, n. 20, p. 5476-5483, 2004.

ROSSETTI, G. H.; ALBIZZATI, E. D.; ALFANO, O. M. Decomposition of formic acid in a water solution employing the photo-Fenton reaction. **Industrial & Engineering Chemistry Research**, v. 41, n. 6, p. 1436-1444, 2002.

RUPPERT, G.; BAUER, R.; HEISLER, G. UV-O_3, UV-H_2O_2, UV-TiO_2 and the photo-Fenton reaction-comparison of advanced oxidation processes for wastewater treatment. **Chemosphere**, v. 28, n.8, p. 1447-1454, 1994.

SAKAMOTO, H.; FUKUI, H.; SOUTA, I.; KANEKO, K. Studies on Bisphenol A and its origins in leachates from solid waste landfills. **Japan Society of Waste Management Experts**, v. 15, p. 511-520, 2004.

SCRIMSHAW, M. D.; LESTER. J. N. **Fate and behavior of endocrine disruptors in sludge treatment and disposal**. Endocrine Disruptors in Wastewater and Sludge Treatment Processes, *CRC Press LLC and IWA Publishing*, pp. 145-176, 2003.

SEHESTED, K.; RASMUSSEN, O. L.; FRICKE, H. Rate constants of OH with HO_2, O_2^-, and $H_2O_2^+$ from hydrogen peroxide formation in pulse-irradiated oxygenated water. **The Journal of Physical Chemistry**, v. 72, n. 2, p. 626-631, 1968.

SHARMA, J.; MISHRA, I. M.; KUMAR, V. Degradation and mineralization of Bisphenol A (BPA) in aqueous solution using advanced oxidation processes: H_2O_2/UV and oxidation systems. **Journal of Environmental Management**, v. 156, p. 266-275, 2015.

SHARMA, J.; MISHRA, I. M.; KUMAR, V. Mechanistic study of photo-oxidation of Bisphenol-A (BPA) with hydrogen peroxide (H_2O_2) and sodium persulfate (SPS). **Journal of Environmental Management**, v. 166, p. 12-22, 2016.

SHARMA, S.; RUPARELIA, J. P.; PATEL, M. L. A general review on advanced oxidation processes for waste water treatment. In: **Nirma University International Conference, Ahmedabad, Gujarat**. 2011.

SILVA, M. P.; DOS SANTOS BATISTA, A. P.; BORRELY, S. I.; SILVA, V. H. O.; TEIXEIRA, A. C. S. C. Photolysis of atrazine in aqueous solution: role of process variables and reactive oxygen species. **Environmental Science and Pollution Research**, v. 21, n. 21, p. 12135-12142, 2014.

SIMUNOVIC, M.; KUSIC, H.; KOPRIVANAC, N.; BOZIC, A. L. Treatment of simulated industrial wastewater by photo-Fenton process: Part II. The development of mechanistic model. **Chemical Engineering Journal**, v. 173, n. 2, p. 280-289, 2011.

SIN, J. C.; LAM, S. M.; MOHAMED, A. R.; LEE, K. T. Degrading Endocrine Disrupting Chemicals from Wastewater by TiO_2 Photocatalysis: A Review. **International Journal of Photoenergy**, p. 1-23, 2012.

SODRÉ, F. F.; MONTAGNER, C. C.; LOCATELLI, M. A. F.; JARDIM, W. F. Ocorrência de interferentes endócrinos e produtos farmacêuticos em águas superficiais da região de Campinas (SP, Brasil). **Journal of Brazilian Society of Ecotoxicology**, v. 2, n. 2, p. 187-196, 2007.

STAEHELIN, J.; HOIGNE, J. Decomposition of ozone in water in the presence of organic solutes acting as promoters and inhibitors of radical chain reactions. **Environmental Science & Technology**, v. 19, n. 12, p. 1206-1213, 1985.

STAPLES, C. A.; DOME, P. B.; KLECKA, G. M.; OBLOCK, S. T.; HARRIS, L. R. A review of the environmental fate, effects, and exposures of bisphenol A. **Chemosphere**, v. 36, n. 10, p. 2149-2173, 1998.

SUN, Y.; IRIE, M.; KISHIKAWA, N.; WADA, M.; KURODA, N.; NAKASHIMA, K. Determination of bisphenol A in human breast milk by HPLC with column switching and fluorescence detection. **Biomedical Chromatography**, v. 18, n. 8, p. 501-507, 2004.

SURI, R. P.; NAYAK, M.; DEVAIAH, U.; HELMIG, E. Ultrasound assisted destruction of estrogen hormones in aqueous solution: effect of power density, power intensity and reactor configuration. **Journal of Hazardous Materials**, v. 146, n. 3, p. 472-478, 2007.

TAO, H.; HAO, S.; CHANG, F.; WANG, L.; ZHANG, Y.; CAI, X. Photodegradation of bisphenol A by titana nanoparticles in mesoporous MCM-41. **Water, Air, & Soil Pollution**, v. 214, n. 1-4, p. 491-498, 2011.

TERNES, T. A.; STÜBER, J.; HERRMANN, N.; MCDOWELL, D.; RIED, A.; KAMPMANN, M.; TEISER, B. Ozonation: a tool for removal of pharmaceuticals, contrast media and musk fragrances from wastewater? **Water Research**, v. 37, n. 8, p. 1976-1982, 2003.

TIJANI, J. O.; FATOBA, O. O.; PETRIK, L. F. A review of pharmaceuticals and endocrine-disrupting compounds: sources, effects, removal, and detections. **Water, Air, & Soil Pollution**, v. 224, n. 11, p. 1770-1794, 2013.

TORRES, R. A.; SARANTAKOS, G.; COMBET, E.; PÉTRIER, C.; PULGARIN, C. Sequential helio-photo-Fenton and sonication processes for the treatment of bisphenol A. **Journal of Photochemistry and Photobiology A: Chemistry**, v. 199, n. 2, p. 197-203, 2008.

UMAR, M.; RODDICK, F.; FAN, L.; AZIZ, H. A. Application of ozone for the removal of bisphenol A from water and wastewater–a review. **Chemosphere**, v. 90, n. 8, p. 2197-2207, 2013.

UNITED STATES ENVIRONMENTAL PROTECTION AGENCY, **BPA action plan,** 2010, accessed on**,** https://www.epa.gov/sites/production/files/2015-09/documents/bpa_action_plan.pdf

URASE, T.; MIYASHITA, K. I. Factors affecting the concentration of bisphenol A in leachates from solid waste disposal sites and its fate in treatment processes. **Journal of Material Cycles and Waste Management**, v. 5, n. 1, p. 77-82. 2003.

VANDENBERG, L. N.; HAUSER, R.; MARCUS, M.; OLEA, N.; WELSHONS, W. V. Human exposure to bisphenol A (BPA). **Reproductive Toxicology**, v. 24, n. 2, p. 139-177, 2007.

VERHOEVEN, J. W. Glossary of terms used in photochemistry (IUPAC Recommendations 1996). **Pure and Applied Chemistry**, v. 68, n. 12, p. 2223-2286, 1996.

XU, J.; WU, L.; CHANG, A. C. Degradation and adsorption of selected pharmaceuticals and personal care products (PPCPs) in agricultural soils. **Chemosphere**, v. 77, n. 10, p. 1299-1305, 2009.

YAMADA, K.; URASE, T.; MATSUO, T.; SUZUKI, N. Constituents of organic pollutants in leachates from different types of landfill sites and their fate in the treatment processes. **Journal Japan Society on Water Environment**, v. 22, p. 40-45, 1999.

YAMAMOTO, T.; YASUHARA, A.; SHIRAISHI, H.; NAKASUGI, O. Bisphenol A in hazardous waste landfill leachates. **Chemosphere**, v. 42, n. 4, p. 415-418, 2001.

YASUHARA, A.; SHIRAISHI, H.; NISHIKAWA, M.; YAMAMOTO, T.; UEHIRO, T.; NAKASUGI, O.; OKUMURA, T.; KENMOTSU, K.; FUKUI, H.; NAGASE, M.; ONO, Y. Determination of organic components in leachates from hazardous waste disposal sites in Japan by gas chromatography–mass spectrometry. **Journal of Chromatography A**, v. 774, n. 1, p. 321-332, 1997

YUE, P. L. Modelling of kinetics and reactor for water purification by photo-oxidation. **Chemical Engineering Science**, v. 48, n. 1, p. 1-11, 1993.

ZAHORODNA, M.; BOGOCZEK, R.; OLIVEROS, E.; BRAUN, A. M. Application of the Fenton process to the dissolution and mineralization of ion exchange resins. **Catalysis Today**, v. 129, n. 1, p. 200-206, 2007.

ZENG, G.; ZHANG, C.; HUANG, G.; YU, J.; WANG, Q.; LI, J.; XI, B.; LIU, H. Adsorption behavior of bisphenol A on sediments in Xiangjiang River, Central-south China. **Chemosphere**, v. 65, n. 9, p. 1490-1499, 2006.

ZEPP, R. G.; CLINE, D. M. Rates of direct photolysis in aquatic environment. **Environmental Science & Technology**, v. 11, n. 4, p. 359-366, 1977.

ZHANG, A.; LI, Y. Removal of phenolic endocrine disrupting compounds from waste activated sludge using UV, H_2O_2, and H_2O_2/UV oxidation processes: effects of reaction conditions and sludge matrix. **Science of the Total Environment**, v. 493, p. 307-323, 2014.

ZHANG, Y.; ZHOU, J. L.; NING, B. Photodegradation of estrone and 17β-estradiol in water. **Water Research**, v. 41, n. 1, p. 19-26, 2007.